Cell Settling, Migration, and Stochastic Cancer Expression Suggest Potassium Flux Per H^+- Sensitive KCN Members Associated with Oncogenes and Histone/DNA Modulators Potentially Initiates pH-Reversal

Marie E. Beckner[1]*

1 Brain Health Research Institute at Kent State University; mbeckne1@kent.edu
* Correspondence: mbeckne1@kent.edu

ABSTRACT

Attraction of glioblastoma cells to potassium was suspected when cells clustered around dying cells and they migrated towards serum (high [K^+]) and a positive potassium gradient. Potassium channel proteins (KCN family, 90 members) mediating altered transmembrane flux may provide K^+ that releases H^+ bound to inner membranes in cancer cells for cytosolic proton transfer (possibly Grotthuss) to extrusion sites. Cell settling and migration assay results led to collection of 70 studies, unbiased by authors for inclusion of KCN genes, that detected KCN differentially expressed genes (DEG). Of 53 KCN DEG found among 29 malignancies, 62.3% encoded H^+-sensitive proteins. KCN DEG encoding H^+-sensitive proteins were more prevalent in 50 studies involving one or more of 8 categories (7 oncogenes and histone/DNA modifiers) versus those with none, p = 0.0325. Pertinent genes for lactate outflow, etc. had relatively normal expressions. Brain tumors in REMBRANDT (database) showed altered expression of KCN genes encoding H^+-sensitive proteins in glioblastomas versus less invasive oligodendrogliomas of patients on anti-seizure medications, with less *KCNJ16* /Kir5.1, $p = 5.32 \times 10^{-8}$. Altered H^+-sensitive potassium flux via the KCN family downstream of oncogenes and histone/DNA modifiers putatively incites proton transfers for H^+ release during pH reversal in cancer.

Keywords: Potassium Channels, Potassium, *KCNJ16, KCNN4, KCNMA1*, H^+-sensitivity, pH-reversal, Differential Gene Expression, Grotthuss Proton Transfer, Oncogenes

Graphical Abstract

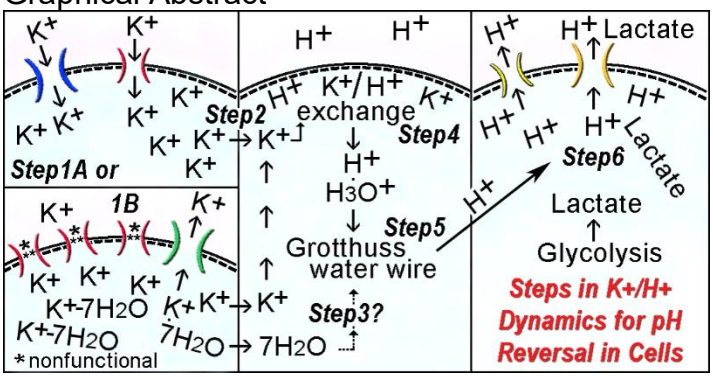

Graphical Abstract Legend: Steps in K^+/H^+ Dynamics for pH Reversal in Cells. Step1. Potassium ions accumulate near cell membranes if (A) inward flow channels bring in more

K^+ than normal or (B) if the diffuse low outward flow channels are nonfunctional with compensation by channels in a few locations that are high flow requiring contributions of solvated potassium (K^+-$7H_2O$) from deeper cell regions. Step2. K^+ reaches the inner cell membrane where H^+ is bound diffusely to its negative charges. Step3. As K^+-$7H_2O$ desolvates (for channel exit or membrane binding), the release of $7H_2O$ may augment or form Grotthuss water wires near inner membrane surfaces. Step4. At the inner membrane K^+ exchanges with H^+. As H^+ is released, it becomes H_3O^+ and diffuses into the cytosol. Step5. H_3O^+ enters a Grotthuss water wire that enables rapid proton transfer (conformational) to H^+ exit sites. Step6. H^+ leaves the cell with lactate or it exits via other H^+ extruders. The cytosolic pH increases and the external pH decreases for pH reversal.

1. Introduction

1.1. General

Potassium flux is already known to maintain cell membrane potential in all cells, to assist volume changes in migrating cells, and permits neurons to fire action potentials as they release potassium that is buffered by glial cells. Potassium, as cytoplasmic monovalent cations, is now proposed to also exchange with fixed H^+ on inner membranes to incite proton transfer and extrusion for shifts in pH that favor tumor cell survival and invasion. If so, then K^+/H^+ cation exchange may help to explain the attraction of glioblastoma cells (highest grade malignant glial tumors) to axons in CNS white matter tracts and peripheral nerve fibers [1,2] that release K^+ via axonal action potentials as well as their growth factors. Experiments performed to study cell morphology and viability in a microaqueous environment suggested malignant cell attraction to K^+. Glioblastoma cells tightly clustered around single dying cells, putatively releasing their cytoplasmic stores of K^+. It had already been observed that glioblastoma cells migrated towards fetal bovine serum, known to have levels of 5-15 mM K^+ [3]. This clustering behavior was similar to how glioblastoma cells rim necrotic foci (pseudopalisading) which is a typical histologic feature of these tumors [4-6]. Also, pseudopalisading glioblastoma cells have an enhanced migratory phenotype [6,7]. Additionally, in regard to reversal of pH, i.e. intracellular pH (pHi) is greater than extracellular pH (pHe), there are related metabolic features reported for benign astrocytic cells, such as (*i*) an increase of their intracellular pH with neuronal stimulation, possibly triggered by membrane K^+ redistribution during depolarization [8,9]. Also, intracellular alkalinization detected in benign mammalian astrocytes has been attributed to their uptake of potassium released by repetitive neuronal firing of action potentials *in vivo* [10] as astrocytic cell membranes depolarize. Also, (*ii*) the rate of glycolysis (inhibited by lactic acid produced in hypoxia) is stimulated by changes in intracellular [H^+] rather than [HCO_3^-] in astrocytes [11]. Cytoplasmic alkalinization in malignant and transformed cells occurring via efflux of protons resulting in extracellular acidosis has been attributed to mechanisms involving ion transporters, pumps, exchangers, etc. with the “active” ones requiring ATP [12-19]. Redistribution of K^+ has been previously suggested as being a contributing factor in tumor cell alkalinization [12] and pH-sensitive ion channels, including those for K^+, have been mentioned as “sensors” in descriptions of pH reversal [13,14,16,17]. Data in this study suggests the possibility of potassium flux as playing a role in glioblastoma cell behavior.

The large size of the KCN (potassium channel) family with its complex interactions among family members, an extensive complement of non-family regulators, functional reliance on contents of biological milieus, and a wide distribution across the genome serving as a relatively large target for genetic damage, were characteristics that supported further investigation of potential anomalous potassium flux in cancer through gathering data on this family in a stochastic manner. Retrieval of reported data unbiased for KCN gene expression in tumors allowed retrieval of data on differentially expressed genes (DEG) of KCN family members and associated non-KCN DEG in 70 studies of many types of cancer to provide an overall view of anomalous potassium flux in cancer. Also, a brain tumor database REMBRANDT [20,21], and a published whole genome analysis of 6 glioblastoma cell lines, Patil, et al. [22], were queried for data on KCN genes. The H^+-sensitivity of a large proportion of the KCN family members detected and the high likelihood of K^+ as a replacement cation for H^+ suggest that potassium ion flux across plasma membranes or accumulation near them may play a role in the pH reversal commonly seen in malignancy. Deregulated, passive inward channel flux (without requiring ATP) or loss of normal diffusely distributed outward K^+ flow (necessitating focally concentrated outward flow as needed) leading to accumulations of K^+ ions at inner cell membranes with H^+ bound to fixed anions potentially leads to K^+/H^+ exchange to release H^+ as an initial step leading to pH reversal.

1.2. Cytosolic Proton Transfer Related to K^+ and Hydration

The proposed K^+ replacement of bound H^+ would augment adjacent hydronium ion (H_3O^+) accumulation which can be seen at water-lipid interfaces [23], such as along inner cell membranes. This putatively sets the stage for pH reversal via subsequent steps. The mobility of unbound H^+ (H_3O^+ at 36.2×10^{-4} cm^2 $V^{-1}s^{-1}$) is very high compared to other univalent cations such as K^+ and Na^+ [24]. In immortalized human embryonic kidney cells, H^+ diffusion through the cytosol occurred 60-fold faster than when limited to the inner plasma membrane surface, i.e. 0.6 $\mu m s^{-1}$ versus 0.01 $\mu m s^{-1}$ [25]. In cardiac myocytes a comparable high speed of cytoplasmic H^+ distribution, 0.7 $\mu m s^{-1}$, has been detected. This was based on using HCl in KCl (140 mM) solutions (pH 3.0) for acid diffusion studies with membrane acid transport simultaneously inhibited [26]. Another study has shown dissociation of HCl in a microaqueous environment so that the acid's protons were each transferred to a neighboring water molecule and then another in clusters of $HCl(H_2O)_n$, where n=1 to 5 and 7. With the addition of a fifth and sequential seventh water molecule, the covalent H-Cl bond transitioned to the contact ion pair, $H_3O^+Cl^-$, plus free hydrogens. The $HCl(H_2O)_5$ and $HCl(H_2O)_7$ clusters were spontaneously dissociated structures with contact ionic bonds [27]. Thus, H_3O^+ may be distributed to the cytosol after putative K^+/H^+ exchange on inner membranes and after spontaneous dissociation of acids (multiple types in cancer cells) within cytosols, possibly microaqueous in nature.

Cytosolic proton transfer has been previously attributed to small molecules, such as taurine, carnitine, carnosine, or homocarnosine, behaving as mobile buffers that shuttle H^+ to enable cytosolic proton transfers [26]. However, proton transfers from H_3O^+ may also be enabled by a rapid mechanism consistent with behavior described originally by C.J.T. Grotthuss in 1806 [28] that fits with this scenario. Proton transfers may occur within the cytoplasm via H-bonded complexes, possibly involving Eigen and Zundel cations,

$H_9O_4^+$ and $H_5O_2^+$, respectively, or by wires of protonated water molecules linked by interconversions in a manner that is consistent with the behavior of salts and water observed between electrodes in the early 1800s. According to the Grotthuss mechanism, due to interconversions, a proton that enters a chain or matrix of water molecules is not the same proton that exits elsewhere [24,28-34]. The conformational changes for proton transfer in water can occur as a rapid falling domino effect. Thus, a wide-reaching, flexible delivery of cytoplasmic protons to membrane extruders may result. Putative K^+/H^+ exchange that frees bound H^+ from cell membranes would generate water cations because free H^+ becomes H_3O^+ almost immediately which then potentially interacts with cytosolic chains of $H_9O_4^+$ and $H_5O_2^+$ or protonated water wires for distribution. Extended hydrogen bonded chains that undergo rapid conformational changes potentially mediate proton release distal from the point of proton entry much faster than by simple diffusion. H^+ can be transferred in this manner to cell exit sites, such as exchangers swapping out H^+, monocarboxylate transporters venting lactate that requires accompanying protons, one for one, exiting through gap junctions, etc. This type of rapid transfer of H^+ in water has also been referred to as a "proton jump" [35]. Although in a previous study, the Grotthuss mechanism was not thought to mediate extracellular tumor acidity [36], it was not ruled out as occurring intracellularly. The Grotthuss mechanism describes a potential almost "everywhere, all at once" strategy for delivery of free protons to cell exit sites as needed. Therefore, putative inner membrane proton replacement by K^+ to initiate formation of H_3O^+ is probably a highly regulated process in normal cells, consistent with the large, complex KCN family controlling K^+ flux. Loss of regulation with differential expressions of KCN genes in malignant cells offers one approach to begin investigating the potential ionic dynamics of tumor cells related to pH reversal. Genetic damage of the KCN family members or altered regulation by activated oncogenes and/or modified histones/DNA putatively plays a role in pH reversal for tumor cell survival in glycolytic cells producing lactate if it cannot be removed in another way (such as by forming intracellular glycogen).

Also, potassium has a relationship with water that is important. A lack of water due to poor circulation, cell crowding, pressure from fibrotic, stiff surroundings, etc., especially during invasion, produces generalized microaqueous conditions within cancer cells. Regional hydration may be possible by redistribution of water molecules loosely associated with solvated ions, such as potassium, K^+-$7H_2O$. Redistribution of water via its association with potassium may enhance Grotthuss type protonated water structures close to the inner surface of cell membranes but this is unknown.

Volume changes related to ions are known to occur in malignant cells during division and migration. Protrusion of pseudopodia or invadopodia (increased volume in cell projections) and shrinkage of their retracted rear cell bodies that are accomplished with oscillations of cell membrane potential and osmotic changes via KCl uptake and release per potassium and chloride channels, along with aquaporin participation, and possibly with K^+ refilling/recycling [37-42]. The spontaneous dissociation of acids generated in a microaqueous environment undergoing changes in the number of water molecules available for solvation of acids into ion pairs [27], along with rapid proton transfers via the Grotthuss mechanism, putatively enhance proton delivery to the leading edge of migrating cells for efflux to preserve glycolysis from lactate inhibition. Pseudopodia are glycolytic as indicated by proteomic analysis [43]. Also, enhanced proton release from cancer cells

leads to extracellular acidosis that aids tumor invasion via activation and induced expression of metalloproteases for matrix degradation [44-50]. Thus, tumor cells can escape poorly perfused or crowded, microaqueous tissue regions via pH reversal relying on proton release putatively following K^+/H^+ exchange as the initiating step.

1.3. Need for Proton Extrusion in Cancer

The metabolism of cancer cells produces excess protons [51]. In addition to acids produced by metabolic pathways, free radicals generated are also acidic [52-54]. Extrusion of protons avoids cytoplasmic acidosis within tumor cells, so this not only protects glycolysis via lactate release but also prevents cytochrome c-mediated activation of caspase-3 to stop apoptosis [55], protects gap junctions to maintain cell to cell exchange of ions and metabolites [56-59], and increases the activity of ATP citrate lyase (ACLY) that connects lipid and carbohydrate metabolism. The optimal pH of ACLY is in the 8.5 - 8.7 range [60,61]. ACLY's removal of citrate (inhibitor of glycolysis) is protective in glioblastomas [62]. ACLY also regulates histone acetylation in response to growth factor stimulation [63,64]. Thus, proton removal from the cytoplasm favors cell fitness in tumor cells [65] as well as enabling migration for their escape from adverse conditions.

1.4. Complexity of K^+ Flux

As mentioned earlier, direction (inward or outward) and strength of K^+ channel flow is complex. The KCN family has more than 90 members [66,67]. Complexity is also due to numerous regulators (in addition to those encoded by KCN genes) present in biological milieus. Regulators, gating agents, and cofactors, include polyamines, voltage, H^+, Ca^{2+}, Mg^{2+}, Zn^{2+}, Na^+, ATP, miR-133b, reactive oxygen species (ROS), reactive nitrogen species, reactive sulfur species, nitric oxide, hydrogen sulfide, hypoxia, hyperglycemic levels of glucose, nucleotides, protein kinase A, protein kinase C, protein kinase G, guanosine-triphosphate-binding proteins (G-proteins), regulator of G protein signaling (RGS) proteins, phosphatidyl inositol 4,5 bisphosphate (PIP2), steroids (estrogen, testosterone, etc.), cholesterol, sulfonylurea, β-hydroxybutyrate, hypoxia inducible factor 1α, the 14-3-3 protein, β-coat protein, dipeptidyl aminopeptidase-like proteins, the neurotransmitter GABA, NAD(+), NADP(+), NADH, NADPH, glutathione, glutathione disulfide, mechanical stimulation, cell cycle progression, products of *LINGO1, 2*, and BKγ1-4 encoded by *LRRC26*, *52*, *55*, and *38* [68-90]. Also, 19% (or more) of proteins targeted by small-molecule drugs used to treat numerous diseases include ion channels [91-93]. Thus, the complexity of K^+ channel flux hinders planning studies to identify specific regulatory mechanisms lost in cancer.

Complexity is further enhanced because the ROS affecting potassium channels are generated via multiple sources such as (*i*) mitochondrial respiratory chain electron transport redox reactions [84,94-97], as well as (*ii*) the NOX family (6 members) of NADPH oxidases [71,94,95,98]. ROS from these sources can reach the cytoplasm [95]. Colon carcinoma cell lines with acid-resistant growth showed significantly upregulated mRNA levels of *NOX1* encoding NADPH oxidase 1 [99] that produces ROS. Interestingly, isolated intact respiring rat brain mitochondria increased ROS production when their

medium was alkalinized which raises the possibility that this could also happen in alkaline cytosol of cancer cells as pH reversal develops [100].

The widespread chromosomal distribution of the 90 (or more) KCN genes plus those of the numerous non-family regulators suggests that failsafe redundancies for genomic damage may exist that increase the chances of selecting cells that can maintain levels of K^+ for survival but not in a manner that is optimal for differentiation and normal activity. Numerous genomic/expression scenarios selected in rapidly dividing tumor cells may work around mutational losses or gains with adaptations so that cells maintain their K^+ levels for supporting membrane integrity and are putatively also able to exchange with fixed H^+ on inner membranes in invasive cells to incite pH reversal. Not only do the monocarboxylate transporters, MCT1 and MCT4, transport negatively charged lactate molecules coupled one-for-one with protons across the cell membrane [101], protons can also be extruded from cancer cells via Na^+/H^+ exchanger family members, ATP driven pumps, etc. as detected in numerous studies [102] and in earlier cited studies. Therefore, pertinent genes among the non-KCN DEG are also of stochastic interest in this study.

Mediators of potassium flux, despite their complexity, and the relationship of K^+ and H^+ at cell membranes should be clarified. K^+ accumulation due to a lack of normal diffuse K^+ efflux or buildup of K^+ around large outwardly conducting potassium channels, could putatively exchange with bound protons on inner membranes or it could happen with deregulated inwardly channeled K^+ flux (possibly with K^+ being recycled for refilling as needed if efflux becomes excessive). These events with K^+ could occur without affecting the functions of key structural proteins that would be seen if Na^+ was used [103]. Although both potassium and sodium are the available monovalent cytoplasmic cations to potentially replace membrane bound H^+, there should be a preference for potassium due to its weaker binding of water compared to sodium ions. Less energy is required to displace water from potassium than sodium [104,105]. K^+ ions permeate their membrane channels in a desolvated ('naked') state rapidly so at this point they release their associated water molecules. Also, there is exclusion of smaller Na^+ ions that have stronger water binding from the channels selective for potassium [106-108]. Also, compared to Na^+, K^+ is better at maintaining solubility of cell components containing carboxylates and phosphates to help explain its higher concentration in the cytoplasm [105,109]. Numerous KCN family scenarios may be involved with anomalous potassium flux in cancer. Deregulated diffuse, passive K^+ entry, such as the *KCNJ*/Kir (inwardly rectifying, also bidirectional, flux), or disrupted K^+ outflow via KCN family members, such as the numerous members of the Kv (voltage dependent) KCN subfamily and the *KCNK*/K2P (tandem two pore "leak") subfamily members, may be important. Also, Ca^{2+} activated potassium channel families, *KCNM*/BK for *MA1* plus other members that regulate it, and the *KCNN*/SKs and *KCNN4*/IK family members that mediate outward flow, with BK and IK providing large and medium flux, respectively, likely play important roles due to their relatively high flow rates. High flow rates may indicate localized versus diffuse K^+ release and in addition these channels can be affected by the release of calcium from cancer cells. However, all types of K^+ transits may be involved and a role for Na^+ in releasing H^+ cannot be ruled out given the abnormally high levels of Na^+ found in tumor cells [110-112]. Additionally, some K^+ channels are influenced by Na^+.

Loss of normal cellular responses to pH via loss of KCN channels that function with H^+-sensitivity may alter cells in cancer. Malignant cell behavior suggests that tumor cells

respond opportunistically to sources of K^+, thus achieving levels of K^+ ions at inner membrane surfaces or flow rates that force K^+/H^+ exchanges that initiate pH reversal to improve tumor cell survival and invasion. Deregulated potassium uptake by glioblastoma cells may occur from the available sources *in vivo* as briefly mentioned earlier. These (with additional information) include (*i*) neurons and axons firing action potentials where K^+ is released to maintain electroneutrality, (*ii*) dying cells, including red cells (K^+, 80 - 120 mmol/L) and necrotic tissue releasing cytoplasmic K^+ [113-116], and (*iii*) damaged blood vessels leaking plasma (potassium, 3.8 - 5.0 mmol/L [117]). Importantly, deregulation via loss of a K^+ channel is illustrated by showing in an experimental mode that the loss of H^+-sensitive *KCNK1* (among a small group of genes identified) was advantageous for breast cancer cell survival of induced necrosis I [118].

1.5. Biological Milieu Constituents to Consider in Studying K^+ Flux

Biological milieus contain many factors regulating potassium channels as described earlier. More details to consider in studying these channels in cancer are listed here. Serum includes calcium (2.30 - 2.74 mmol/L), magnesium (0.74 - 1.23 mmol/L), phospholipids (1.50 - 3.80 g/L), sodium (136 - 142 mmol/L, adult plasma value) [117], and polyamines (0.1 - 1.0 μM, fetal bovine serum [3]). Magnesium and polyamines (positively charged) are important gating molecules of inwardly-rectifying *KCNJ*/Kir family channel members [119]. Removing fetal bovine serum from the medium of cultured fibroblasts resulted in decreased potassium intracellularly [120]. Also, fetal bovine serum lost the ability to depolarize the resting membrane potential of airway smooth muscle cells after dialysis against distilled water but its freeze-dried dialysate retained this ability after reconstitution [121], consistent with potassium as the responsible constituent. Elevations of polyamines have been reported in cerebrospinal fluid in instances of brain tumors [122] and are in the tumor-associated myeloid cells that infiltrate glioblastomas [123]. Also, polyamines are formed when L-arginine, released from apoptotic bodies, is metabolized by Arg1 [124]. Other agonists and modifiers in biological milieus within regions of necrosis include heme and other hemoglobin break-down products [125,126]. Tumor associated macrophages are influenced to promote malignancy (increased expression of *ARG1, VEGF*, *TGFB*, etc.) by lactate, presumably shuttled from cancer cells, such as seen in transitional cell carcinoma of the bladder, gastric cancer, and others [127-129]. As mentioned earlier, many types of tumors outside of the CNS exhibit perineural invasion [130-133].

There may be reciprocal gain of potassium by tumor cells from nerves and axons as the tumor cells provide lactic acid back to neurons and axons as energy substrate for a mutually beneficial metabolic interchange. If constituents of biological milieus modulate K^+ transits indirectly via their effects on downstream potassium channel activity, then sources of extracellular potassium may attract tumor cells to fulfill their needs. Although specific sources of K^+ *in vivo* have not been generally appreciated for influencing the behavior of cancer cells, they may be important as loss of regulation required for complex normal cell functions occurs in dedifferentiation.

1.6. Highlighted Findings in This Study

Fetal bovine serum (with and without hepatocyte growth factor (HGF)) had been seen previously to promote glioblastoma cell migratory behavior, including protrusion of pseudopodia through 3 μm filter pores, migration of whole cells through 8 μm filter pores, and invasion through a Matrigel matrix and rat brain tissue slices, often under glycolytic conditions [43,62,134-136]. Glioblastoma cell clustering around dying cells and their migration to serum, with compelling background information on astrocytes, suggested that anomalous potassium flux could play a role in tumor cell behavior. Cell migration of multiple glioblastoma cell lines to serum among eight tested in this study and the response in a separate assay to a positive gradient of potassium supported abnormal membrane flux or lack of it via some of the potassium channels as a putative aid for tumor cells.

The large scope of K^+ channel candidates for loss or gains in expression and the potential influence of numerous known modulators were daunting. However, stochastic analysis of numerous published studies to gather unbiased data was reasonable to survey as many contributing factors as possible at this point. Incidentally detected KCN DEG and related non-KCN DEG in genomic landscapes of experimental cancer scenarios and databases permitted a search for pertinent functional similarities among the DEG of the large KCN family. Meta-analysis of 70 malignant (or models related to cancer) expression studies found that the studies fell into 8 categories of 7 oncogenes and histone/DNA modifiers. These categories were determined by the authors of the expression (E), E1-E70, studies if related DEGs were also detected in any of the 70 studies. The studies included 29 types of malignancy (breast, lung, brain, etc.) that incidentally detected one or more KCN DEG. *KCNMA1* and *KCNN4* were the most frequently detected KCN DEG. The encoded products of the 53 detected KCN DEG are predominantly H^+-sensitive (62.26%) and 52 (74.3%) of the 70 studies identified at least one H^+-sensitive KCN DEG. There was a significant propensity for KCN DEG to encode H^+-sensitive family members in the studies among the 8 categories of 7 oncogene and histone/DNA modifier related scenarios compared to the 20 studies in “no category”. A concurrent search of the National Institutes of Health REpository of Molecular BRAin Neoplasia Data (REMBRANDT) database for expression levels of KCN genes in invasive glial brain tumors (glioblastomas versus oligodendrogliomas that are less invasive) of patients on anti-seizure medications showed a significant decrease in *KCNJ16* and trends in three other KCNs also encoding H^+-sensitive proteins in glioblastomas. Correlation with a genomic study of 6 glioblastoma cell lines [22] confirmed relatively decreased RNA expression of *KCNJ16* among KCN genes and provided additional relevant genomic data. Altered expression of KCN family members, possibly with compensatory activities of other KCNs and non-KCN factors, may provide quantities of K^+ sufficient for preservation of cell membrane integrity and putative K^+/H^+ exchange on inner membranes to release bound H^+. As an initial step K^+/H^+ exchange may incite pH reversal and invasive behavior.

2. Materials and Methods

2.1. Materials and Cell Culture

All chemicals and reagents were from Sigma-Aldrich (RRID:SCR_008988), St. Louis, MO, USA, unless otherwise stated. Anti-Met was from Cell Signaling Technology, Beverly, MA, USA, Cat# 4560, RRID:AB_2143887), 1:1000 dilution, for the beta Met

subunit (145 kDa). Diff Quik (Allegiance, McGaw Park, IL, originally developed by Harleco, now a product line of Sigma-Aldrich (RRID:see above) is sold as Hemacolor Solutions I, II, and III. It is also sold by many medical suppliers with reference to Harleco and/or the cytology literature [137]. A172 (RRID:CVCL_0131), C6 (TKG Cat# TKG 0242, RRID:CVCL_0194), F98 (ATCC Cat# CRL-2397, RRID:CVCL_3510), LN18 (RRID:CVCL_0392), LN229 (RRID:CVCL_0393), T98G (RRID:CVCL_0556), U87 (RRID:CVCL_0022), and U373 (RRID:CVCL_2219) glioblastoma/astrocytoma cell lines (human (A172, LN18, LN229, U87, U373) and rat (F98 and C6)) were obtained from the American Type Culture Collection, Manassas, VA, USA RRID:SCR_021346. No cell lines were generated from live animals for this study by the author. The cells were maintained in Minimal Essential Media (MEM) Eagle(138) or alpha-MEM (Cellgro, Mediatech, Herndon, VA, USA) with 10% fetal bovine serum, FBS, (Invitrogen, Carlsbad, CA, USA).

2.2. Statistics Section

Pearson product-moment correlation, R, also termed cor (with *p* values for a true correlation being greater than 0), the Student's t-Test, paired and unpaired, and Fisher's Exact Test for Count Data, in either Excel Statistics (RRID:SCR_017294) or the R Project for Statistical Computing (RRID:SCR_001905) were used.

2.3. Databases

For general gene information, the National Institutes of Health database, https://www.ncbi.nlm.nih.gov , the Online Mendelian Inheritance in Man (OMIM) database, OMIM (RRID:SCR_006437), https://omim.gov , and GeneCards (RRID:SCR_002773) https://www.genecards.org/ were used. GeneCards was also used to obtain protein-protein interaction data. The Ensembl https://www.ensembl.org/ database (RRID:SCR_002344) was used to obtain information on the structure of genes, including features of exons and introns. The National Library of Medicine's PubMed database, https://pubmed.ncbi.nlm.nih.gov/ , was searched for the numbers of publications available using 2 and 3 word searches for subjects of interest. The Online Mendelian Inheritance in Man (OMIM) database was searched for KCN family member genes expressed in the nervous system with exclusion of genes uniquely expressed in heart, kidney, and other non-neural sites, and to identify their chromosomal loci (March 2019). The REpository for Molecular BRain Neoplasia DaTa (REMBRANDT) (RRID:SCR_004704), originally at the NIH, became part of the Georgetown Database of Cancer (G-DOC), https://sites.google.com/georgetown .edu/g-doc/home or via the G-DOC Hub platform at https://gdochub.georgetown.edu/ as a project of the Georgetown Lombardi Comprehensive Cancer Center, Washington, D.C., designed to provide translational research tools to the scientific community [20,21]. It was queried for gene expression on microarrays of KCN family members, selected genes important in cancer and brain tumors, and housekeeping genes. Medians of reporter probes for each gene were available in Adobe Flash (RRID:SCR_017258) readouts through 12/31/2020 (date of last service). Genomic sequence and expression results of 6 glioblastoma cell lines were obtained from the Supplemental Materials of Patil et al. [22].

2.4. Ethics Statement

No human subjects or animal experiments were used by the author in this study. Only commercially available human and rat cell lines were used i*n vitro* for laboratory studies. Published medical science manuscript information, mostly open access, with the authors of the studies following the guidelines of each their institutions, was also used for data.

2.5. Cell Settling with Fluid Removal Assays

Human glioblastoma cells (U87, LN229, A172, T98G) were maintained in routine culture conditions. On the day of each assay, cells were detached with trypsin and allowed to recover for 4 hours in MEM with 10% FBS at 37° C in a CO_2 tissue culture incubator. For each assay, a Cell Settling Chamber Kit (Neuro Probe, formerly Gaithersburg, MD, USA, Ph: (301) 417-0014, email info@neuroprobe.com), with 8 wells, each 7 mm in diameter, was assembled. A provided glass slide, 1 mm thick, 25 x 75 mm, was placed in the recessed bottom plate. A provided pre-punched piece of blotting paper, pre-moistened with PBS, a gasket, and the upper plate were stacked on top of it. Thumbnuts fitted on the top plate were securely hand tightened. Cells were centrifuged (500 rpm, 5 min) and resuspended with gentle pipetting, 500,000 cells per ml in culture media with 10% FBS. Cell suspensions were added, 50 microliters per well. After 30 minutes with media visibly absorbed out of the wells by the blotting paper, the chamber was disassembled, the slide was removed and stained with Diff Quik solutions, I, II, and III followed by 3 quick rinses in tap water in beakers. At least two replicate wells per cell line were prepared. Stained cells were examined microscopically. Cell vacuoles in U87 cells (single and clustered) were counted in the settled cellular monolayers. When vacuoles collectively had a diameter of at least one third of an average nuclear diameter in the same 100X microscopic field, the cell was counted as positive for vacuolization (surrogate indicator of degeneration). Cells were analyzed in a midline sweep of the 100X microscopic fields across the 7 mm width of each well. Pearson product moment correlation coefficient, R, determinations, were performed for the percentage of cells vacuolated versus the number of cells in each cluster. Morphological features, such as cell clustering, were noted. An Olympus BH2 microscope (Olympus Corp., Lake Success, NY, USA) with an Olympus FV II digital camera using Olympus Microsuite Five Software for Imaging Applications (Soft Imaging System, Lakewood, CO, USA) was used to capture the black and white images. An American Optical Spencer Microscope (Buffalo, NY, USA, sold to Reichert Technology, then Leica Microsystems, Inc. (Deerfield, IL (RRID:SCR_008960)) with an OptikamB9 Digital Camera 10 MegaPixels (Optika, www.optikamicroscopes.com, Via Rigla 32, 24010 Ponteranica (BG), Italy) with Adobe Photoshop v5.1 and Adobe Photoshop Elements 2024 for Windows (Adobe Systems Incorporated, San Jose, CA, USA (RRID:SCR_014199) was used to generate the color microscopic images.

2.6. Cell Migration Assays

Cells of A172, C6, F98, LN18, LN229, T98G, U87, and U373 glioblastoma cell lines were maintained in normal tissue culture conditions with half volumes of culture media

changed one day prior to each assay. Confluent cells were detached with trypsin on the day of assay and allowed to recover in media with 10% FBS for 2 hours at 37°C in a CO_2 tissue culture incubator. Cells were centrifuged (<500 rpm, 5 min) and resuspended at 2 million/ml with gentle pipetting in media for migration, MEM (includes 5.4 mM KCl [138] but it is 5.3 mM according to Thermo Fisher among its inorganic salts), with 0.1% bovine serum albumin (BSA). Chemoattractant/chemokinetic stimulants, recombinant hepatocyte growth factor (HGF) and/or FBS were added to the bottom wells (29-30 μl total volume) as indicated in Figure 2. The 48-well modified Boyden Chambers (Neuro Probe) were assembled with porous (8 μm diameter pores, 1,000 pores/mm^2, laser generated), air-dried polycarbonate filters, 8 μm thick (Neuro Probe), coated with 0.01% porcine gelatin (solution of 1 ml 10% acetic acid, 1 ml 1% gelatin (fully dissolved, no floating globules) from refrigerated stock (10%, gently warmed to liquify), and 98 ml H_2O). One corner of each filter was diagonally cut off sufficient for orientation before each assay. Cell suspensions were added to the upper wells, 60 μl each well. The chambers were incubated at 37°C for 5 hours in a CO_2 (5%) tissue culture incubator. Upon completion of the assay, each filter (easily disturbed by air flow) was removed by lifting one end with a pair of fine, curved tip tweezers, and then clamped into a large square plastic clip at the other end of the filter and then releasing the tweezers without disturbing any cell pellets. The filter attached to the large clip was stained with Diff Quik solutions (I-III) by hanging the filter by its attached clip on a metal weighing spatula placed over tops of beakers with Diff Quik solutions, followed by rinses in 3 different beakers of water using quick dips, and then carefully placed on a large glass slide (2" x 3") using tweezers and the clip with migrated cells on the downside of filters. Unmigrated cells were gently removed from the upper side of a filter with cotton swabs or Kimwipes so that only the stained migrated cells remained, located between the filter and glass slide. There were 4 replicates per data point unless pre-assay cell harvests only allowed fewer replicates. Slides with migrated cells were digitized using a regular scanner (HP OfficeJet Plus 8715 printer/scanner (Hewlett Packard (formerly RRID:SCR_011873), Spring, TX, USA). Densitometry (UN-SCAN-IT Gel Analysis Software, 7.1 (RRID:SCR_017291) Silk Scientific, Inc., Provo, UT, USA) with correction for background filter staining density to quantify cell migration results. An Epson Perfection 2450 PHOTO (Epson America, Long Beach, CA, USA) was also used for obtaining some of the images of migration assays. The first two rows of migrated cell pellets, digitized for densitometry, were the results used to calculate cell migration specifically to HGF, i.e. HGF cell migration, defined as the 2nd rows of cells which had migrated to HGF divided by the 1st rows of cells representing background (unstimulated) migration because they migrated to media without the added chemoattractants, HGF and/or FBS. HGF cell migration results are stated as times(X) the corresponding unstimulated, background cell migration for each cell line. Additional migration assays of U87 cells evaluated the motogenic/chemokinetic properties of FBS and HGF by placing them in either the bottom or both top and bottom wells and also separately, MEM versus Dulbecco's PBS was evaluated in the bottom wells in a small dose curve of FBS with Migration media (Dulbecco's PBS (contains 2.7 mM KCl, 1.8 mM KH_2PO_4, 137.9 mM NaCl, 10 mM Na_2HPO_4) with added 0.210 mM $MgCl_2$, 0.243 mM $CaCl_2$, 5 mM pyruvate, 5.551 M glucose, and 0.1% bovine serum albumin) in all of the top wells.

2.7. Immunoblot of Met, Receptor for HGF

One dimensional gel electrophoresis was performed for immunoblotting. Lysates of unmigrated cells from 8 cell lines, equalized for total protein content (10 µg per lane), were electrophoresed in separate lanes of 10% polyacrylamide gels under reducing conditions. Protein standards (MagicMark, MultiMark, Invitrogen (now merged with Thermo Fisher Scientific (RRID:SCR_008452)) were loaded 8 µg per lane. The gel was stained with Coomassie blue (Novex Colloidal Blue Stain Kit, Invitrogen, now merged with Thermo Fisher Scientific (RRID:SCR_008452)), as shown, and destained with tap water. Gel contents were transferred onto polyvinylidene difluoride membranes (Invitrogen, now merged with Thermo Fisher Scientific (RRID:SCR_008452)), blocked (Detector Block, Protein Detector Western Blot Kit Lumi-GLO System, Kirkegaard & Perry Laboratories, Gaithersburg, MD, USA, now merged with SeraCare Lifesciences:(RRID:SCR_004535)) and reacted with anti-Met (1:1000), reactive with a 145 kDa band. The secondary antibody 1:1000 (Kirkegaard & Perry Laboratories, now merged with SeraCare Lifesciences:(RRID:SCR_004535)) was horseradish peroxidase-labeled anti-mouse. Immunoreactive bands were visualized via horseradish peroxidase's conversion of a luminol-based solution to produce chemiluminescence, and the reactive blot was scanned to generate a digital image. An Epson Perfection 2450 PHOTO was used for obtaining digital images with densitometry obtained using UN-SCAN-*It* gel, early version 5.1.

2.8. Differentially Expressed Genes of Potassium Channels

Potassium channel (KCN) family members were found as differentially expressed genes (DEG) in cancer genomic landscapes described in 70 studies (1301 authors) recently published (2007-24) in 15 journals through subscriptions and open access. The KCN DEG were detected with non-KCN DEG in at least one published figure (heatmap, Venn diagram, volcano plot, etc.) or table (none from Supplemental Materials of the manuscripts) in each publication. Detection of one or more KCN genes in a group of genes designated as DEG by the authors (with no initial focus on KCN genes) was used for selecting these studies. Types of studies included mostly common malignancies, such as breast, lung, gastrointestinal, brain, bone marrow, liver, soft tissue sarcomas, etc. Categories (determined after all E1-E70 studies were completed) were according to descriptions by the authors of each paper with the caveat that there had to also be a relevant DEG reported in at least one of the E1-E70 studies.

2.9. Expression of Potassium Related Genes in Glial Tumors

REMBRANDT (G-DOC) contained tumor expression data on 67 oligodendrogliomas (Oligo) and 220 glioblastoma (GBM) patients, including subgroups treated with anti-seizure (AS) medications, i.e. 24 Oligo-AS and 75 GBM-AS. Gene expressions were determined by reporter probes on microarrays with their median values provided. Differences in median values for multiple probes (when available) were found with t-tests, paired via reporter probes for the two comparison groups when possible, and otherwise, unpaired t-tests were performed. Housekeeping genes (HKG) that lacked relevance for glial tumors via literature searches were also analyzed for comparisons. Additionally,

Oligo-minus-GBM (OMG) differences were calculated for each probe. OMG differences for each gene of interest were compared to the OMG differences for HKG (*B2M*, *PPIA*, *RRLP0*, and *YWHAZ*). The *t*-tests were performed for unpaired samples with unequal variance in OMG comparisons. Published studies [22,139,140] were used for confirmation of REMBRANDT results.

3. Results

3.1. Settled Glioblastoma Cells with Fluid Removed

At the end of each cell settling assay, the extracellular fluid had been wicked away. Cell groups could be seen macroscopically in some as viewed in Appendix A (Figure. A1). For each cell line (A172, LN229, T98G, and U87) a striking feature was the clustering of robustly viable tumor cells around single degenerating cells of the same lineage on slide surfaces in low numbers. Cell surfaces were exposed to ambient air, glass, or surfaces of other cells by the end of the assays. The tight clustering of viable cells suggested an opportunistic attraction to the dying single cells by possibly taking up released contents from moribund cells to enhance fitness. Although the tint of staining varied, some viable cells clustered around single dying cells displayed basophilic cytoplasmic staining (Figure 1A-B). Although some faint, thin connecting strands between cells may have been present, mostly there was a narrow linear open space between the apposed cells, best seen in black and white photographs. Cells, single and in groups without visible degenerating central cells, and scattered debris were also seen. Cytoplasmic vacuolization was most prominent in the U87 cells (Figure 1A-C). The number of vacuoles was highest in single cells and decreased as the size of cell clusters increased. Representative U87 cells, single and in groups, were layered together into one image with a broad white stroke added around each layer for delineation and contrast with the added pink background (Figure 1C). In counts of vacuolated settled cells performed on the cell monolayers from two separate wells, 15% and 72% of single cells were vacuolated whereas vacuolated cells were only 11% and 18% in cell groups comprised of greater than twenty cells in the 1st and 2nd wells, respectively. Pearson regressions of the cells in clusters with vacuoles for the two wells had significant R^2 values of 0.266 (p = 0.0410) and 0.544 (p = 0.0062), 1st and 2nd wells, respectively, as seen in scatterplots (Figure 1D). The cells in clusters exhibited less vacuolization as a sign of less degeneration possibly due to sharing their cytoplasmic contents as needed and also

possibly due to the contributions of contents from dying cells of the same lineage.

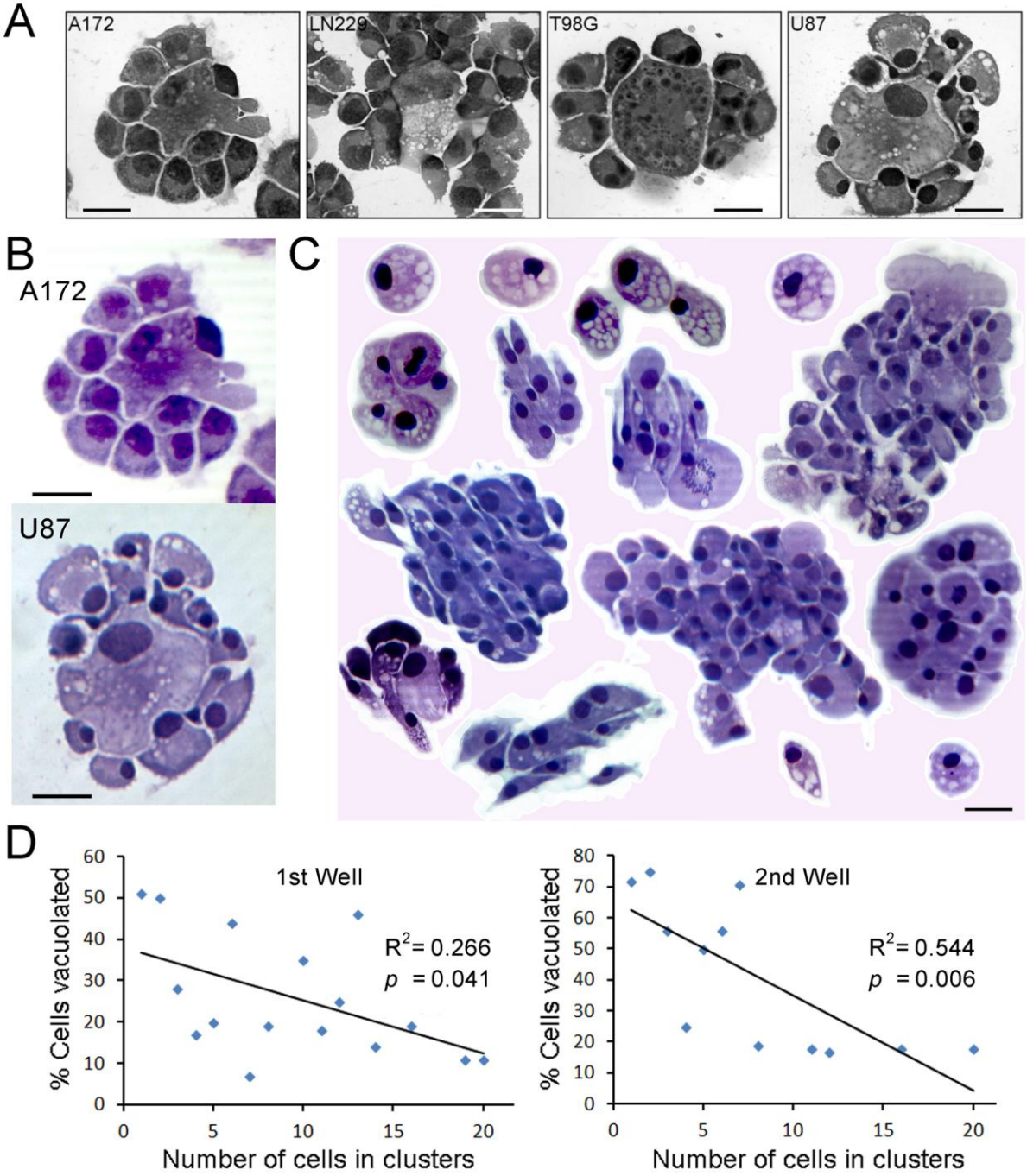

Figure 1. Settled glioblastoma cells deprived of extracellular fluid. (A and B) The morphology of each cell line (A172, LN229, T98G, and U87) after cell settling with fluid wicked away, included a few clumps of robust appearing, viable tumor cells clustered around single degenerating cells of the same lineage. Cell surfaces, after settling and withdrawal of suspension media, were exposed to ambient air, glass, or surfaces of other cells. Although the tint of Diff Quik staining varied, some viable clustered cells' cytoplasm stained relatively basophilic. The black and white photographs suggest some thin connections between cells

crossing the narrow linear open spaces separating them. Single and grouped cells without a visible degenerating central cells and scattered cell debris were also seen in wider views. (C) Cytoplasmic vacuolization, most prominently seen in U87 cells, is shown in the representative single and grouped cells that were outlined with digital white strokes around each merged layer for delineation and contrast with the added pink background. More basophilic cytoplasmic staining with Diff Quik seen in some cell groups would be consistent with an alkaline pH but no pH measurements were made. The numbers of vacuoles were highest in single cells and decreased as the numbers of cells in the cellular groups increased. (D) In counts performed on the cell monolayers from two separate wells, 51% of 75 and 72% of 25 single cells were vacuolated, 1st and 2nd wells, respectively. However, vacuolated cells in groups were only 11% of 122 and 18% of 39 cell groups comprised of greater than twenty cells, 1st and 2nd wells, respectively. As shown in the 2 scatterplots, Pearson regressions of the numbers of cells contiguous in groups or clusters that had vacuoles had R^2 values of 0.266 (p = 0.0410) and 0.544 (p = 0.0062), 1st and 2nd wells, respectively. Scale bars, 25 μm.

3.2. Cell Migration with HGF and Serum Chemoattraction

Earlier studies of U87 and LN229 glioblastoma cell lines and fresh glioblastoma cells from a clinical specimen reported chemoattraction to HGF and serum [43,62,134-136]. Testing additional glioblastoma cell lines for migration to HGF and FBS, their chemokinetic effects (more extensively than previously), comparing cellular levels of HGF's receptor, Met, and including a comparison of MEM versus Dulbecco's PBS as the media in bottom wells for chemoattraction in a FBS dose curve with U87 cells are reported here. Boyden chamber assays (48 well chambers), 3 per cell line, for 2 rat astrocytoma cell lines (C6 and F98) and 5 human glioblastoma cell lines (T98G, LN18, U87, LN229, and U373) showed cell migration to HGF alone as a chemoattractant (row 2), HGF and FBS together as chemoattractants (rows 3-9), and to FBS alone as a chemoattractant in a dose curve (rows 10-12) compared to background (unstimulated) cell migration in the top rows. Concentrations of chemoattractants are indicated in the left columns. Notably, with the same amount of HGF present, adding increased amounts of FBS increased cell migration in 7 of the 8 cell lines (Figure 2A).

Portions of scanned assay images of FBS alone as the chemoattractant in a dose curve are shown as migrated cell pellets with densitometry results in bar charts below their images. All cell lines, except A172, showed significant migration to FBS alone. U87 and U373 results showed the most impressive stepwise increase in chemotactic migration at all 3 concentrations of FBS versus background migration with all p values < 0.0005 and 0.000005, respectively. U373 chemotaxis to 0.5% FBS, 3.8 times the background (unstimulated) migration, was the highest level for all cell lines. A172 cells showed a trend for increased migration to 0.5% FBS, p = 0.0638. Some of the cell lines showed flattening of their responses as levels of FBS increased (Figure 2B). All assays (3 per cell line) are shown in Appendix A for C6, F98, T98G, and LN18 (Figure A2) and U87, LN229, A172, and U373 (Figure A3). Cell migration specifically for HGF in each cell line is stated as a multiple (X) of the background cell migration, obtained by dividing the 2nd row of assays' cell pellets densitometry results by the corresponding 1st row of

background cell migration, bottom row (Figure 2C). The immunoblot shows reactivity for HGF's receptor, Met (β subunit, 145 kDa). The Met reactivity with U87 and LN229 has been published previously [134] but here the relative amounts of Met in 8 cell lines are reported, including rat (C6 and F98) and human glioblastomas (T98G, LN18, U87, LN229, A172, and U373). As shown in the bar chart there was a lack of correlation with the cell motility results shown below it (Figure 2C). In Appendix A, the gel image showing equalized protein loading for all 8 cell lines in the immunoblot is available (Figure A4A). The order for HGF cell migration from highest to lowest results for all 3 assays of each cell line was T98G (2.11X), U373 (1.93X), LN229 (1.52X), U87 (1.49X), C6 (1.33X), A172 (1.30X), LN18 (1.15X), and F98 (1.13X). Twelve of the 92 data points of visibly migrated HGF cell pellets had densitometry results showing slightly less than 1X background cell migration and were rounded up to 1X for these results. A few replicates did not show visible unstimulated or stimulated cell pellets.

Earlier studies had noted chemokinesis with HGF and 0.1% FBS in U87 cell migration assays [136] and also chemokinesis with 5% FBS alone in LN229 cell invasion assays [135]. The dose curve for FBS includes additional data points as shown in Figure 2D. A dose curve was also published earlier with fewer data points for chemoattraction using HGF, FBS, and both for U87 and LN229 cells previously (134) but the assays here include additional data points and 6 more cell lines. The chemoattractant strength of HGF alone (row 2), and with 0.1% and 1% FBS (rows 5 and 8, respectively) was enhanced by both FBS concentrations in the U87 cells. Chemokinetic strength of HGF alone (row 3), with 0.1% and 1% FBS (rows 6 and 9, respectively) was also enhanced by FBS. Chemotaxis and chemokinesis at 0, 0.1, and 1% FBS demonstrated strong enhancement of FBS versus HGF alone for either type of U87 cell migration. The combination of HGF, 2.5 ng/ml, and 1% FBS for chemoattraction significantly, $p = 0.012$, outperformed their chemokinetic effects on cell migration (Figure 2D). A scanned image of the assay is also available in Appendix A (Figure A4B). A portion of the immunoblot for Met in U87 and LN229 cells with the gel was published previously (134) but without the entire immunoblot for U87 and LN229 cells plus 6 additional cell lines and all standards as included in this study

Another assay to evaluate MEM for migration studies included gradients of K^+ and Cl^- in migration assays of U87 cells. Both ions are redistributed with volume changes during cell migration. In the absence of FBS, Dulbecco's PBS in the bottom wells provided K^+ as 2.7 mM KCl + 1.8 mM KH_2PO_4 (**4.5 mM K^+**) and Cl^- as 2.7 KCl + 137.9 mM NaCl (**140.6 mM Cl^-**). MEM in the lower wells provided K^+ as 5.3 mM KCl (**5.3 mM K^+**) and Cl^- as 5.3 mM KCl + 1.8 mM $CaCl_2$-$2H_2O$ (**8.9 mM Cl^-**). See Methods for a minor issue with KCl molarity in MEM. For all upper wells without FBS, the Migration media provided K^+ as 2.7 mM KCl + 1.8 mM KH_2PO_4 (**4.5 mM K^+**) and Cl^- as 2.7 KCl + 137.9 mM NaCl + 0.21 mM $MgCl_2$ + 0.243 mM $CaCl_2$ (**141.5 mM Cl^-**). Potassium did not generate any gradient for cells migrating from upper to lower wells when Dulbecco's PBS was used in the bottom wells and there was almost no gradient for chloride either. However, when MEM was used in the lower wells a reverse gradient for Cl^- was generated with more Cl^- in the upper versus the lower wells. With MEM in the lower wells there was a positive gradient to potassium for migrating cells (5.3 mM in the lower

wells versus 4.5 mM in the upper wells). Chloride ions present in a negative gradient are probably not responsible for the 1.7X increase in cell migration when MEM was used in the bottom wells. However, the positive gradient for K^+ may have contributed to the significantly increased migration, $p = 0.0144$, without FBS present. MEM as the media in the lower wells was also associated with significantly increased cell migration when 0.1 and 1% FBS were present, $p = 0.0136$ and $p = 0.000442$, respectively, compared to using Dulbecco's PBS for the media in the lower wells having the same FBS concentrations (Figure 2E). MEM contains 5.6 mM dextrose, 1 mM pyruvate, and 2 mM l-glutamine, whereas Migration media contained 5.6 M glucose and 5 mM pyruvate. Therefore, MEM as a source of fuel in the bottom wells was probably not a significant differentiating factor in the results. MEM also contains 17.856 mM sodium bicarbonate, 0.8 mM magnesium sulfate (more Mg^{2+} than Migration media (0.21 mM $MgCl_2$), less sodium than Dulbecco's PBS and Migration media, amino acids, vitamins, etc. A scanned image of the assay is available in Appendix A (Figure A4C). These results support the role of K^+ in enhancing cancer cell migration. Variable background migration, as shown in the top rows of representative assays (Figures 2A-B) and assay-to-assay variation for each cell line as shown in Appendix A files (Figures A2 and A3) are routine for cell migration assays.

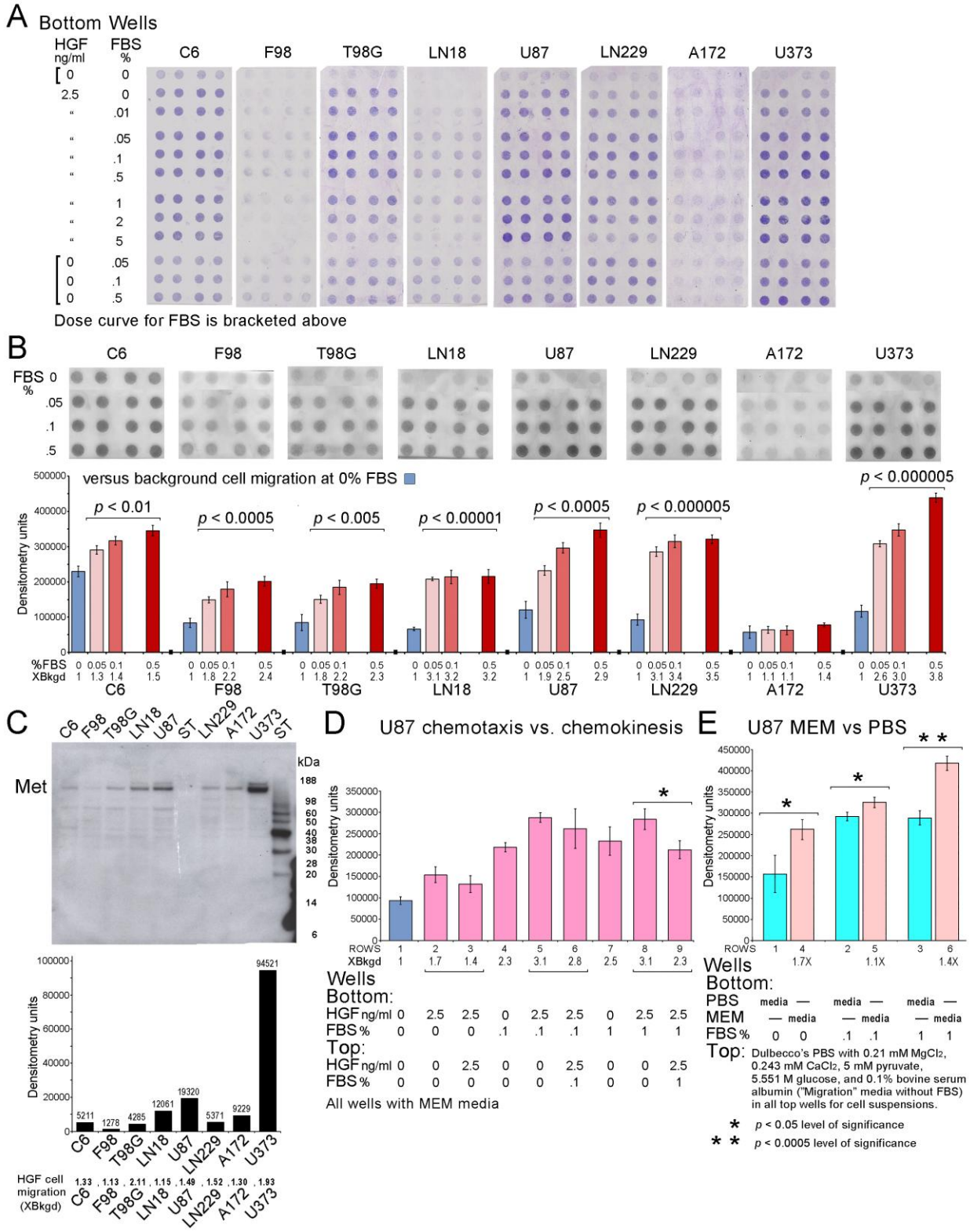

Figure 2. Migration of glioblastoma cell lines to hepatocyte growth factor (HGF) and fetal bovine serum (FBS). (A) Representative Boyden chamber assays of 2 rat astrocytoma (C6 and F90) and 6 glioblastoma

cell lines (T98G, LN18, U87, LN229, A172, and U373) showed unstimulated (background) cell migration (row 1, at the top), cell migration to HGF (row 2), HGF and FBS (rows 3-9), and to FBS alone (rows 10-12) using concentrations in the bottom wells as indicated in the left columns. All cell lines, except for A172, migrated to FBS alone. With the same amount of HGF present, adding increasing amounts of FBS increased chemotactic cell migration in the other 7 cell lines. These images were obtained by using a transparency scanner. (B) Portions of scanned (regular scanner) assay images using FBS alone as the chemoattractant were digitized for densitometry (total pixels for units) with results shown as bar charts. All cell lines showed significant migration to FBS except for A172 which only had a trend, $p = 0.0638$, for 0.5% FBS. The entire collection (3 assays per cell line) is available in Appendix A for C6, F98, T98G, and LN18 (Figure A2) and U87, LN229, A172, and U373 (Figure A3). The first assays for C6, F98, LN18, and LN229, the second assay for T98G, and the third assays for U87, A172, and U373, were digitized for densitometry. (C) An immunoblot with a bar graph of densitometry results underneath shows the relative amounts of HGF's receptor, Met (β subunit, 145 kDa) in each cell line. Also, HGF-stimulated cell migration is listed below the bar graph. HGF-stimulated cell migration (digitized densitometry of row 2 of the migration assays divided by background (no stimulation) migration for row 1 cell pellets in B) is stated in units of times(X) background cell migration. The HGF-stimulated cell migration compared with levels of Met lacks notable correlation. The gel for the immunoblot showing equalized protein loading is available in Appendix A (Figure A4A). (D) Unstimulated cell migration (blue bar representing the average of the assay replicates) in U87 cells is shown for contrast with the chemotactic and chemokinetic strength of HGF and FBS (pink bars representing averages of replicates in each row of the assays using HGF alone or HGF and FBS) that were both greater than unstimulated cell migration. The chemoattractant strength of HGF alone (bar for row 2) and with 0.1% and 1% FBS (bars for rows 5 and 8, respectively) shows impressive enhancement by FBS. Chemokinetic strength of HGF alone (bar for row 3), with 0.1% and 1% FBS (bars for rows 6 and 9, respectively) also showed impressive enhancement by FBS. The combination of HGF, 2.5 ng/ml, and 1% FBS for chemoattraction (bar for row 8) significantly, $p = 0.012$, outperformed their chemokinetic effects (bar for row 9) on cell migration. The scanned image of the assay is also available in Appendix A (Figure A4B). (E) An assay that evaluated MEM for U87 migration studies included gradients for K^+ and Cl^-. In the absence of FBS, Dulbecco's PBS in the bottom wells provided K^+ as 2.7 mM KCl + 1.8 mM KH_2PO_4 and Cl^- as 2.7 KCl + 137.9 mM NaCl. MEM in the lower wells provided K^+ as 5.3 mM KCl, and Cl^- as 5.3 mM KCl + 1.8 mM $CaCl_2$-$2H_2O$. For all upper wells without FBS, the Migration media provided K^+ as 2.7 mM KCl + 1.8 mM KH_2PO_4 and Cl^- as 2.7 KCl + 137.9 mM NaCl + 0.21 mM $MgCl_2$ + 0.243 mM $CaCl_2$. See text for total mM for each ion. When the bottom wells contained Dulbecco's PBS there was no significant gradient created for K^+ or Cl^-. However, when MEM was in the bottom wells, positive K^+ and negative Cl^- gradients were generated. Both K^+ and Cl^- ions are used for volume changes in cell migration. The positive gradient for K^+ is supported as being a chemoattractant in view of the significantly increased migration, $p = 0.0144$, in MEM versus Dulbecco's PBS in the lower wells. None of the wells contained FBS for the above comparison. However, MEM in the lower wells was associated with significantly increased cell migration with 0.1 and 1% FBS also present, $p = 0.0136$ and $p = 0.000442$, respectively, compared to Dulbecco's PBS in the lower wells having the same FBS concentrations. Averages of rows for the Densitometry units indicated by bars are shown with 95% confidence limits (B, D, and E). Variability in staining of the background migration, as shown in the top rows of representative assays (A) and assay-to-assay variation for each cell line in Appendix A (Figures A2 and A3), are routine findings. Each circle of stained migrated cells shown is 3 mm in diameter.

3.3. KCN Genes Differentially Expressed in 70 Studies

3.3.1. General Features of Detected Differentially Expressed KCN Genes

The availability of K^+ for cancer cell survival and migration suggested by experimental studies just described led to consideration of the large KCN family of genes being altered in cancer cells. Published genomic landscapes, i.e. heat maps (46 studies), Venn diagrams, volcano plots, tables, etc. were found in 70 cancer studies including KCN (potassium channel) family members as one or more of 53 KCN genes that were differentially expressed genes (DEG) along with numerous co-expressed non-KCN DEG. Selection criteria for DEG (mostly $p < 0.05$ differences, chance of false discovery, etc.) were set by the authors who incidentally detected and reported the KCN DEG among groups of DEG Appendix B (Table B1, sample view, and the full list, FullTblB1DEGalphaAZ, is available after the References in a table format). Parameters were applied in each study for a particular type of malignancy, without or with perturbations, such as tumor treatment, transcription factor, over-expression of an oncogene(s), or according to survival, disease progression, primary versus metastasis, recurrence, etc. The 53 KCN DEG are distributed across 17 chromosomes (1-3, 5-12, 17-21, and X). Although many of these KCN genes encode membrane pore subunits with K^+ selectivity, some provide modulatory/regulatory effects on pore function when present with other subunits that may also function independently as pores. Heterodimers among KCN family members are common. Members of 4 KCN subfamilies, Kv (voltage dependent, related, *KCNA*, *KCNQ*, *KCNH*, etc.), Kir (inwardly rectifying, *KCNJ*), K2P (tandem two pore domain , *KCNK)*, and KCa (calcium dependent, related, *KCNM*, *KCNN*, etc.) were found in 32(46%), 10(14%), 14(20%), and 29(41%), respectively, of the 70 studies.

3.3.2. Proton(H^+) Sensitivity of Detected KCN DEG

In keeping with the connection proposed for K^+ and H^+, the H^+-sensitivity of KCN DEG encoded proteins was relevant. At least 33 (62.3%) of the 53 KCN DEG encode gene products that are H^+-sensitive according to 135 publications listed in Appendix B (Table B2). Fifty-two (74.79%) of the 70 studies contained at least one KCN DEG identified as being H^+- sensitive. One, 2, 3, and 6 H^+-sensitive KCN DEG genes were found in 36, 14, 1, and 1 of the studies, respectively. H^+- sensitive genes in each of the 4 subfamilies, Kv, Kir, K2P, and KCa were found as DEG in 17 (24%), 9 (13%), 13 (19%), and 21(30%) of 70 studies, respectively. The most frequently detected DEG, *KCNN4* and *KCNMA1*, present in 9 and 6 studies, respectively, encode H^+-sensitive proteins (red H^+ above columns) and are also Ca^{2+}-sensitive (Figure 3A).

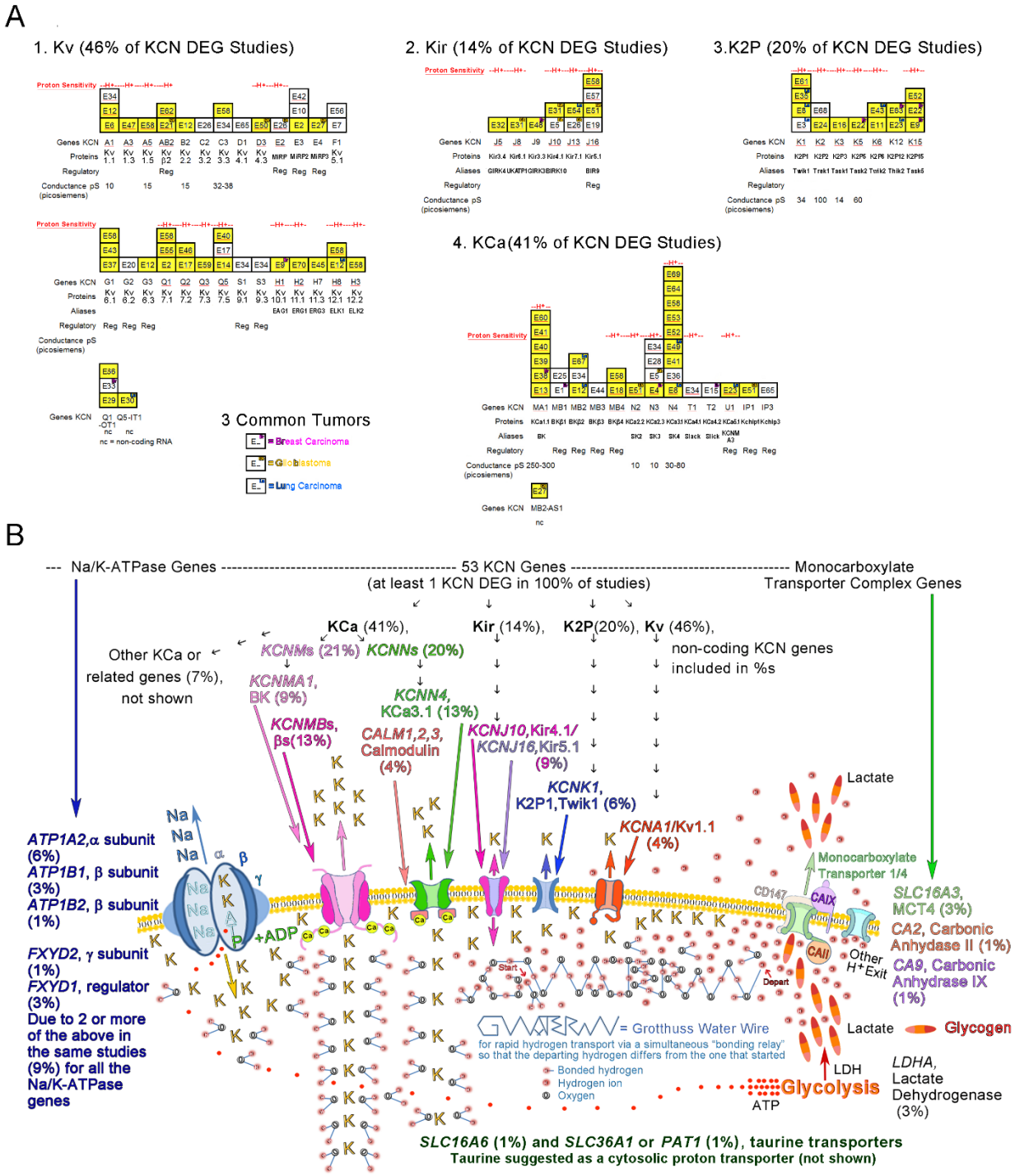

Figure 3. The KCN DEG and related non-KCN DEG detected in E1-E70 studies with relevant information are shown. (**A**) 53 KCN DEG of 4 KCN subfamilies detected are listed along the x-axes in the specific studies that are listed vertically in boxes above the specific KCN gene names, reflecting their frequency in 70 studies. The 3 most frequent types of tumors (breast, glioblastoma, and lung) are highlighted with color-coded superscripts, as listed under the first group of histograms. The 33 (62.26%) of KCN DEG that encode H^+-sensitive proteins are labeled with red H^+ above each column. Studies with KCNs detected

that encode H^+-sensitive proteins also have their names underlined in red within the boxes of the histograms. 52(74.29%) of the 70 studies contain at least one KCN encoding a H^+-sensitive protein. Yellow shading of the boxes labeled for specific studies indicates that these studies were included in 1 or more of 8 categories shown later (Figure 4A). The non-coding KCNs are in separate small histograms included with their appropriate KCN subfamily group. If only studies that included at least one protein-coding KCN DEG are considered, then 52(78.79%) of those 66 studies contained at least one KCN encoding a H^+-sensitive protein. Multiple KCN DEG were detected in 18 (27.27%) of 66 studies. (**B**) A stochastic view of K^+-related dynamics in cancer cells is presented based on collective incidences of both KCN and related non-KCN DEG identified in E1-E70. Images of the most frequent members of each of the 4 KCN subfamilies along with pertinent non-KCN membrane proteins and their complexes are consistent with published graphical representations [141-148]. There were relatively few studies in E1-E70 with differential expressions detected for genes encoding Na/K-ATPases (9% for 5 genes), the monocarboxylase transporter complex (5% for 3 genes), lactate dehydrogenases (3% for 1 gene), taurine transporters (2% for 2 genes), and 0% for related functional analogues not listed. Therefore, abnormal K^+ flux allowing K^+/H^+ exchange, if present in these same cancer studies with KCN DEG present, suggests KCN DEG for playing a role in the pH changes following rapid cytosolic H^+ transport (putatively Grotthuss type) to exit sites that include release of protons with lactate. Also, the lack of DEG for glycogen synthases assumes only normal (if any) intracellular storage of lactate as glycogen. Abnormal accumulations of K^+ at inner membrane surfaces may have occurred due to KCN DEG (in assorted combinations) to exchange with bound H^+, either due to genetic loss or down regulation of any of the numerous KCN membrane proteins mediating outward flux or a gain via KCNs mediating increased inward flux. The movement of K^+-$7H_2O$ (represented by 2 H_2O per K^+ shown in a "cross sectional" view) within the cells may bring water to outer cytoplasmic regions, possibly enhancing Grotthuss conditions near inner membranes in cancer cells. The putative K^+-related changes in cancer cells that at the same time maintain relatively normal expression levels of pertinent non-KCN genes, as seen in the majority of the 70 KCN DEG studies, would be consistent with the complex scenario shown (**B**). E1-E70 citations are listed in *Section 3.3.6. Categories Among Studies with E1-E70 Citations Per Category*.

3.3.3. Coding and Multiplicity of KCN DEG and Non-KCN DEG

Four of the 70 studies identified only non-coding KCN genes, *KCNQ1-OT1* (E29, E33, and E66) and *KCNQ5-IT1* (E30), as DEG. Study E27 identified *KCNMB2-AS1* as well as *KCNE4* as DEG. Disregarding the 4 studies with only non-coding KCNs detected as DEG, multiple (2 - 9) KCN DEG were found in 18 (27.3%) of 66 studies with protein-coding KCN DEG. Thirty-eight (71.70%) of the 53 KCN DEG were detected with other coding KCN DEG in at least one of the 66 studies. There were 102 instances of 53 KCN DEG in a total of 3,238 coding DEG instances (2,490 non-KCN DEG without repeats). The average numbers of KCN DEG and all DEG per study were 1.53 +/- 0.33 (95% CI) and 45.91+/- 7.92 (95% CI), respectively. The correlation coefficient for number of KCN DEG and size of all DEG (KCN and non-KCN) groups was 0.379. If only the studies that included at least one protein coding KCN DEG are considered, then 52 (78.79%) of the 66 studies detected at least one H^+-sensitive KCN DEG (Figure 3A).

3.3.4. Malignancies in E1-E70

The 3 most frequently found types of malignancies in the 70 studies were lung cancer, breast cancer, and glioblastoma with detected genes encoding H^+- sensitive products **bolded** in the following list. The lung cancer studies with their KCNs include: E3(***KCNK1***), E8(***KCNK1***, ***KCNN4***), E12(***KCNH8***, *KCNMB2*), E23(***KCNU1***), E30(*KCNQ5-IT1*), E35(***KCNK1***), E43(***KCNK6***), E49(***KCNN4***), 2), E54(***KCNJ13***), E63(*KCNK12*), and E67(*KCNMB2*). The breast cancer studies include: E1(*KCNMB1*), E4(***KCNN3***), E9(***KCNH1***, ***KCNK15***), E15(*KCNT2*), E22(***KCNK5***, ***KCNK15***), E33(*KCNQ1-OT1*), E38(***KCNMA1***), E48(*KCNJ9*), and E63(*KCNK12*). The glioblastoma studies include: E5(***KCNJ10***, ***KCNN3***), E21(***KCNAB2***), E26(***KCNE2***, ***KCNJ13***), E27(KCNE4, KCNMB2-AS1), E31(***KCNJ10***), E50(***KCND3***), E51(KCNIP1, ***KCNJ16***, ***KCNN2***). H^+-sensitive KCNs were found in 86%, 73%, and 44% of the 7 glioblastoma, 11 lung cancer, and 9 breast cancer studies, respectively. All three of the melanoma studies detected H^+-sensitive KCN DEG. Numerous types of malignancy listed in Appendix B, including NCI-60 cell lines (E16), detected H^+-sensitive KCN DEG, see Appendix B (Figure B1A). Common informative protein abbreviations in the KCN family are also listed (Figure B1B). E1-E70 citations for E1 – E70 are listed in *Section 3.3.6. Categories Among Studies with E1-E70 Citations Per Category*

3.3.5. Stochastic View of K^+-Related Dynamics in E1-E70

A percentage based stochastic view of K^+-related gene expression dynamics in cancer cells is presented based on collective incidences of both KCN and related non-KCN DEG identified by the authors of each paper. Images of the most frequent members of each of the 4 KCN subfamilies along with pertinent non-KCN membrane proteins and their complexes are consistent with published graphical representations [141-148]. In view of the relatively small number of 70 studies with differential expressions detected for genes shown in Figure 3B that encode Na/K-ATPase (9% for 5 genes), the monocarboxylase transporter complex (5% for 3 genes), lactate dehydrogenases (3% for 1 gene), taurine transporters (2% for 2 genes), and 0% for genes encoding functional analogue proteins not listed, the abnormal K^+ flux in these same cancers with KCN DEG can be considered for supplying K^+ for a K^+/H^+ exchange that initiates pH changes. Rapid cytosolic H^+ transport (putatively involving Grotthuss water wires) to exit sites for proton release with lactate is included to complete the pH reversal scenario. The pertinent lack of DEG in the E1-E70 studies for glycogen synthases, to mediate anomalous storage of lactate without extrusion, is included because glycogen storage of lactate occurs in humans, mice, bacteria, etc. [149-152]. Abnormal accumulations of K^+ at inner membrane surfaces are illustrated since they are proposed to promote K^+/ H^+ exchange that releases bound H^+. Accumulations of K^+ occur either due to genetic loss or down regulation of KCN membrane proteins mediating outward flux or increased inward flux due to a gain or loss in copy number and/or expression of the KCN genes found to be differentially expressed in E1-E70. The movement of K^+-$7H_2O$ (indicated with 2 H_2O per K^+, as a “cross-sectional” view in Figure 3B within cells may bring water to outer cytoplasmic regions, possibly promoting Grotthuss conditions in cancer cells near inner membranes. These putative K^+-related changes in cells that maintain relatively normal expression levels of pertinent non-KCN genes as seen in the majority of the KCN DEG studies suggest the scenario shown (Figure 3B).

3.3.6. Categories Among Studies with E1-E70 Citations Per Category

Eight categories describe 50 of the 70 studies (Figure 4A). These were author-designated which also had relevant DEG in at least one of the E1-E70 studies. Some studies belonged in more than one category and 20 studies were in no category as designated last item in the list below.

Of the 18 studies in the first category of histone/chromatin/epigenetic (His/Chr/Epi or histone/DNA), 10 were in this category due to specific genes described by the authors of the studies, including: E2(*N6AMT1*, previously *KMT9*), E13(*MSH2*, *BET*), E32(*H3K27me3*, *EZH2*), E41(*HDAC8*), E46(*KDM2B*), E49(*KMT2D*), and E53(*H3K27*). Also, E27's and E29's authors focused on chromatin access and imprinting, respectively. Two imprinted genes, *KCNQOT1* and *PAX8*, were DEG in E29. Twenty-one imprinted DEG (*AXL*, *DLK1*, *GDAP1L1*, *GNG7*, *GRB10*, *IGF2*, *KCNQ1*, *KCNQOT1*, *LRRTM1*, *MEG3*, *NDN*, *NNAT*, *NTM*, *PAX8*, *PEG3*, *PEG10*, *PHLDA2*, *PLAGL1*, *RHOBTB3*, *RTL1*, and *TFPI2*) were detected among a total of 2560 DEG for a rate of 0.82% in E1 - E70. When repeats are included, there were 32 instances of imprinted genes among 3,242 instances of DEG in E1-E70 for a rate of 0.99%. Detection of 0.82% or 0.99% imprinted genes is expected from the genome (approximately 200, i.e. less than1% of all genes) according to Tucci and colleagues who also provided a list of human imprinted genes [153]. Therefore, the presence of imprinted genes was not used as an inclusion criterion for the His/Chr/Epi category. In addition to the 10 studies per author designations, 8 additional studies detected His/Chr/Epi related DEG as follows: E4(*DNMT3B*), E30(*KDMA-AS1*), E31(*H2A.X*, previously *H2AFX*), E37(*H2AC18*), E43(*H2AC18*, *H2BC5*, *H2BC12*), E45(*NUPR1*), E58(*DNMT3B*), and E66(*BDR4*, *H1-4*(previously *HIST1HIE*)). The entire His/Chr/Epi category includes the following studies with their citations: E2 [154], E4 [155], E13 [156], E27 [157], E29 [158], E30 [159], E31[160], E32 [161], E37 [162], E41 [163], E43 [164], E45 [165], E46 [166], E49 [167], E53 [168], E58 [169], E59 [170], and E66 [171] (Figure 4A, left side).

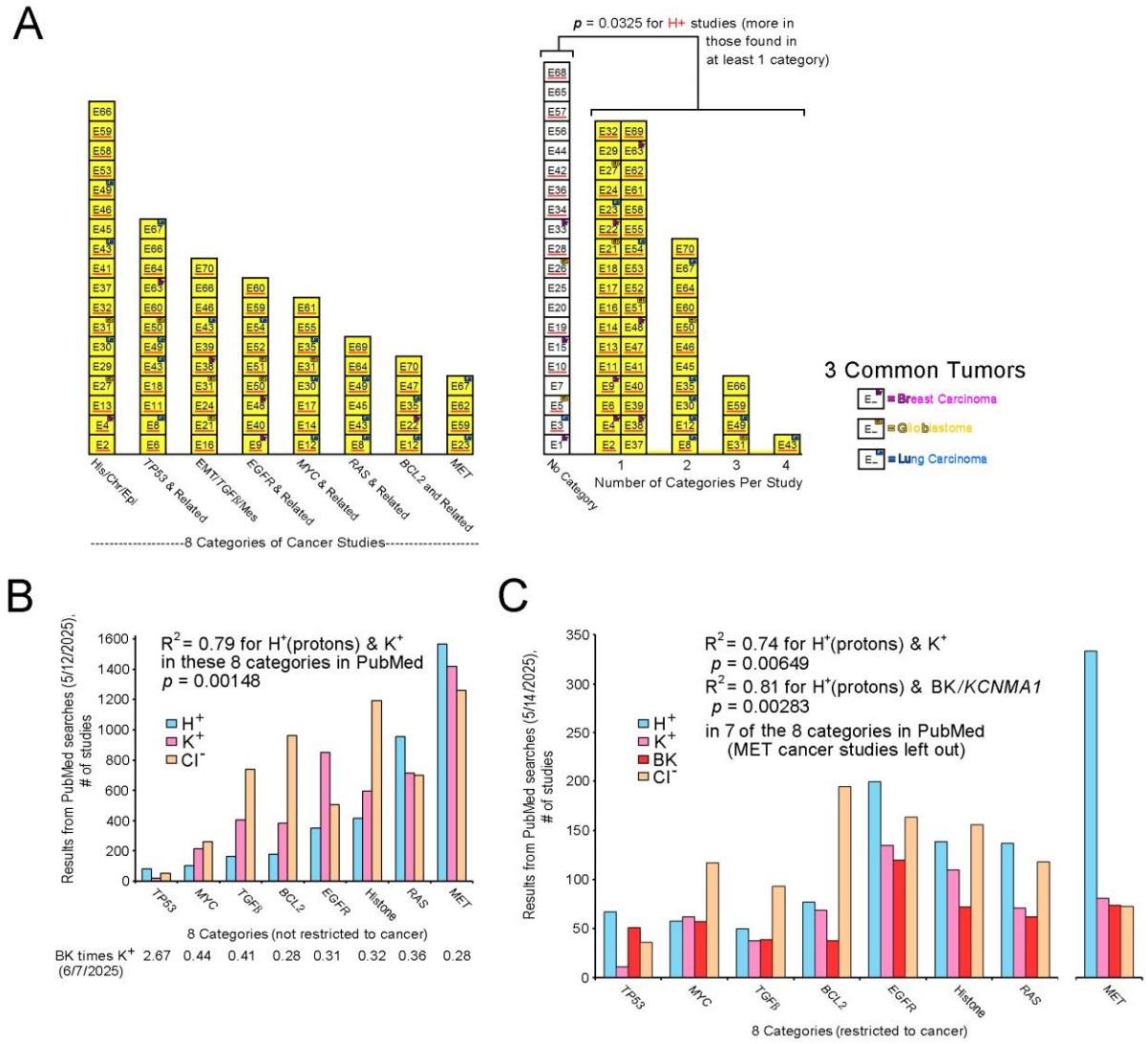

D

8 Categories (not restricted to cancer)

5/13/2025	*TP53*	*MYC*	*TGFbeta*	*BCL2*	*EGFR*	HISTONE	*RAS*	*MET*
TP53	X							
MYC	1709	X						
TGFbeta	408	1382	X					
BCL2	1573	3977	1315	X				
EGFR	2983	1695	1857	1754	X			
HISTONE	1090	2436	1602	1517	1142	X		
RAS	2202	3737	1840	1182	7337	1414	X	
MET	838	506	803	390	4861	609	1432	X

Figure 4. Oncogenes and DNA modifiers may play a role in cancer studies detecting KCN DEG encoding H^+-sensitive proteins. (**A**) The KCN DEG that encode H^+-sensitive proteins are highlighted with red underlining of the study names. Histograms of 8 categories (x-axis) of cancer studies among E1-E70 that contain KCN DEG are shown in the left histogram. The right histogram also includes 20 studies in "no category" (see text) in the first column. Comparison of the studies in “no category” versus those included in at least one of eight categories shown in the left histogram indicated a significant difference for the number of studies detecting KCN DEG encoding H^+-sensitive proteins. With a Fisher's Exact test studies that detected one or more KCN DEG that encoded a H^+-sensitive protein showed a significant difference in

the numbers of studies if the studies were in at least one of the eight categories versus no category, p = 0.0325. (**B – D)** The PubMed database (more than 38 million citations) was checked with word searches for the incidence of oncogene and histone publications related to H^+, K^+, BK (encoded by *KCNMA1*), and Cl^- (contrasting ion) to detect correlations related to findings in the 70 studies selected by detection of KCN DEG. (**B**) On May 12, 2025, searches for each category of "TP53", "MYC", "TGFbeta", "BCL2", "EGFR", "histone", "RAS", and "MET" were performed separately for "proton", "potassium", and "chloride". For all 8 categories, the total numbers of citations for "proton", "potassium", and "chloride" were 1565, 1418, and 1261, respectively, and the Pearson's product-moment correlations for "proton" with "potassium" and "proton" with "chloride" were R = 0.891 (p = 0.00148) and 0.599 (p = 0.0584), respectively. The Pearson's product moment correlation for "potassium" and "chloride" was 0.689 (p = 0.0295). R^2 for "proton" with "potassium" was 0.79. "BK" and "potassium" searches on 6/7/2025 revealed "BK" as a potential large component of the "potassium" citations, approximately one third for 7 of the categories. (**C**) When the same searches also included "cancer" as a third word, the numbers of citations for "proton", "potassium", "BK", and "chloride" on May 14, 2025, were 1061, 577, 513 (88.9% of "potassium" search results), and 952, respectively. However, when MET was left out for better "proton" correlations, the numbers of citations for "proton", "potassium", "BK", and "chloride" on May 14, 2025, were 728, 496, 439 (88.5% of "potassium" search results), and 879, respectively, and the Pearson's product-moment correlations for "proton" with "potassium" and "chloride" were R = 0.860 (p = 0.00649) and 0.462 (p = 0.148), respectively, across the 7 categories. Pearson's product-moment correlation for "proton" with "BK" was R = 0.901 (p = 0.00283) across the 7 categories. R^2 for "proton" with "BK" was 0.81. R^2 for "proton" with "potassium" was 0.74. The results for correlation between numbers of "Met" citations and those for the ions differed in results from the "cancer" searches in (C) compared to search results not restricted to "cancer" shown in (B). (**D**) The numbers of citations shared among the 8 categories of 7 oncogenes and histone are shown. E1-E70 citations are listed in *Section 3.3.6. Categories Among Studies with E1-E70 Citations Per Category*

---

2. In the <u>second category</u> there were 9 studies on *TP53* according to the authors' focus in E6, E8, E11, E49, E49, E60, E63, E64, and E67. Additionally, 3 studies found *TP53* and related genes as DEG as follows: E18(*MDM2*), E43(*TP53INP1A*), and E50(*TP53*). The 12 studies in this category are as follows: E6 [172], E8 [173], E11 [174], E18 [175], E43 [164], E49 [167], E50 [176], E60 [177], E63 [178], E64 [179], E66 [171], and E67 [180] (Figure 4A, left side).

3. In the <u>third category</u> there were 7 studies on Epithelial Mesenchymal Transition (EMT)/ *TGFb*/ Mesenchymal Tumor (EMT/*TGFb*/Mes) according to the authors' focus with specific genes, *CDH1*, *2*, *VIM*, *TGFb1*, *2*, *3*, in some of these studies as follows: E16(*CDH1*,*2*, *TGFb1*, *VIM*), E24(*TGFb1*), E31, E38, E39, E43(*CDH2*), and E46. Three additional studies also found some of these genes as follows: E21(*TGFb1*), E66(*VIM*), and E70(*CDH2*, *TGFb2*, *TGFb3*). The 10 studies this category are as follows: E16 [181], E21 [182], E24 [183], E31 [160], E38 [184], E39 [185], E43 [164], E46 [166], E66 [171], and E70 [186] (Figure 4A, left side).

4. In the <u>fourth</u> <u>category</u> there were 5 studies on *EGFR* and related genes according to the authors with corresponding DEG in two of their studies as listed, E9, E48, E50(*EGFR*, *ERBB2*), E51(*EGFR*), and E52. Additionally, 4 studies found related DEG as follows:

E40(*NRG1*), E54(*NRG2*), E59(*NRG1*), and E60(*ERBB4*). The 9 studies in this category are as follows: E9 [187], E40 [188], E48 [189], E50 [176], E51 [190], E52 [191], E54 [192], E59 [170], and E60 [177] (Figure 4A, left side).

5. In the fifth category there were 5 studies on *MYC* according to the authors with *MYC* as a DEG in 2 of the studies as seen in the following list: E14(*MYC*), E30, E31, E55, and E61(*MYC*). Additionally, 3 studies had *MYC* or one of its related genes as seen here: E12(*MYCL*), E17(*MYCN*), and E35(*MYC*). The 8 studies this category are as follows: E12 [193], E14 [194], E17 [195], E30 [159], E31 [160], E35 [196], E55 [197], and E61 [198] (Figure 4A, left side).

6. The sixth category is comprised of 6 studies on *RAS* per the authors' interest, with *KRAS* found as a DEG in 2 studies as follows: E8, E43, E45, E49, E64(*KRAS*), and E69(*KRAS*). The 6 studies this category are as follows: E8 [173], E43 [164], E45 [165], E49 [167], E64 [179], E69 [199] (Figure 4A, left side).

7. In the seventh category the authors focused on *BCL2* in E47 but did not list it as a DEG. However, 4 other studies identified *BCL2* as a DEG and 1 also identified *BCL2L1* as well, as seen in the following list: E12(*BCL2*), E22(*BCL2*), E35(*BCL2*), and E70(*BCL2*, *BCL2L1*). The 5 studies in this category are as follows: E12 [193], E22 [200], E35 [196], E47 [201], E70 [186] (Figure 4A, left side).

8. In the eighth category the authors focused on *MET* in 1 study and found it as a DEG, E23(*MET*). Additionally, 3 studies also identified *MET* as a DEG, E59(*MET*), E62(*MET*), and E67(*MET*). The 4 studies in this category are as follows: E23 [202], E59 [170], E62 [203], E67 [180] (Figure 4A, left side). All studies in the 8 categories are shaded yellow in Figure 4.

9. No category. Twenty studies were not in any of the above 8 categories and are listed as follows: E1 [204], E3 [205], E5 [206], E7 [207], E10 [208], E15 [209], E19 [210], E20 [211], E25 [212], E26 [213], E28 [214], E33 [215], E34 [216], E36 [217], E42 [218], E44 [219], E56 [220], E57 [221], E65 [222], and E68 [223] (Figure 4A, right histogram, no yellow shading).

3.3.7. H^+-Sensitivity Significant in E1-E70 Studies Within 8 Categories

A histogram (Figure 4, right side) shows the studies collectively in the 8 categories versus those not in any category, with the studies that detected H^+-sensitive KCN DEG underlined with red. The difference for detection of H^+-sensitive KCN DEG was significant between the two groups, $p = 0.0325$, Fisher's Exact Test for count data. Eleven studies were in 2 categories (E8, E12, E30, E35, E45, E46, E50, E60, E64, E67, and E70). Four studies were in 3 categories (E31, E49, E59, and E66), and E43 was included in 4 categories. All 8 categories were among those that were shared in studies (Figure 4A**,** right histogram, yellow shading). E1-E70 citations are listed in *Section 3.3.6. Categories Among Studies with E1-E70 Citations Per Category.*

3.3.8. PubMed Citations for "Proton". "Potassium", Etc. in Categories

The PubMed database was checked with word searches for the incidence of 7 oncogenes and histone publications being related to those for H^+, K^+, BK (encoded by *KCNMA1*), and Cl^-(a potential contrasting ion), without and with "cancer", to compare with the 70 studies selected based on detection of KCN DEG. On May 12, 2025, searches for each category of TP53, MYC, TGFbeta, BCL2, EGFR, histone, RAS, and MET were performed separately for "proton", "potassium", and "chloride" and "cancer" was not included. For all 8 categories, the total numbers of citations for "proton", "potassium" and "chloride" were 1565, 1418, and 1261, respectively, and Pearson's product moment correlations for "proton" with "potassium" and "chloride" were R = 0.891 (p = 0.00148) and 0.599 (p = 0.0584), respectively. Pearson's product-moment correlation for "potassium" with "chloride" was 0.689 (p = 0.0295). R^2 for proton with potassium was 0.79. Later searches on 6/7/2025 for "BK" and "potassium" revealed "BK" citations were probably a large component of those for "potassium", possibly about one third in 7 categories (TP53 was much greater than one third) and are listed also below the x axis (Figure 4B). When the searches also included "cancer" as a third word, the numbers of citations for "proton", "potassium", "BK", and "chloride" on May 14, 2025, were 1061, 577, 513, and 952, respectively. However, when MET was left out, the numbers of citations for "proton", "potassium", "BK", and "chloride" on May 14, 2025, were 728, 496, 439, and 879, respectively, and Pearson's product-moment correlations for "proton" with "potassium" and "chloride" were improved, R = 0.860 (p = 0.00649) and 0.462 (p = 0.4623), respectively, using only 7 categories. Analysis prior to MET removal is not shown. R^2 for "proton" with "potassium" for 7 categories after MET removal was 0.74. Pearson's product-moment correlation across the 7 categories for "proton" with "BK" was R = 0.901 (p = 0.00283). R^2 for correlation of "proton" with "BK" across the 7 categories was 0.81. It is unknown why citations in the MET category no longer positively participated in the correlation seen in previous searches without "cancer" for "proton" and "potassium" but may have been due to the tendency for negative studies to remain unpublished. The answer could be important but is beyond the scope of this study. It also was noted that compared to searches without "cancer" shown in Figure 4B, the "BK" citations appeared to constitute an even larger proportion of "potassium" searches when "cancer" was included, while assuming that "potassium" in the searches included all or most of "BK" citations (Figure 4C). Numerous citations were shared pairwise in 2-word searches (not restricted to cancer) among the 8 categories of 7 oncogenes and histone with the numbers shown (Figure 4D). Thus, many studies involving the 8 categories describe them collectively. The E1-E70 studies provide a broad view of KCN genes among potassium studies. Citation searches of several KCN proteins other than BK did not produce sufficient numbers for comparisons.

3.3.9. Non-KCN DEG Repeats in E1-E70

The non-KCN DEG found repeatedly in up to 5-7 studies were often detected with *KCNN4* and some with *KCNMA1*. Among the non-KCN repeat DEG, *ITGA2*/Integrin Alpha-2 was detected most frequently (7 studies). Six of these also included H^+-sensitive

KCN DEGs which are bolded as follows: **E8** (***KCNK1, -N4***)**,** E15, **E39** (***KCNMA1***), **E41**(***KCNMA1***, ***-N4***), **E49**(***KCNN4***), **E64**(***KCNN4***), and **E69**(***KCNN4***). *KCNN4* was the most frequently found DEG, 9 times total and in 5 of 7 studies with *ITGA2* as a DEG. The four studies of co-expressed *KCNN4*, *ITGA2*, and *PLAUR*, E8 [173], E41 [163], E49 [167], and E69 [199], included 2 lung cancers, 1 melanoma, and 1 pancreatic cancer, in the categories of *His/Chr/Epi*, *TP53*, and *RAS* as listed (Figure 5A**,** left Venn diagram). *HMGA2/*High Mobility Group AT-hook 2, *LIF/*Leukemia Inhibitory Factor, and *PLAUR/*Plasminogen Activator, Urokinase Receptor (UPAR) were identified as non-KCN DEG in 6 studies each that also often detected *KCNN4* as a DEG.

A

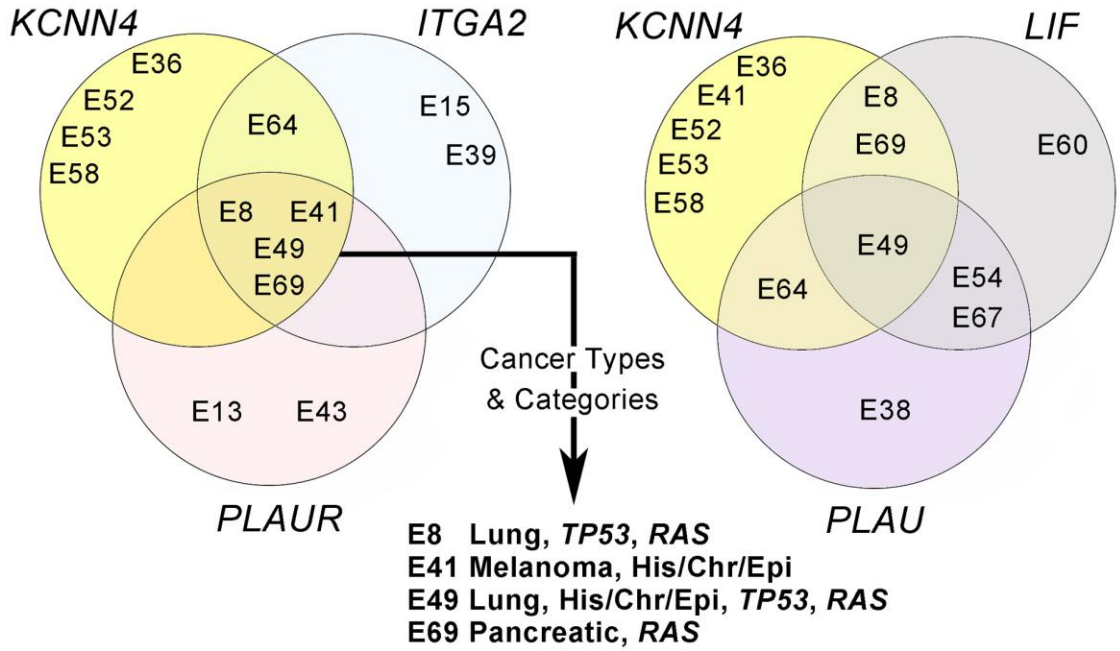

B

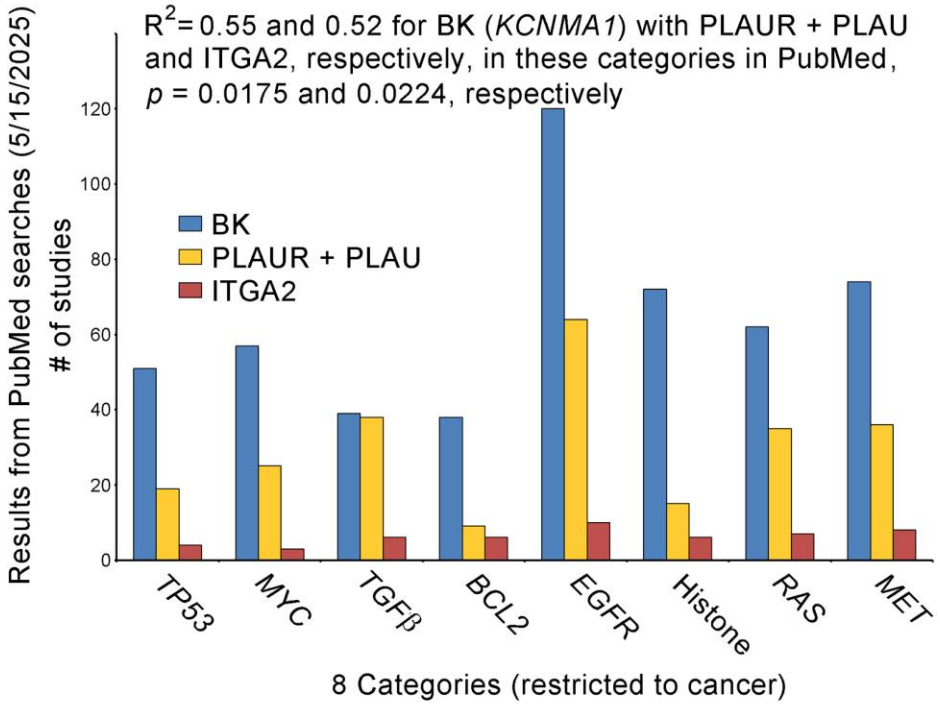

KCNMA1/BK
KCNN4/KCa3.1, IK, SK4, or Gardos channel
ITGA2/Integrin A2
LIF/Leukemia Inhibitory Factor
PLAU/Urokinase-Type Plasminogen Activator (uPA)
PLAUR/uPA Receptor

Figure 5. Repeat non-KCN DEG were found, often with *KCNN4* and some with *KCNMA1*. (A) Among the non-KCN repeat DEG, *ITGA2*/Integrin Alpha-2 was detected most frequently (7 studies). Six of these studies also included H^+-sensitive KCN DEGs which are bolded as follows: **E8** (***KCNK1, -N4***), E15, **E39** (***KCNMA1***), **E41**(***KCNMA1***, ***-N4***), **E49**(***KCNN4***), **E64**(***KCNN4***), and **E69**(***KCNN4***). *KCNN4* was the most frequently found DEG, 9 times total and in 5 of 7 studies for *ITGA2*. The four studies of co-expressed *KCNN4*, *ITGA2*, and *PLAUR*, E8 [173], E41[163], E49 [167], and E69 [199] , included 2 lung cancers, 1 melanoma, and 1 pancreatic cancer, in the categories of *His/Chr/Epi*, *TP53*, and *RAS* as listed (top left Venn diagram). One study detected *KCNN4*, *LIF*, and *PLAU* together as DEG (top right Venn diagram). One study, E41 [163], detected *KCNMA1*, *KCNN4, ITGA2*, and *PLAUR* together as DEG (not shown). (**B**) PubMed word searches for shared citations among "BK" (encoded by *KCNMA1)* and "PLAUR" + "PLAU" and "ITGA2" found correlations of $R^2 = 0.55$, $p = 0.0175$, and $R^2 = 0.52$, $p = 9.0224$, respectively, across the 8 categories of 7 oncogenes and histone.

Two studies detected *KCNN4*, *ITGA2*, and *PLAU* (found in 5 studies, ligand for PLAUR) together as DEG (not shown). *PLAUR* and *PLAU* were DEG together in only one study. Ten studies had either *PLAUR* and/or *PLAU* as DEG. Three studies detected *KCNN4*, *ITGA2*, and *LIF* together (not shown) and one study detected *KCNN4*, *LIF*, and *PLAU* together as DEG (Figure 5A, right Venn diagram). One study, E41 [163], detected *KCNMA1*, *KCNN4, ITGA2*, and *PLAUR* together as DEG (not shown).

Searches of PubMed for shared citations in cancer searches with "BK" with "PLAUR + PLAU" and then "ITGA2" in 3-word searches including "cancer" found significant Pearson's product-moment correlations of R = 0.742 ($p = 0.0175$) and 0.718 ($p = 0.0224$), respectively, and $R^2 = 0.55$ and 0.52, respectively, across the 8 categories of 7 oncogenes and "histone" when each was used as a third word (Figure 4B). Although none of the other potassium channels could be checked in this way, repeats in E1-E70 may have value for eventually identifying functionally relevant co-expressed non-KCN DEG's products to study experimentally with KCN gene products, especially *KCNN4* and *KCNMA1*.

Also, non-KCN DEG found in E1-E70 overlap with those in recent studies of genes encoding circulating proteins associated with risk for numerous types of cancer. The following genes found as DEG in 4 - 6 of the E1-E70 studies, that are shared with the two studies, are as follows with their frequency (X = times): *FGFR3* (5X), *GDF15* (4X), *IGFBP3* (5X), *IGFBP7* (4X), *KRT19* (4X), and *PLAUR* (6X) [224,225].

3.3.10. Non-KCN DEG Superfamilies in E1-E70

Nine superfamilies of non-KCN DEG were detected in E1-E70 with at least 15 occurrences. The instances of superfamily occurrences included as follows: 74X for SLC (Solute Carrier), 32X for COL (Collagen), 27X for ITG (Integrin), 22X for TMEM (Transmembrane), 21X for CD (Cluster of Differentiation), 19X for GPR (G-Protein coupled Receptor), 18X for SOX (Sry-related HMG bOX), 15X for SERPIN (SERine Proteinase INhibitors), and 15X for TNFRSF (Tumor Necrosis Factor Receptor Super Family) superfamily members. DEG repeated in at least 2 studies were present in all of the superfamilies listed.

The largest numbers of repeat non-KCN DEG occurrences were the 7X, 5X, and 4X DEG occurrences of *ITGA2* (previously mentioned), *SOX2*, and *SLC1A2/*Excitatory Amino Acid Transporter 2 (EAAT2), respectively, among the superfamilies. EAAT2 clears glutamate from the extracellular space at synapses [226-228]. *SLC16A3*, monocarboxylate transporter 4, was a DEG in 2 studies as shown (Figure 3B). Six Regulators of G protein Signaling (RGS) family members were also found as DEG in 7 studies. Eighteen (25.7%) of the 70 studies had either GPR or RGS family member DEG. Among the GPR DEG found, none are known as being H^+-sensitive as described in Appendix B (Text B1). Four carbonic anhydrase genes, *CA2*, *CA9*, *CA12*, and *CA14* were found among 5 studies. *CA2* and *CA9* are shown (Figure 3B). Genes encoding subunits of Na/K-ATPases, *ATP1A2*, *ATP1B1*, and *ATP1B2*, were DEG in 4, 2, and 1 of the E1-E70 studies, respectively (See Fig. 3B). Aquaporin family genes, *AQP1*, *AQP3* and *AQP4*, were collectively DEG in ten of the E1-E70 studies.

3.3.11. KCNs Encoding H^+-Sensitive Proteins in E1- E70 in Ten Cancer Reviews

Ten reviews describing KCN family members in malignancy were compared with detection of KCN members in E1-E70. The numbers of KCN genes described in reviews are listed as follows: 7 in a review of glioblastomas [229], 3 in a meeting report for a colloquium on cancer [230], 23 in a review listing 18 cancer types [231], 13 in a review that listed 10 cancer types [232], 9 in a review mentioning 17 cancer types [233], 21 in a review that listed 14 cancer types [234], 12 in a review mentioning at least 13 cancer types [235], 15 in a review that listed 7 cancer types [236], 13 in a review that listed 13 cancer types [237], and 13 in a review that mentioned 11 cancer types [238]. Twenty KCNs found in 35 (one half) of E1 - E70 studies overlap with those in the reviews and are listed as follows: *KCNA1*, *A3*, *A5*, *D1*, *H1*, *H2*, *H7*, *J5*, *J8*, *J10*, *K2*, *K3*, *K5*, *K15*, *MA1*, *N2*, *N3*, *N4*, *Q1*, and*T2*. The ten reviews combined with E1-E70 highlight KCN genes that encode H^+-sensitive proteins. At least one KCN gene in each of 29 studies (82.85% of 35 overlapping studies from E1 – E70) encodes a H^+-sensitive protein and these studies are listed as follows: E4, E5, E6, E8, E9, E12, E13, E16, E22, E24, E28, E31, E32, E34, E36, E38, E39, E40, E41, E47, E49, E52, E53, E58, E60, E64, E68, E69, and E70. The remaining overlapping studies included E15, E29, E33, E45, E65, and E66. Citations for E1-E70 are in *Section 3.3.6. Categories Among Studies with E1-E70 Citations Per Category*.

3.3.12. Long Introns (20,000 bp or longer) in E1-E70's KCN DEG

Many genes in the KCN family have long introns (at least 20,000 bp in length). Long introns can affect gene expression and may play a role in gene regulation. Also, they may be affected by genetic damage as cancer develops and evolves. Thirty-one (58.5%) of the 53 KCN DEG detected in E1-E70 contain long introns, some much greater than 20,000 bp. Seven KCN DEG (*KCNC2*, *D3*, *H1*, *H8*, *MA1*, *Q1*, and *T2*) each contain at least one intron that is 100,000 – 199,999 bp in length. Five KCN DEG (*KCNH7*, *IP1*, *Q3*, *MA1*, and *MB2*) each contain at least one 200,000 - 299,999 bp intron and *KCNB2* and *KCNQ5* each contain at least one intron that is 300,000 – 399,999 bp long. Fourteen of the KCN DEG in E1-E70 contain multiple long introns. *KCNMA1* and *KCNT2* each

contain seven long introns. *KCNN4* is among the KCN DEG that do not contain any long introns. Forty-one (58.6%) of the E1-E70 studies contained at least one KCN DEG that had at least one long intron. Nine studies had multiple (2 – 4) KCN DEG with long introns. However, *KCNA3*, *A5,* and *F1* in E1-E70 have only one exon and therefore do not contain any introns. Intron data from the Ensembl database, was obtained in 2023 and 2025, last accessed 6/22/2025, Ensembl browser 114 (May 2025 release). The contrast between the introns of *KCNMA1* and *KCNN4* is striking and raises the possibility of increased preservation of *KCNN4* as a smaller target when genetic damage occurs but this is unknown.

3.4. Study of Selected KCN DEG in REMBRANDT

3.4.1. Rationale and Preliminary REMBRANDT Survey

Based on glioblastoma cell adherence to dying cells, "palisading" around necrotic tumor regions, chemotaxis to serum and possibly a potassium gradient, and the tendency of glioblastoma cells to invade white matter tracts, the possibility of potassium acting as a chemoattractant in the CNS biological milieu led to a search for KCN DEG in the brain tumor database, REMBRANDT, concurrently while searching for KCN DEG in studies of various cancer types already described. REMBRANDT (as a part of the online Georgetown Database of Cancer (G-DOC) was queried. Among potassium channel related genes, KCN family members were selected because of their H^+- sensitive and modulatory/regulatory members, independence from energy requirements for many members, susceptibility to genomic damage due to the wide genomic distribution of the large KCN family (at least 90 members), potential to be downstream effectors of oncogenes, possible interactions with G-proteins, complex relationships with biological milieus, and additionally their major roles in glial and neuronal functions. Initial queries in the Online Mendelian Inheritance in Man (OMIM) database (https://omim.gov) in 2018-2019 and literature descriptions of KCN genes [239] yielded 41 KCN genes with neuronal as well as astrocytic expressions in the human brain to consider. All 41 genes were found in loci that corresponded to known regions of chromosomal losses, gains, or both in glioblastomas, published as Figure 3-76 in a book authored by Burger PC and Scheithauer BW [1]. These genes are distributed as follows: Chromosome (Ch) 1 (*KCNA2*, *A3*, *C4*, *N3*, *J9*, *J10*, *K2*, *K1*); Ch2 (*KCNJ3*, *J13*); Ch3(*KCNMB2*, *MB3*); Ch5 (*KCNN2*, *MB1*); Ch6 (*KCNK17*), Ch8 (*KCNQ3*); Ch9 (*KCNT1*); Ch10 (*KCNMA1, K18*), Ch11 (*KCNJ11*, *C1*, *A4*, *K4*, *J5*); Ch12 (*KCNA1*, *A5*, *A6*, *J8*, *MB4*); Ch14 (*KCNK10*), Ch17 (*KCNJ12*, *J16*, *J2*); Ch19 (*KCNN1*, *N4*, *C3*); Ch20 (*KCNB1*, *Q2*); Ch21 (*KCNJ15*, *J6*); and Ch22 (*KCNJ4*). The most numerous were in the KCNJ subfamily genes (*KCNJ2*,*3*,*4*,*5*,*6*,*8*,*9*,*10*,*11*,*12*,*13*,*15*, and*16*) encoding inwardly rectifying potassium channel forming proteins(Kir) and their modulators/regulators, Kir2.1, 3.1, 2.3, 3.4, 3.2, 6.1, 3.3, 4.1, 6.2, 2.2, 7.1, 4.2, and 5.1. Kir channels can be relatively occluded by Mg^{2+} or polyamines when cell membrane potentials are positive relative to the equilibrium potential of K^+ that allows only a small outward current. At membrane potentials negative to the equilibrium potential of K^+, Mg^{2+} and polyamines leave the channels by flowing into the cell so a large inward K^+ current can occur [240,241]. Kirs, including Kir4.1, may also extrude K^+. Kir 4.1 and 5.1 are present in both astrocytes and oligodendrocytes [39,242].

A preliminary survey of REMBRANDT for expression of 21 KCN family members,12 other potassium flow related genes, and 4 housekeeping genes (HKG) checked for differences in glioblastomas from patients, with and without a history of seizure medications. Seizures could be an indicator for abnormal levels of potassium [243-245]. With "unknowns for gene expression" included, there were 84 and 18 glioblastomas, with and without a history of anti-seizure medication, respectively. Compared to the absolute difference in the expression of HKG (*PPIA*, *RPLP0*, *YWHAZ*, and *B2M*) between the two groups, the single or average absolute median values of reporter probes for *KCNJ10*, *KCNK3*, *ATP1A1*, *KCNN3*, *KCNJ13*, *KCNMB2*, *SLC12A7*/KCC4, *KCNN2*, *KCNMB1*, *GJA1*, *KCND2*, *KCNK9*, *SLC1A2*/EAAT2, *KCNJ2*, and *KCNJ16* exceeded the average HKG difference (0.1131) of median values. Others, including *ATP1A2*, *KCNA2*, *KCNA3*, *KCNK1*, *KCNIP3*, *KCNMB3*, *SLC1A3*/EAAT1, *SLC12A2*/NKCC1, *KCNT1*, *KCNMA1*, *LRRC55*, *KCNA1*, *KCNMB4*, *GJB2*, *GJB6*, *SLC12A6*/KCC3, and *FXYD7*, did not exceed the average HKG difference in expression. The preliminary data (not further analyzed) suggested that the subset of glioblastomas in patients with seizures (according to medication history) had expressions of KCN family member genes that could be compared to the same genes in oligodendrogliomas (less invasive glial tumor) from patients who also had seizures. Abnormalities in potassium-related gene expressions, such as among the KCN family members, resulting in potassium flux related to worse malignant behavior could potentially underly differences in behavior between the related gliomas, oligodendrogliomas and glioblastomas.

3.4.2. Specificity in Gene Expressions Reflecting Cell of Origin

Checks were made for expected findings. Expression of *ATP1A2* (alpha subunit of Na/K-ATPase specific for glial cells) was higher in both types of glial tumors versus its neuronal specific counterpart (*ATP1A1*) in the patients on anti-seizure medications. The medians of two reporter probes available for each gene yielded significant differences, $p = 0.0345$ and 0.0278, respectively, for oligodendrogliomas and glioblastomas using 2-tailed, unpaired t-tests (Figure 6A). The specificity of expression for connexin genes in astrocytic cells, *GJA1*/Cx43, *GJB6*/Cx30, and *GJB2*/Cx26, was used to verify the expected cells of origin for the two types of glial tumors, oligodendrogliomas and glioblastomas [242,246,247], in REMBRANDT patients on anti-seizure drugs. The medians of single reporter probes for expression of astrocytic type connexins, collectively as a group, were significantly greater in the glioblastomas, $p = 0.0477$ (1-tailed, paired t test), (Figure 6B). Results using multiple reporters for oligodendrocyte type connexins were not available. More prominent vascularization of glioblastomas versus oligodendrogliomas was consistent with a trend for greater expression of *VEGFA*, $p = 0.166$, in the glioblastomas among the patients with known anti-seizure treatment (not shown).

REMBRANDT

(REpository for Molecular Brain Neoplasia DaTa)

A Anti-seizure Rx

Gene	Oligo	GBM
ATP1A1	2.92049	2.91169
versus	5.08693	4.84342
ATP1A2	9.58621	9.49969
	9.90387	10.03376
p values	0.03449*	0.02776*

B Anti-seizure Rx

Gene	Oligo	GBM	
GJA1	3.79493	3.92367	*p* value for
GJB2	4.61600	4.93627	Oligo versus GBM
GJB6	6.89208	7.01980	= 0.04765*

C

	Large Group		Anti-seizure Rx	
Gene	Oligo	GBM	Oligo	GBM
KCNJ10	7.88072	6.94161	7.88221	6.82805
	3.35772	3.27711	3.31175	3.19652
KCNJ16	8.12864	6.81784	8.30402	7.30945
	7.41947	6.30007	7.59016	6.54826
KCNK3	5.25703	5.33609	5.09866	5.41457
	7.22861	7.62468	7.36709	7.52793
KCNK10	5.26409	5.21112	5.31340	5.01056
	11.18701	10.50502	11.33574	10.54029
	8.66476	8.52497	8.84111	8.53841
CA12	9.36679	9.25853	9.31132	9.29754
	8.39995	8.14632	8.43690	8.03071
	10.92476	10.72416	10.92042	10.68890
	6.29452	6.07502	6.00293	5.98906
	5.39249	5.50748	5.84638	5.23676
	7.07346	5.45519	7.74194	5.83069
TP53	11.58190	12.11004	11.43341	12.11586
	7.86090	7.95125	7.79580	8.06428

D Anti-seizure Rx

Gene	Gene OMG difference	HKG	Oligo	GBM	HKG OMG difference
KCNJ10	1.05416	*PPIA*	6.90772	7.09117	- 0.18345
	0.11523		10.16633	9.76835	0.39798
KCNJ16	0.99457		9.45655	9.81833	- 0.36178
	1.04190		7.43305	6.78537	0.64768
KCNK3	- 0.31591		6.63263	6.71673	- 0.08410
	- 0.16084		6.64463	6.92428	- 0.27965
KCNK10	0.30284		8.79386	8.84473	- 0.05087
	0.79545		8.68471	8.74586	- 0.06115
	0.30270	*RPLP0*	9.77174	9.73344	0.03830
CA12	0.01378		9.26984	9.68827	- 0.41843
	0.40619		9.98964	9.80454	0.18510
	0.23152		9.82984	9.70374	0.12610
	0.01387		9.54447	9.22953	0.31494
	0.60962	*YWHAZ*	5.91707	4.53647	1.38060
	1.91125		5.59831	5.48575	0.11256
TP53	- 0.68245		7.86566	8.97262	- 1.10696
	- 0.26848		5.82757	6.57399	- 0.74642
		B2M	5.15497	5.61879	- 0.46382
			8.55786	8.41906	0.13880
			9.17194	8.68818	0.48376

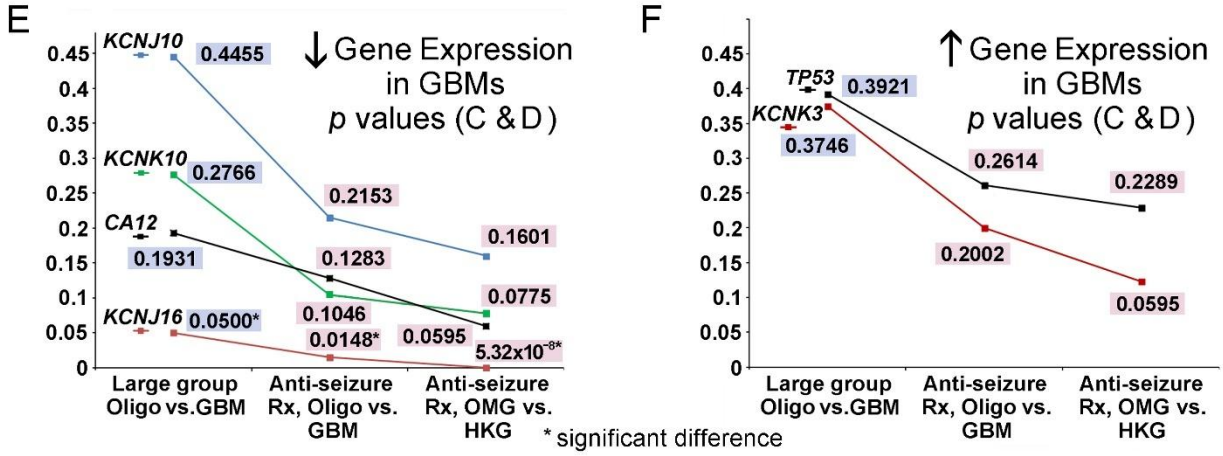

Figure 6. Results for oligodendrogliomas (Oligo) and glioblastomas (GBM) from REMBRANDT. (**A – D**) Median reporter probe values of microarray gene expression results from Oligo and GBM tumor tissue are shown in columns as indicated. Pink backgrounds (A – F) indicate results are from patients on anti-seizure medications (Anti-seizure Rx). Results with a blue background (C, E, F). are from Large Group patients (medication history not used for criteria). (**A**) The *p* values of t-tests are at the bottoms of columns for comparisons of *ATP1A1*/Na/K-ATPase subunit alpha 1, neural specific, versus *ATP1A2*/Na/K-ATPase subunit alpha 2, glial specific in Oligo and GBM with significant differences confirming glial origins. (**B**) Single median reporter probe values for astrocytic-specific (versus oligodendroglial) values for gap junction genes with higher levels of expression in GBM versus Oligo as expected. (**C**) Values listed for median

reporter probes for 4 KCN genes (See text) and 2 other genes, *CA12*/carbonic anhydrase 12 and *TP53*/p53. (**D**) An additional method to evaluate expression of genes shown (C)**,** calculated Oligo Minus GBM (OMG) differences of the median probe results for each gene of interest and the housekeeping genes (HKG). These differences were then compared to correct for variation in tissue handling, assay-to-assay variation within and between institutions, etc. (**E – F**) The *p* values are shown graphically for decreased and increased gene expressions in GBM, respectively. Significance improved dramatically for *KCNJ16* with this approach and trends became stronger for other genes. Oligo = oligodendroglioma, GBM = glioblastoma, Rx = medication, HKG = housekeeping genes. REMBRANDT (part of the Georgetown Database of Cancer (G-DOC).

3.4.3. KCN Gene Expressions in Patients on Seizure Medications

Limiting tumor comparisons to patients on anti-seizure medications improved detection between the two types of invasive glial tumors. Without using the history of seizure medications, a difference in expression of *KCNJ16*/Kir5.1 in glioblastomas (less expression), $p = 0.05$, of borderline significance, became significant in glioblastomas using the smaller group of patients on anti-seizure drugs, $p = 0.0148$. Trends also improved for differences in expressions of *KCNJ10*Kir4.1, *KCNK3*/TASK1, and *KCNK10*/TREK2, (all H^+-sensitive, Appendix B (Table B2) and [248,249]) with reporter probe data (Figure 6C) and *p* values (Figures 6E - F) shown along with other genes, *CA12*/carbonic anhydrase 12 and *TP53*/p53. *SLC16A1*/MCT1, *PTEN*, and other non-KCN genes (not shown), also showed some improvement in the difference between oligodendrogliomas and glioblastomas when comparisons were limited to patients on anti-seizure drugs. Median results of five *SLC16A1*/MCT1 probes indicating increased expression in glioblastomas, but without significance, had $p = 0.269$ and $p = 0.255$ in the smaller group with a history of anti-seizure medication.

3.4.4. Oligodendroglioma Minus Glioblastoma (OMG) Normalization

Housekeeping gene (HKG) normalization was used to correct for loss of genomic integrity, differences in tissue handling, assay to assay variation within and between institutions, etc. in the comparisons using the microarrays of two different type of tumors in REMBRANDT. It was used for comparisons in patients on anti-seizure medications. Oligodendroglioma Minus Glioblastoma (OMG) differences (increased or decreased) were calculated for each reporter probe's median expression. These OMG differences for each DEG were compared to the OMG differences for all 4 HKGs. Enhancement of the previously detected differences resulting in better *p* values as shown (Figures 6D-F). The OMG difference for *KCNJ16*, decreased in glioblastomas, became highly significant, $p = 5.532 \times 10^{-8}$. The trends for several other genes improved. The *t*-tests were calculated for unpaired samples with unequal variance in the OMG comparisons. The median probe data (Adobe Flash format) in Figures 6A-D is no longer available online in REMBRANDT (Georgetown website, see Materials and Methods, Subsection *2.3. Databases*).

3.5.1. KCN DEG Shared in E1-E70, REMBRANDT, and Glioblastoma Cell Lines [22]

Whole exome and RNA sequencing data of LN18, LN229, T98G, U87, U343, and U373 human glioblastoma cell lines, available as Open Access in Patil et al.'s Supplementary Materials [22], revealed data for many of the KCN DEG and genes of interest found in the E1-E70 and REMBRANDT studies. Also, 3 and 5 of these cell lines were also used for the cell settling and cell migration studies, respectively, described earlier. Their data availability is described in the **Data Availability Statement** that follows this article's text. They described their methodology in detail [22], with some information also included here. For each of the GBM cell lines, U87, T98G, LN229, LN18, U343, and U373, a 62 Mb region of the genome was targeted. Alignment was to human reference genome hg19. Their single nucleotide variant (SNV) was considered to be a potential Cancer Specific Mutation (CSM) if present in the COSMIC database (Reference 18 in [22]) and/or was present in GBM TCGA exome sequencing data (their references 8,9). Data for 4 cell lines, U87, T98G, LN229, and LN18, had an average concordance of 65.3% with the COSMIC database (their reference 18) and 74.74% with the Broad Institute's CCLE database (their reference 19). In addition to CSMs, Patil et al. reported small insertions and deletions (indels) in a size range of -49 to +29 bases. Differential gene expression data per Patil and colleagues was obtained via comparisons of their RNA-seq data from six GBM cell lines, U87, T98G, LN18, LN229, U343, and U373, with expression data of five normal brain tissue samples from TCGA, with a cut off value of a 2-fold change in absolute expressions. Their results for 2,214 genes compared with those that were also present in TCGA GBM tumor samples had a concordance of approximately 73%. Of the 2,214 genes in the Patil study,1,831 (82.7%) were down regulated. For the 1,621 genes similarly up or down regulated in both the TCGA and Patil et al. studies, 79.64% were down regulated.

Among the KCN genes identified by Patil and colleagues, 42 KCN genes had CSM and indels. The DNA changes identified in 18 of the 42 KCN genes occurred in at least 3 of their glioblastoma cell lines. The KCN family group, with the highest number of members (ten) with reported DNA changes, included *KCNJ1*, *2*, *3*, *5*, *6*, *10*, *12*, *13*, *14*, and*16*. Patil and colleagues identified 69 CSM among KCN family member genes, representing 4.33% of 1,594 CSM found in all the genes they sequenced. Also, the 68 indels (25 insertions and 43 deletions) that they found in KCN family members represented 1.75% of all 3,892 indels found in the 6 glioblastoma cell lines. For comparison with this study of KCN DEG in E1-E70 and genes of interest in REMBRANDT, shared KCN DEG with their sequencing results revealed DNA alterations including CSM, INS, and DEL. Twenty-three of the E1-E70 KCN DEG and 4 of the REMBRANDT study's KCN genes of interest based on expression had changes described in the genomes of 6 glioblastoma cell lines by Patil et al. Those detected in E1-E70 (glioblastomas (7) with 28 other cancer types) are marked with light green squares on the right side of lists, and genes of interest (significant difference or trends) found in REMBRANDT are bolded (*KCNJ10*, *KCNJ16*, *KCNK3*, and *KCNK10*), (Figure 7A). Patil et al. found that all 51 KCN family members with gene expressions detected in the six glioblastoma cell lines were down regulated versus normal with the 51 expressed KCN family member genes representing 1.48% of all 3428 genes found to be differentially expressed in the cell lines. Average gene expression levels of RNA determined by Patil et al. are listed in descending order of abundance, including 27 and 4 of the E1-E70 and REMBRANDT KCN genes, respectively, along with names of encoded proteins (Figure 7B). *KCNJ16*, which was

significantly down regulated in REMBRANDT's glioblastomas, when compared to oligodendrogliomas, was ranked among the lowest detectable expressing genes in the 6 glioblastoma cell lines studied by Patil et al. Only four of the 51 KCN genes with expression values ranging from <0.001 to 803.719 (modeled counts) had lower expression than detected for *KCNJ16* (Figure 7B). The log2 fold RNA changes from normal calculated using their Supplementary Table S6 [22], are shown for the 51 KCNs with detectable RNA in the glioblastoma cell lines. The 27 genes (52.94%) with encoded H^+- sensitive proteins and the 24 KCN genes with DNA changes are highlighted on the graph (Figure 7C). Of the 53 KCNs in E1-E70 there are 38 (71.70%) also described by Patil et al. in their glioblastoma cell lines, either with the DNA changes shown and/or with RNA expressions detected. Of the seven GBM studies in E1-E70, six (85.71%) each shared 1 - 3 KCN DEG with those described by Patil et al. The specific glioblastoma studies in E1-E70 with these KCN DEG are E5, E21, E26, E27, E31, and E51. Only one, E50, of the E1-E70 glioblastoma studies did not detect a KCN DEG corresponding to those with RNA expression detected by Patil et al. [22]. There is a large overlap of KCNs encoding proteins with H^+-sensitivity in E1-E70, REMBRANDT, and those described by Patil et al. (Figure 7C). References for H^+-sensitivities are cited in Appendix B, Table B2, and earlier in Section *3.4.3. KCN Gene Expressions in Patients on Seizure Medications,* for the encoded proteins of *KCNA1*, *KCNA3*, *KCNA5*, *KCNAB2*, *KCNH1*, *KCNH3*, *KCNJ10*, *KCNJ16*, *KCNK1*, *KCNK3*, *KCNMB4*, *KCNN3*, *KCNQ1*, *KCNQ2*, *KCNQ3*, *KCNQ5*, and *KCNT1*. References for H^+-sensitivity of the proteins encoded by additional KCN genes shown (Figure 7C) are as follows: *KCNA2*/Kv1.2 [250], *KCNA4/*Kv1.4 [251,252], *KCNC4*/Kv3.4 [253], *KCNH4*/ELK1 [254], *KCNJ3*/GIRK1 [255,256], *KCNJ11*/Kir6.2,IKATP [257,258], *KCNJ12*/Kir2.2,HIRK1 [259] (variant), *KCNK9*/K2P9,TASK3 [260,261], and *KCNK17*/K2P17.1,TALK2,TASK4 [262].

A

Gene	Ch	5'UTR	Protein coding	Introns	3'UTR	# Cell Lines
KCNA1	12				DEL	1
KCNA3	1				INS,CSM	3
KCNA6	12				INS(2)	5
KCNA7	19		DEL			1
KCNAB1	3				DEL(5)	6
KCNB1	20				CSM	1
KCNC1	11				CSM	1
KCNC3	19				INS	2
KCNC4	1		CSM		CSM	2
KCND1	X	CSM	CSM			2
KCND2	7	CSM				1
KCNE1	21				INS	4
KCNE4	2				INS	3
KCNG3	2		CSM		CSM	2
KCNG4	16	CSM				1
KCNH1	1		CSM		DEL(2),CSM(2)	5
KCNH8	3		CSM		CSM	2
KCNIP3	2				CSM	1
KCNIP4	4			INS(2),DEL(5), CSM	INS(3), DEL(3)	6
KCNJ1	11				INS	1
KCNJ2	17				INS,DEL	3
KCNJ3	2				INS,CSM	5
KCNJ5	11	CSM(4)			INS,DEL	5
KCNJ6	21				CSM(2)	1
KCNJ10	1				DEL,CSM	2
KCNJ12	17		DEL,CSM(23, 10 silent)		INS,DEL(3)	6
KCNJ13	2	DEL				1
KCNJ14	19				INS,CSM	2
KCNJ16	17			DEL	INS(2),DEL	4
KCNK2	1		CSM		INS(3),DEL, CSM	6
KCNK3	2				CSM	1
KCNK10	14			CSM	INS,DEL(4), CSM(2)	6
KCNK16	6		CSM			1
KCNMA1	10				DEL,CSM	3
KCNMB1	5				DEL	1
KCNMB3	3	INS,DEL	DEL			4
KCNN1	19		CSM			1
KCNN2	5		INS			4
KCNN3	1		CSM(5,2silent)			1
KCNQ1	11		CSM(2,1silent)	DEL(6) CSM(2)		6
KCNS1	20				DEL	1
KCNT2	1		CSM		CSM	2

■ = DEG in E1 - E70 & REMBRANDT DEG are bolded

UTR = Untranslated Region, DEL = Deletion, INS = Insertion, CSM = Cancer Specific Mutation (Single Allele Substitution)

B

	Gene	Ave. RNA	Protein Name
■	1. *KCNAB2*	803.719	Kvβ2
	2. *KCNC4*	351.847	Kv3.4
■	3. *KCNMB4*	217.130	BKβ4
■	4. *KCNIP3*	191.967	KChIP3
	5. *KCNB1*	155.982	Kv2.1
■	6. *KCNN3*	129.440	KCa2.3, SK3
■	7. ***KCNJ10***	94.083	Kir4.1
■	8. *KCNF1*	74.733	Kv5.1
	9. *KCNIP4*	72.195	KChIP4
■	10. *KCNK1*	60.489	K2P1,TWIK1
■	11. *KCNC3*	60.440	Kv3.3
■	12. ***KCNK3***	54.020	K2P3,TASK1
■	13. *KCNQ5*	51.475	Kv7.5
	14. *KCNIP2*	47.120	KChIP2
■	15. *KCNH3*	46.225	Kv12.2,ELK2
■	16. *KCNA1*	45.318	Kv1.1
	17. *KCNAB1*	36.674	Kvβ1
	18. *KCNJ6*	36.411	Kir3.2,GIRK2
	19. *KCNJ4*	35.865	Kir2.3,HIRK2
	20. *KCNK9*	26.810	K2P9.1,TASK3
■	21. *KCNQ3*	22.001	Kv7.3
	22. *KCNJ12*	21.544	Kir2.2,HIRK1
	23. *KCNA2*	19.745	Kv1.2
■	24. *KCNT2*	17.533	KCa4.2,SLICK
	25. *KCND2*	16.774	Kv4.2
	26. ***KCNK10***	13.840	K2P10.1,TREK2
■	27. *KCNQ1*	13.662	Kv7.1
	28. *KCNN1*	11.494	KCa2.1, SK1
	29. *KCNJ11*	11.242	Kir6.2,IKATP
■	30. *KCNIP1*	10.936	KChIP1
■	31. *KCNS1*	6.771	Kv9.1
■	32. *KCNT1*	6.494	KCa4.1,SLACK
	33. *KCNJ3*	6.335	Kir3.1,GIRK1
	34. *KCNH4*	5.574	Kv12.3,ELK1
■	35. *KCNJ9*	5.470	Kir3.3,GIRK3
	36. *KCNC1*	5.398	Kv3.1,NGK2
	37. *KCNK12*	5.346	K2P12.1,THIK2
	38. *KCNS2*	3.877	Kv9.2
	39. *KCNA4*	3.813	Kv1.4
■	40. *KCNH1*	3.485	Kv10.1,Eag1
	41. *KCNV1*	2.739	Kv8.1,
■	42. *KCNG2*	2.675	Kv6.2
	43. *KCNK13*	0.965	K2P13.1,THIK1
■	44. *KCNA5*	0.947	Kv1.5
■	45. *KCNA3*	0.833	Kv1.3
■	46. *KCNB2*	0.833	Kv2.2
■	47. ***KCNJ16***	0.833	Kir5.1
	48. *KCNA6*	0.584	Kv1.6
■	49. *KCNQ2*	0.432	Kv7.2
■	50. *KCNC2*	<0.001	Kv3.2
	51. *KCNK17*	<0.001	K2P17.1,TALK2

C

KCN Genes with Detected RNA in 6 Glioblastoma Cell Lines (ave. in B. above, LN18,LN229,T98G,U87,U343,U373)

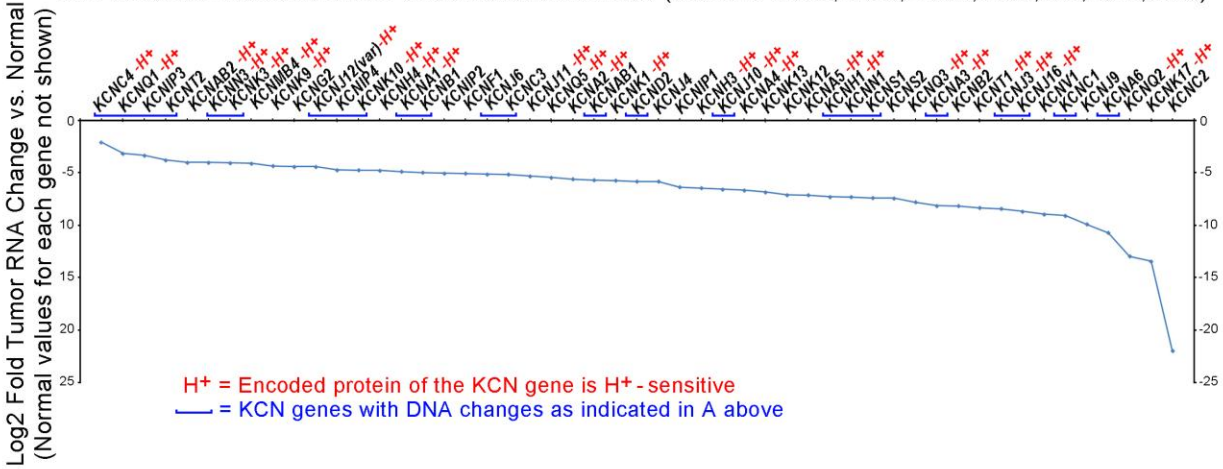

Figure 7. Many KCN DEG detected in E1-E70 studies (Figures 3 - 5). and in REMBRANDT (Figure 6). were included in whole genome and expression studies of 6 glioblastoma cells lines by Patil et al. [22]. They reported on LN18, LN229, T98G, U87, U343, and U373 cell lines. For comparisons, the shared KCN DEG detected in E1-E70 (29 cancers including 7 glioblastomas) are marked with light green squares and the KCN DEG found in REMBRANDT are bolded (**A** and **B)**. (**A**) Sequencing results revealed DNA alterations including cancer specific mutations (CSM), insertions (INS), and deletions (DEL). Twenty-three KCN DEG (of 53 in E1-E70, See Figures 3 and 4) and those with potential significance in REMBRANDT (3 with trends and 1 significant KCN DEG, See Figure 6C - F), were detected with changes in the genomes of 6 cell lines (usually > 1) by Patil et al. Several shared KCN DEG were genetically altered in all 6 cell lines. (**B**) Average gene expression levels of RNA determined by Patil et al. are listed in descending order of abundance, including 27 and 4 of the E1-E70 KCN DEG and REMBRANDT's KCN DEG and genes of interest, respectively, along with names of their encoded proteins. (**C**) Log2 fold RNA changes in the combined tumor cell lines versus normal (see text) are shown graphically. KCNs encoding H^+-sensitive proteins are highlighted as red (H^+) and the KCNs found to have DNA changes in (A) are highlighted with underlining blue brackets (␣). Of the 51 KCNs with detectable RNA in the glioblastoma cell lines, 27 (52.94%) encoded proteins that are H^+- sensitive. Of the 53 KCNs in E1-E70 there are 38 (71.70%) also described by Patil et al. in glioblastoma cell lines, either with altered DNA and/or RNA expression values. Of the seven GBM studies in E1-E70, six (85.71%) shared 1 - 3 KCN DEG with those described by Patil et al. [22]. See the text and Appendix B (Figure B1A) for specific glioblastoma studies in E1-E70 and the references for each study are given in Section *3.3.6. Categories Among Studies with E1-E70 Citations Per Category.*

4. Discussion

4.1. Input of Functional U87 Studies

The decision to stochastically investigate potassium in cancer was based on earlier FBS cell migration assays and then observing cytology of glioblastoma cell in settling assays. After fluid was wicked away as cells settled on glass slides, not only was expected cell death and cytoplasmic vacuolization seen, but also small groups of cancer cells clustered around single dying cells. Although malignant cells from body fluid specimens sometimes ingest whole cells, the tight cell adherence of robustly viable cells to dying settled cells that were formerly in cell suspension was a surprise. Uncentrifuged cancer cells from clinical body fluid specimens viewed microscopically, after gentle filtration and dissolution of filters [263,264], do not have this appearance, at least routinely. However, the morphology of the settled, viable cells clustered around single necrotic cells did resemble characteristic rimming of deeply staining glioblastoma cells ("pseudopalisades") around necrotic foci in glioblastoma tumor tissue as described in the Introduction, Section *1.1. General*. Also, basophilic staining in tumor cells of tumors with central necrosis with more alkaline cytoplasmic pH detected in necrotic areas has been established experimentally in cervical cancer cells [265]. Clues, as mentioned earlier, to form a hypothesis for the glioblastoma cells in settling assays and their rimming around necrosis in tissue included (*i*) the viability of cancer cells rimming single dying cells seemed protected from the negative effect of fluid removal, (*ii*) relatively darker staining of some viable clustered tumor cells possibly reflected a pH change in them, and (*iii*) when

ATP is depleted, cells open their cation channels to release K^+ (major cation) before rupturing [266-268]. Potassium efflux has been seen in cancer cells [269].

A chemotactic role for potassium was supported in view of cell migration assays, previously performed for planning the use of FBS to optimize glioblastoma cell lines migrating to HGF. Results could not rule out an unidentified serum constituent acting as a chemoattractant. Multiple cell lines migrated to FBS alone with dose responses. Also, U87 cells migrated significantly (p = 0.0144) with a positive gradient present of K^+ generated by MEM (5.3 mM K^+ in a milieu of amino acids, vitamins, etc.) versus 4.5 mM K^+ in "Migration" media, in the absence of FBS and HGF, and was improved in the presence of FBS (Figure 2E). Support for potassium as the chemoattractant possibly inciting their reversal of pH is also considered.

4.2. Mechanistic Proposal for a New Route to pH Reversal

The KCN family members, many pH sensitive, cooperate to control potassium levels at cell membranes in a putatively H^+-sensitive manner. A new hypothesis is that K^+, as a monovalent exchange cation for H^+, frees bound protons from inner cell membranes for rapid cytoplasmic transfers to proton extruders, and instigates pH reversal in cancer if the control of potassium flux is deregulated. Whether rapid delivery of H^+ to exit sites occurs via the Grotthuss mechanism during pH reversal is also a new consideration that could explain how freed protons become available for rapid cytoplasmic proton transfers to cell exit sites during pH reversal in at least some malignancies. Although the Grotthuss mechanism of rapid proton transfer via "water wires" has been described for proteins and the tight junction of the blood brain barrier [270-272], cytoplasmic Grotthuss type proton transfer in cancer cells has not been recognized. As migrating tumor cells flatten and squeeze into small spaces such as between a nerve fiber and its surrounding nerve sheath or along and then through dense basement membranes, bone, cartilage, etc. there should be microaqueous intracellular regions of tumor cells generated temporarily. The cell settling assays removed fluid to create a microaqueous condition for all cells with simultaneous exposure to K^+ from single dying cells within some clusters of cells. These centralized dying cells could also have become "sinks" for protons released from the surrounding viable tumor cells.

Putatively, entry of K^+ across membranes into the viable cells in settling assays provided replacement ions for H^+ bound to fixed inner membrane anions (and possibly to H^+ bound to cytosolic proteins) that permitted newly freed H^+ (rapidly formed H_3O^+) to diffuse through the cytoplasm, possibly via cytosolic Grotthuss water wires formed under microaqueous conditions to serve as a "root system" for supplying protons to extruders. In tissue, viable microaqueous malignant cells may use a potassium flux, K^+/H^+ exchange, proton transfer in water, and then cell exit of protons as a response to stress or oncogenes to acidify the microenvironment with activation of proteases, etc. for cell migration. Simultaneously a higher cytosolic pH is provided to activate alkaline-sensitive intracellular proteins promoting cell survival. An alkaline pHi leads to maximal tumor cell proliferation coupled with increased glycolysis and adaptation to hypoxia *in silico* [273] and is associated with increased flux of glycolytic enzymes, migration, and invasion experimentally [274]. Also, when pHi increases, H^+ diffusion increases [275], possibly enhancing pH reversal for survival of single, migrating cancer cells.

4.3. Further Consideration of KCN Genes in Cancer, Including Key Negative Findings

Simultaneous studies of multiple KCN genes of interest in REMBRANDT and those in KCN cancer reviews, including those with H^+-sensitivity, supported the ongoing stochastic investigation of KCN family members as DEG in unbiased cancer studies. The relatively large number of studies allowed investigation of H^+-related associations with the expression of the KCN gene family's numerous members differentially expressed in malignancy. KCNs in E1-E70 studies overlapped with KCNs DEG in REMBRANDT (*KCNJ16*, *KCNJ10*, *KCNK3*, and *KCNK10*, all 4 encoding H^+-sensitive proteins), and with 20 KCN genes covered in ten reviews. At least one KCN DEG in each of 29 studies (82.85% of the 35 studies from E1-E70 overlapping with the KCNs in ten reviews) encodes a H^+-sensitive protein. Potassium ions may redistribute in cancer cells to exchange with H^+ in pH reversal via differential expression in the KCN family members that encode H^+-sensitive proteins, possibly related to oncogenes, genetic damage, etc.

The KCN family offers the possibility of a large variety and range of dynamic distributions of K^+ via its numerous members, networking, biological milieus, modulation by oncogenes, histone/DNA modifiers, etc. Also, potassium is supplied by blood pulsing through the vascular system, although locally haphazard in cancer, and by the firing of action potentials along axons in nerve fibers and white matter tracts. The formation of synapses between tumor cells and neurons provide K^+ as well as other synaptic substances [276]. These sources may be increased or decreased in cancer. Activation of proteases by extracellular acidosis that degrade connective tissues provide increased access to neural and vascular K^+ during migration and metastasis. Multiple proton extruders have been proposed for glycolytic/plurimetabolic type glioblastoma cells [277]. Also, the microaqueous surface conditions in cell settling assays and during tissue invasion *in vivo* suggest a lower probability of CO_2 dissolving in surrounding extracellular fluid to form carbonic acid that dissociates to hydrogen and bicarbonate ions for cell uptake. The possibility of having taurine function significantly as a carrier of cytoplasmic H^+ seems less likely since the only taurine transporters found as DEG in E1 – E70, *SLC16A6* and *SLC36A1* (or *PAT1*, former name), were present in low numbers (Figure 3B). No non-KCN DEG were found for carnitine transporters. Adaptations took place in the cell settling assays and in some invasive scenarios without extracellular fluid being available. Also, the aquaporin genes, *AQP1* and *AQP4* genes, whose products mediate water flux, were only found in 3 of the E1-E70 studies. *AQP3*, found in 4 studies, encodes aquaglyceroporin that mediates glycerol, uncharged solutes, and water flux [278].

In the E1 - E70 studies important negatives include non-KCN DEG representing proton extruders, carbonic anhydrases, etc. with some mentioned in the Results and earlier in this section of the Discussion. Importantly, only a few studies found *ATP1A2* encoding Na/K-ATPase and related genes (as a group < 10%) to be differentially expressed in E1-E70. Its role as an important negative is supported by a report that digoxin, an inhibitor of Na^+/K^+ ATPase, an active inward K^+ transporter, has been found to reduce the size of circulating tumor cell clusters in women with metastatic breast cancer, -2.2 cells per cluster [279]. Others are also shown (Figure 3B). Some negatives (lacking significant differential expression) were described in the REMBRANDT analysis.

In support of finding *KCNK* genes as DEG in 20% of E1-E70, with *KCNK1*/K2P1 being most frequent, this is consistent with the loss of *KCNK1* being associated with breast cancer cell survival when necrosis was induced [118]. Also, the ten reviews of KCN genes found in cancer as described in the RESULTS, Section 3.*3.3.11. KCNs Encoding H^+-Sensitive Proteins in E1- E70 in Ten Cancer Reviews*, included overlap with 4 members of the K2P (*KCNK* genes) and 4 members of the KCa (*KCNM* and *KCNN* gene groups) subfamilies and others. In E1-E70, *KCNN4* and *KCNMA1*, were the most frequently detected KCN DEG, 9 and 6 studies, respectively.

4.4. E1-E70 Studies Related to 7 Oncogenes and Histone/DNA Modulation

Among the E1-E70 studies, 50 were in 8 categories of histone/DNA modulator involvement and/or having relationships to one or more of 7 oncogenes (*TP53*, *TGFβ*, *EGFR*, *MYC*, *RAS*, *BCL2*, and *MET*). Sixteen studies were in more than one category. Migration of 7 of the 8 glioblastoma cell lines responded to HGF, the ligand of *MET*'s encoded Met [280,281] as shown (Figure 2). Others have proposed a role of multiple oncogenes, including *EGFR*, *RAS* (*KRAS* and H*RAS*), *MYC*, and *TGFβ*, that overlap with the oncogenes in E1-E70 studies, and histone/DNA modifiers to interact on paths to malignancy in a context driven manner [282]. Lactate can activate *TGFβ* [283-286]. Also, "upregulation of oncogenic pathways" has been described in clinically evident precancerous lesions of 12 different types of malignancies in studies reviewed recently [287].

The collective influence of multiple oncogenes on downstream potassium channels may promote K^+ flux at inner membranes of tumor cells, possibly with refilling needed if outflow via large flow K^+ channels is anomalously high. Oncogenes could be involved upstream in promoting K^+/H^+ exchange leading to pH reversal. The 50 KCN studies related to 7 oncogenes and/or histone/DNA modulation were significantly (p = 0.0325) more likely to have at least one or more KCN DEG encoding a H^+-sensitive protein than the other 20 KCN studies in “no category”.

Retrieval of citation data from PubMed revealed a significant correlation in the numbers of studies of H^+ with K^+ across all 8 categories of 7 oncogenes and histone in 2-word searches without restriction to cancer. However, the category for MET had to be removed to achieve a comparable correlation of H^+ with K^+, when searches were restricted to “cancer” using 3-word searches (Figure 4C). Although explanations require definitive studies, this may reflect under-reporting of negative studies. The PubMed citations reveal that citations for BK (*KCNMA1* encoded) probably constitute a large proportion (approximately one third) of studies involving K^+ and H^+ across the categories of 7 oncogenes and “histone” not restricted to cancer and the BK citations may represent most of the studies when restricted to “cancer” (Figure 4B-C). Findings in this study are consistent with at least some H^+-sensitive KCN DEG in addition to *KCNMA1*/BK being influenced by six oncogenes (those listed previously but not MET) and histone modulation related to K^+ flux (possibly via activation of ACLY, see *Section 1.3. Metabolic Need for Proton Extrusion in Cancer*). Oncogenes and histone modulation through KCN genes/proteins may play a role in H^+ dynamics.

4.5. Non-KCN DEG in Multiple E1-E70 Studies

In E1-E70, the most frequent non-KCN DEG found was *ITGA2* in 7 studies, and *HMGA2*, *LIF*, and *PLAUR* were each found in 6 studies with *ITGA2*, *LIF*, and *PLAUR* shown in Venn diagrams (Figure 5A). Also, to support the relevance of cancer gene expression studies with unbiased detection of KCN DEG, six non-KCN DEG, i.e. *FGFR3*, *GDF15*, *IGFBP3*, *IGFBP7*, *KRT19*, and *PLAUR*, each included in at least 4 of the E1-E70 studies, were also identified by others as encoding circulating proteins associated with a risk of cancer [224,225]. *PLAUR*, found in 6 of E1-E70 studies, was also co-expressed with the most frequent KCN genes that are also H^+-sensitive, *KCNN4* and *KCNMA1* in 4 and 2 studies, respectively. *KCNN4*, *PLAUR*, and *PLAU* were detected together as DEG (Figure 5A) in E49 [167], a study associated with 3 categories, RAS, TP53, and His/Chr/Epi. BK (encoded by *KCNMA1*) citations in PubMed correlated with those for PLAUR + PLAU and ITGA2 (Figure 5B).

4.6. Specific Roles for Redistribution of K^+ in Cancer

Studies on intracellular pH-regulating systems, potassium channel inhibitors have been used with interesting results, including "slower recovery from CO_2 acidification" in early frog skeletal muscle experiments [288]. Potassium channels have been recognized as playing important roles in cancer, including volume changes [289,290] but without also considering K^+ for exchange with H^+ on fixed anions to then incite cytoplasmic proton transfers to cell exit sites. The intermediate step of rapid cytoplasmic proton transfer is plausible. Volume changes in cancer cells, problems in their blood supply, stiff tissues constraining migrating cells, etc. that lead to microaqueous conditions in the cytoplasm may help generate Grotthuss conditions that build a putative water-wire type root system to supply proton extruders.

Removal of K^+ from cell interiors may occur via flux of unsolvated K^+ through KCN channels after it has lost its aggregated water. Large outward (*KCNMA1*/BK), intermediate outward (*KCNN4*/IK), bidirectional (*KCNJ10-KCNJ16*/Kir4.1-Kir5.1 dimers or homomeric versions), etc. may alter cytosolic flows to bring centrally located intracellular water via K^+-$7H_2O$ (loosely aggregated) to the cell periphery where water wires form to provide rapid proton transfers. Alternatively, simultaneous changes in Cl^- channels (CLCN detected only once as a DEG in E1-E70 was *CLCN7*) and aquaporins (only a few DEG in E1-E70, see earlier Discussion) could help redistribute intracellular water but stochastically their participation as major players seemed unlikely in E1-E70 based on DEG detected. Na^+ binds water tightly so it is probably not responsible for water redistribution (See Introduction *1.4. Complexity of K^+ Flux,* 4th paragraph for related information on Na^+). Redistributed water regionally within cells may promote appropriate Grotthuss conditions, especially during cell migration but is not established as doing so.

K^+ released outside the cells through high volume calcium gated K^+ channels, etc. could be recycled via refilling through KCN channels (if available) or by Na/K-ATPase that brings K^+ in across cell membranes that could also displace fixed H^+ ions. Accumulated K^+ near the high flow outward channels prior to its release may displace fixed H^+ ions. The intermediate and large conductance K^+ channels encoded by, *KCNN4* and *KCNMA1*, respectively, found 9 and 6 times, respectively, and other KCNNs (*KCNN2*, *3*) and the KCNMBs (*KCNMB1*, *2*, *3*, *4* whose products regulate *KCNMA1*/BK) were found as DEG

in 5 and 8 studies, respectively, (only a few in the same studies) in E1-E70. Kir4.1 and Kir5.1 encoded by *KCNJ10* and *KCNJ16*, respectively, were found in 2 and 4 studies, respectively, in E1-E70 studies. Also, *KCNJ16* was detected as a DEG (less expression in glioblastomas versus oligodendrogliomas) in REMBRANDT, and with less expression in the 6 glioblastoma cell lines versus normal when studied by Patil, et al. [22]. Also, *KCNMB2* and *KCNJ16* are genes predicted to be negatively affected on chromosomes 3 and 17, respectively, in U87 glioblastoma cells, Supplemental Table 3 in Clark et al. [139]. Additionally, redistribution of K^+ away from mitochondria within the cells' interior may affect mitochondrial K^+-dependent enzymes to influence malignant behavior. The alkaline pH of cancer cell cytoplasm in pH reversal activates ACLY which can lead to histone changes to possibly help explain the correlation of 50 studies in E1-E70 with KCN DEG that encode H^+-sensitive proteins with 8 categories of histone/DNA modulators and 7 oncogenes (Figure 4B).

The E1-E70 study results only revealed gene expressions that crossed thresholds set by the authors of each study for significance (mostly $p < 0.05$) independently of any KCN consideration. Lower gene expression levels may be collectively biologically relevant in a network of KCN encoded proteins mediating potassium flux. Co-expression of non-KCN DEG (Figure 5) may become relevant as a signature of K^+ dynamics if they occur in additional studies.

SUMMARY

Migration and settling assays provided data to support and focus further experimental investigation of potassium flux in cancer cells. Although the reversed pH of cancer cells, generated via acid export by multiple extruders, is well established and of potential therapeutic value, the initiating events potentially involving potassium in providing intracellular protons to proton extruders could yield additional therapeutic targets. The multiple tumor models and range of study approaches used by many authors produced stochastic evidence for the large KCN potassium channel family playing a role in at least a subset of malignancies, with H^+-sensitive members as potential downstream effectors of oncogenes. Although any future therapeutic suggestions regarding alterations of potassium channels carries concern regarding effects on the heart [291], the role for potassium channels as mediators of K^+ flux that promotes K^+/H^+ exchange for proton transfer and subsequent efflux needs further exploration in cancer. The stochastic view of cancers based on unbiased studies detecting KCN genes incidentally in genomic landscapes suggests that encoded H^+-sensitive KCN proteins may be downstream effectors of one or more drivers in cancer. Oncogenes may promote adaptation to adverse events and genetic damage to cells, including KCN genes, to optimize cell fitness for survival, possibly as a spectrum of ongoing changes that include the extreme outcome of becoming dedifferentiated, single migrating cells, via pH reversal. Also, cancer specific structural alterations of surface proteins encoded by genetically flawed KCN genes may add to the repertoire of targets for immune attack in personalized medical treatments. Author curated, published gene landscapes in complex cancer studies are useful for stochastically identifying candidates in the large KCN gene family that encode downstream effectors of oncogenes that may initiate pH reversal. They also offer cancer

antigens to consider. Also, tumor models are identified in this manner where significant changes in KCN gene expression have been seen in malignancy.

Funding: The cell settling and cell migration research was funded by the Walter L. Copeland Fund for Cranial Research, The Pittsburgh Foundation, Pittsburgh, PA, D2003-0305 and D2006-0379; The Nick Eric Wichman Foundation, Ellicott City, MD, No Number; The Beez Foundation, Somerset, NJ., No Number; and the American Heart Association, Ohio Valley Affiliate, AHA 9960398V.

Data Availability Statement: Data generated in this study will be available upon request from the corresponding author. Please note that data from REMBRANDT per Adobe Flash (not available after 12/31/2020) can be seen in Figure 6 except for a few instances described which can also be made available on request. KCN gene data obtained from the published manuscript by Patil, V. et al. (22) follows the terms of their statement "an open access article distributed under the terms of the Creative Commons Attribution License, which permits unrestricted use, distribution, and reproduction in any medium, provided the original author and source are credited". 34%, 31%, 13%, and 6% of the papers used in the E1-E70 study were found in Cancer Research, Cancer Cell, Nature Communications, and Journal of Molecular Diagnostics, respectively. Others are from 11 journals, 1 paper each. Papers for E1 – E70 are cited in Section *3.3.6. Categories Among Studies with E1-E70 Citations Per Category*.

Acknowledgements: Ian F. Pollack, MD, University of Pittsburgh, Children's Hospital of Pittsburgh, provided laboratory space, supplies, technicians, and glioblastoma cell lines, George K. Michalopoulos, MD, PhD, Department of Pathology, University of Pittsburgh, provided information on hepatocyte growth factor and MET. The Departments of Pathology and Neurological Surgery, University of Pittsburgh, provided institutional support for cell settling and migration experimental work. The 1301 authors of 70 papers (E1-E70) are thanked for outstanding contributions to the medical science literature used for gathering stochastic information on the KCN gene family while at Kent State, Kent, OH. I thank the Brain Health Research Institute of Kent State University, Kent, Ohio, as a current member, for technical advice and ongoing academic research activities.

Conflicts of Interest: The author declares no conflicts of interest. The funders had no role in the design of the study; in the collection, analyses, or interpretation of data; in the writing of the manuscript; or in the decision to publish the results.

Abbreviations

The following abbreviations are used in this manuscript.

ACLY	ATP Citrate Lyase
Arg1	Arginase 1
AS	Anti-seizure
BK	Big K (encoded by *KCNMA1)*
BSA	Bovine serum albumin
CD	Cluster Differentiation
CLCN	Chloride Channels gene family, *CLCN1,2,3*, etc.
COL	Collagen
CSM	Cancer Specific Mutation

Cx	Connexin
DEG	Differentially expressed gene(s)
E	Expression
EAAT	Excitatory Amino Acid Transporter
EAG1	Ether-A-Go-Go-K^+ Channel Protein 1
ELK1,2	EAG Like K^+ Channel Proteins 1,2
EMT	Epithelial Mesenchymal Transition
ERG1,3	EAG Related Gene K^+ Channel Proteins 1,3
FBS	Fetal bovine serum
GABA	Gamma-aminobutyric acid
GBM	Glioblastoma
G-DOC	Georgetown Database of Cancer
Girk3,4	G protein-activated Inward Rectifier K^+Channel Proteins, 3,4
GPR	G-protein Coupled Receptor
G-proteins	Guanosine-triphosphate-binding proteins
GWATERW	Grotthuss water wire
HGF	Hepatocyte growth factor
His/Chr/Epi	Histone/Chromatin/Epigenetic
HKG	House-keeping gene
IK	Intermediate K (encoded by *KCNN4*)
Indels	Insertions and Deletions
ITAG2	Integrin 2
ITG	Integrin
K2P	Tandem 2 pore domain KCN subfamily proteins
Kca	Calcium stimulated KCN subfamily proteins
Kchip1,3	Kv channel interacting proteins 1,3
KCNA	Subgroup of KCN genes, *KCNA1,2,3,etc.*
KCNAB	Subgroup of KCN genes, *KCNAB1,2,3*
KCNB	Subgroup of KCN genes, *KCNB1,2*
KCNC	Subgroup of KCN genes, *KCNC1,2,3,etc.*
KCND	Subgroup of KCN genes, *KCND1,2,3*
KCNE	Subgroup of KCN genes, *KCNE1,2,3, etc.*
KCNG	Subgroup of KCN genes, *KCNG1,2,3,etc.*
KCNH	Subgroup of KCN genes, *KCNH1,2,3, etc.*
KCNIP	Subgroup of KCN genes, *KCNIP1,2,3, etc.*
KCNJ	Subgroup of KCN genes, *KCNJ1,2,3, etc.*
KCNK	Subgroup of KCN genes, *KCNK1,2,3, etc.*
KCNM	Subgroup of KCN genes, *KCNM,A1,B1,B2, etc.*
KCNN	Subgroup of KCN genes, *KCNN1,2,3, etc.*
KCNQ	Subgroup of KCN genes, *KCNQ1,2,3, etc.*
KCNS	Subgroup of KCN genes, *KCNS1,2,3, etc.*
KCNT	Subgroup of KCN genes, *KCNT1,2*
Kir	Inwardly directing KCN subfamily proteins
Kv	Voltage dependent KCN subfamily proteins

LDH	Lactate dehydrogenase
LIF	Leukemia Inhibitory Factor
MCT	Monocarboxylate transporter
MEM	Minimal Essential Media
Mes	Mesenchymal
MiRP	MinK (minimal K^+channel protein related peptide)
Na/K ATPase	Sodium/potassium ATPase
NOX	NADPH oxidases
Oligo	Oligodendroglioma
OMG	Oligodendroglioma Minus Glioblastoma
OMIM	Online Mendelian Inheritance in Man
PBS	Phosphate buffered saline
pHe	Extracellular pH
pHi	Intracellular pH
PIP2	Phosphatidyl inositol 4,5 bisphosphate
R	Pearson product-moment correlation
REMBRANDT	Repository of Molecular Brain Neoplasia Data
RGS	Regulator of G protein signaling
ROS	Reactive oxygen species
RRID	Research Resource Identifier
SERPIN	Serine proteinase inhibitors
SNV	Single Nucleotide Variant
SK	Small K (encoded by some *KCNN* genes)
Slack	Sequence like a calcium -activated K^+ channel protein
SLC	Solute Carrier
Slick	Sequence like intermediate Con-ductance K^+ channel protein
SOX	Sry-related HMG BOX
TasK1,2,5	Twik-related Acid Sensitive K^+ channel proteins 1,2,5
Thik2	Tandem pore domain Halothane Inhibited K^+ channel protein 2
TMEM	Transmembrane
TNFRSF	Tumor Necrosis Factor Receptor Super Family
Trek1	Twik-Related K^+ channel protein 1
TwiK1,2	Tandem pore domain in Weak Inward Rectifying K^+ Channel proteins 1,2
uPA	Urokinase-Type Plasminogen Activator

Appendix A

Figure A1.

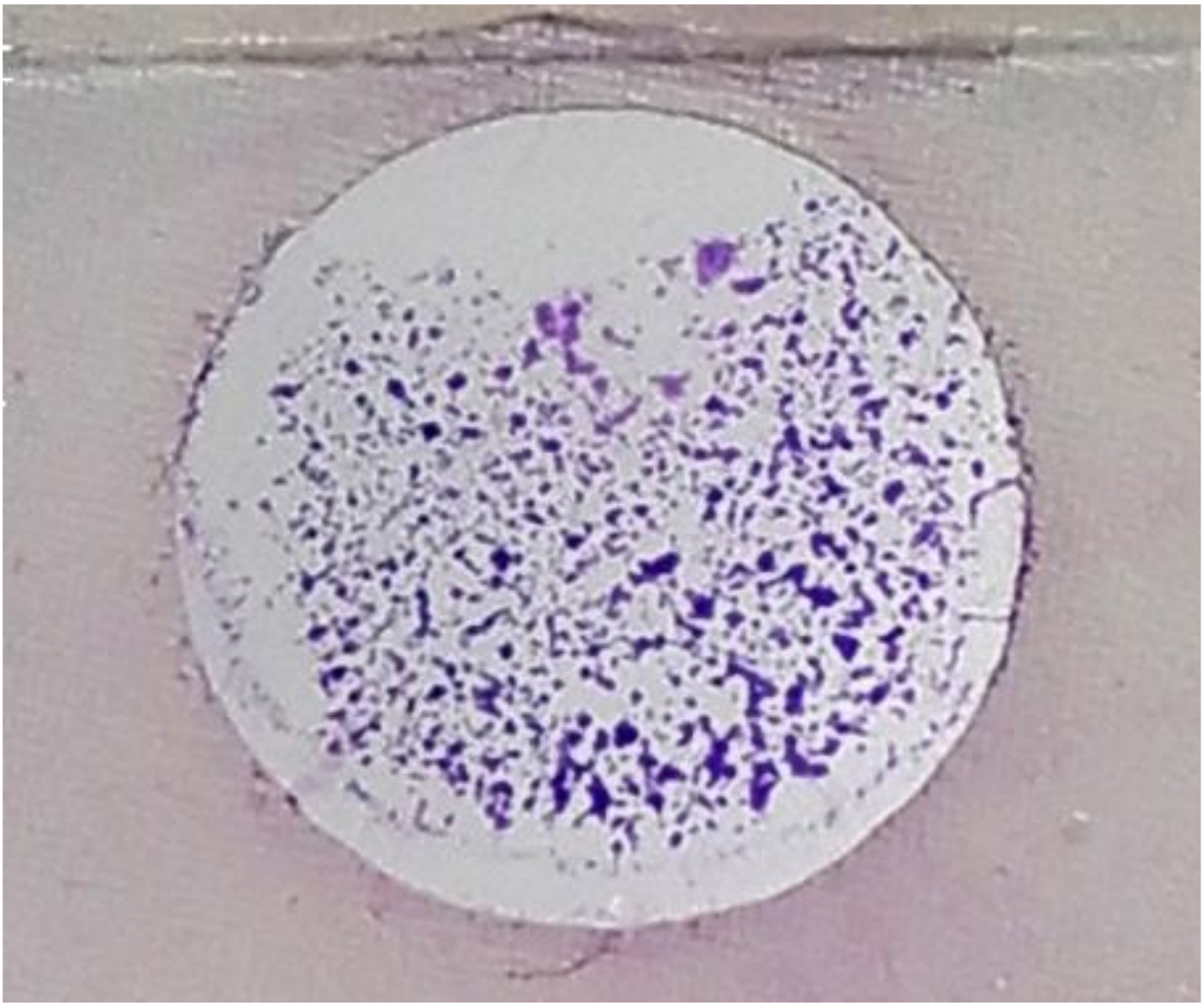

Figure A1. Macroscopic view of settled T98G glioblastoma cells on a Neuro Probe microscopic slide. One of 8 round 7 mm diameter areas that had been the bottom of a settling chamber well. Some cell clumping is noted. Diff Quik stain.

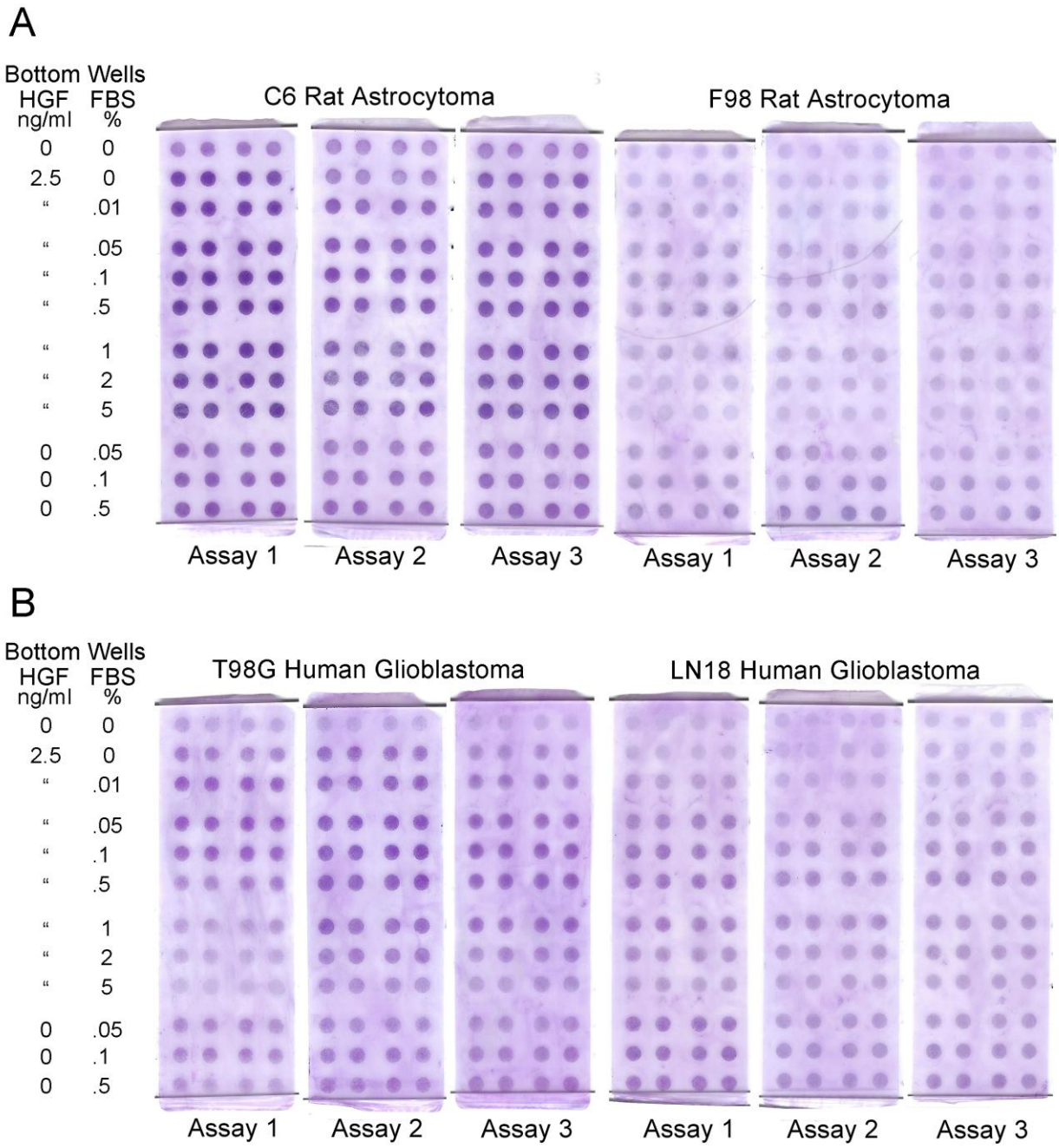

Figure A2. All three migration assays for each cell line (C6, F98, T98G, and LN18) in studies of HGF and FBS chemoattraction. One assay per cell line is shown in Figure 2A. Portions of assays that were digitized and analyzed are shown in Figure 2B. Text in Section 3.2. *Cell Migration with HGF and Serum Chemoattraction* and the Figure 2 legend provide additional information. Each circle of stained migrated cells is 3 mm in diameter.

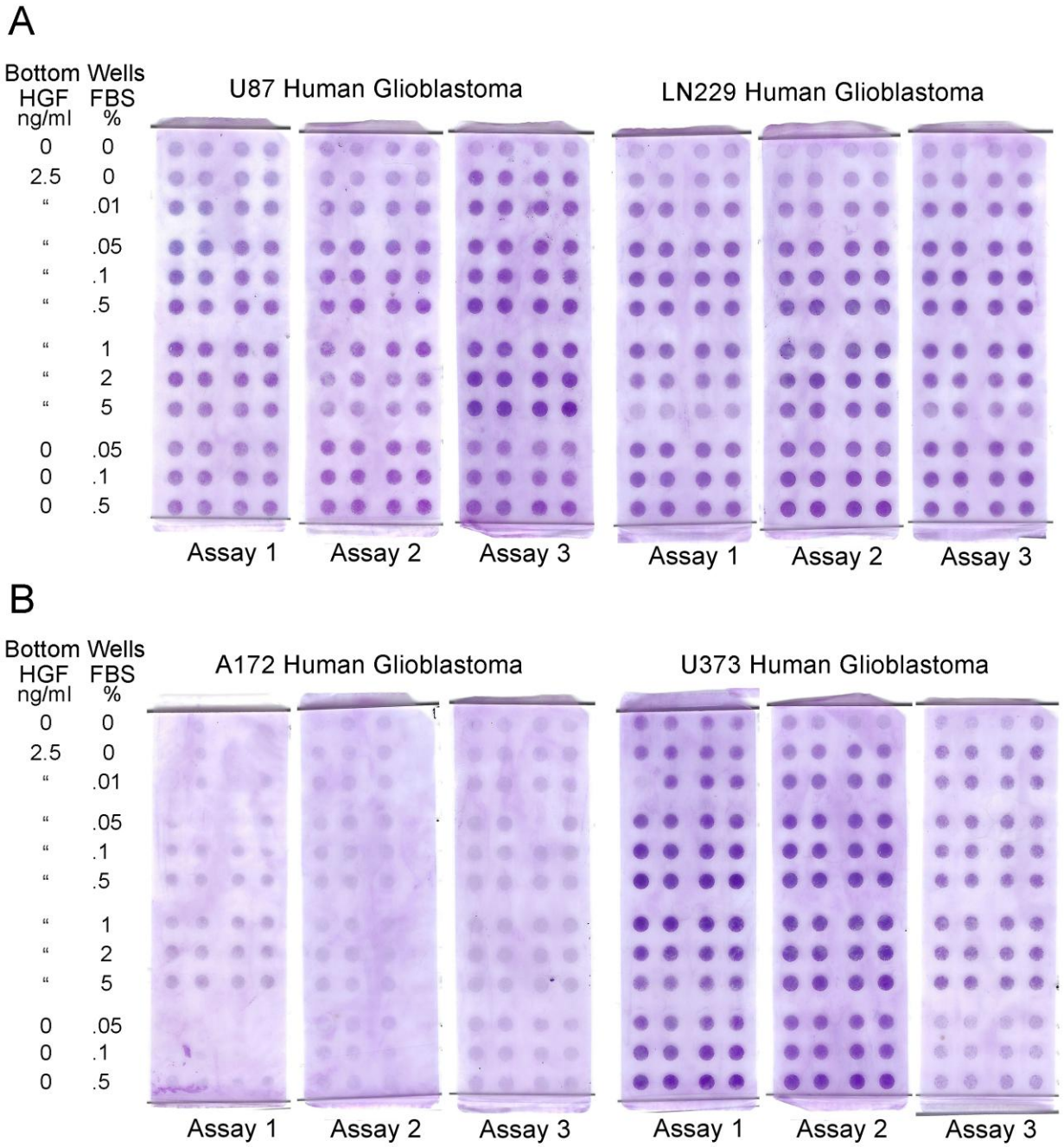

Figure A3. All three migration assays for each cell line (U87, LN229, F98, A172, and U373) in studies of HGF and FBS chemoattraction. One assay per cell line is shown in Figure 2A. Portions of assays that were digitized and analyzed are shown in Figure 2B. Text in Section 3.2. *Cell Migration with HGF and Serum Chemoattraction* and the Figure 2 legend provide additional information. Each circle of stained migrated cells is 3 mm in diameter.

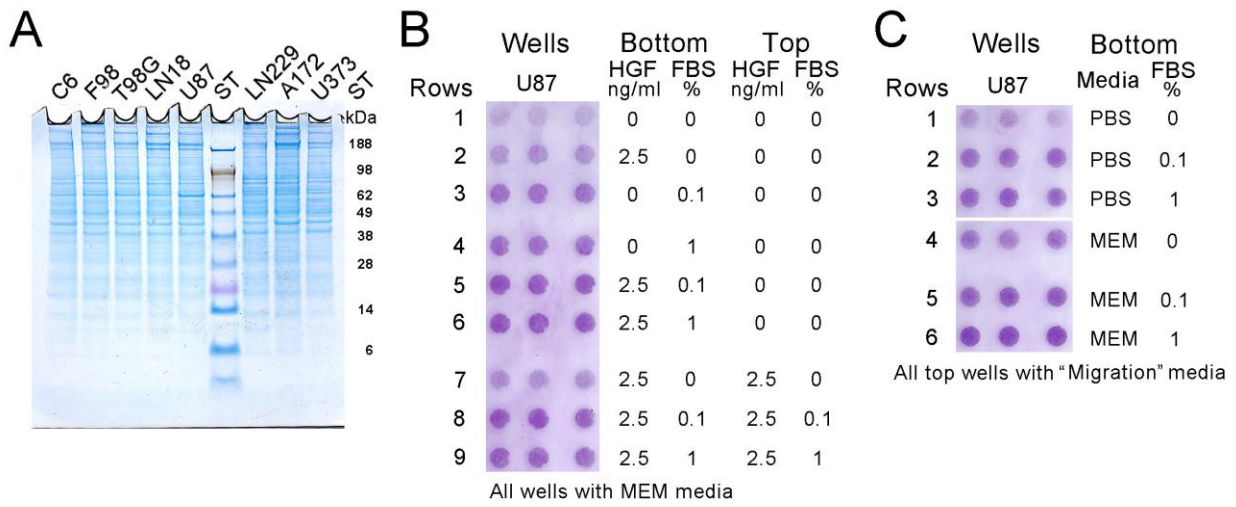

Figure A4. Additional images for Figure 2. (A) Gel image for the immunoblot in Figure 2C showing equal loading of protein in each lane for all 8 cell lines. (B) Scanned image of the U87 migration assay shown in Figure 2D. Chemoattraction of HGF and 2 concentrations of FBS and chemokinesis of HGF, with and without 2 concentrations of FBS, were analyzed in U87 cells. (C) Scanned image of the U87 migration assay shown in Figure 2E. Dulbecco's PBS and MEM were tested as media in the lower wells for migration without and with 2 concentrations of FBS present. The image of the filter removed (white horizontal line) an unrelated portion of the assay that tested a different batch of FBS for suitability in future migration assays. Text in Section 3.2. *Cell Migration with HGF and Serum Chemoattraction* and the Figure 2 legend provide additional information. Each circle of stained, migrated cells is 3 mm in diameter.

Appendix B

Table B1. A sample of alphabetized differentially expressed genes (DEG) in E1-E70 studies. See FullTblB1DEGalphaAZ for the entire list of DEG in a table format after the References.

DEG Name	Study Number
A2M	E21
AAK1	E65
AATK	E54
AB113AP	E1
ABCA1	E50
ABCA12	E54
ABCB10	E48
ABCB1A	E69
ABCC3	E70
ABCD1	E31
See full list…	See full list…

Table B2. KCN genes in E1-E70 studies that encode H^+-sensitive proteins.

KCN Gene	Protein	Reference
KCNA1	Kv1.1	[292]
KCNA3	Kv1.3	[293,294]
KCNA5	Kv1.5	[295-301]
KCNAB2	Kvbeta2	[302,303]
KCND3	Kv4.3	[304-306]
KCNE2	MiRP1	[85,307-311]
KCNE3	MiRP2, R83H variant	[253]
KCNH1	Kv10.1, EAG1	[254,312]
KCNH2	Kv11.1, HERG1	[254,313-325]
KCNH3	Kv12.2, ELK2	[254]
KCNH8	Kv12.1, ELK3	[254,326]
KCNJ5	Kir3.4, GIRK4	[255,256,327]
KCNJ8	Kir6.1, KATP-1	[327-333]
KCNJ10	Kir4.1, BIRK10	[334-336]
KCNJ10/KCNJ16	Kir4.1/Kir5.1heterodimer	[72,326,337-343]
KCNJ13	Kir7.1	[72,327,344]
KCNK1	K2P1, TWIK1	[343,345-350]
KCNK2	K2P2, TREK1	[343,348,351-357]
KCNK3	K2P3, TASK1	[343,346,348,355,358-361]
KCNK5	K2P5, TASK2	[237,343,346,348,362-369]
KCNK6	K2P6, TWIK2	[346,370,371]
KCNK15	K2P15, TASK5	[372]
KCNMA1	KCa1.1, BK, Slo1, maxiK	[96,373-388]
KCNMB4	BKbeta4	[389-393]
KCNN2	KCa2.2, SK2	[394]
KCNN3	KCa2.3, SK3	[394]
KCNN4	KCa3.1, SK4, Gardos	[394-397]
KCNQ1	Kv7.1, KvLQT1	[85,237,307-309,311,399-405]
KCNQ2	Kv7.2	[402(described data),406,407]
KCNQ3	Kv7.3	[406]
KCNQ5	Kv7.5	[408]
KCNT1	KCa4.1, Slo2.2, KNa1.1	[409-412]
KCNU1	KCa5.1, Slo3, KCNMA3	[389,412-418]

A

	Types of Malignancy with KCNs Among Differentially Expressed Genes (DEG)	# of Studies	Specific studies with H+-sensitive KCN DEG underlined
1	Adrenocortical carcinoma/?precursor	2	E32 (J5), E68 (K2)
2	Acute myelogenous leukemia	2	E11 (K6), E59 (Q3)
3	Bladder carcinoma	1	E7
4	Breast carcinoma (See E_)	9	E1, E4 (N3), E9 (H1, K15), E15, E22 (K5, K15), E33, E38 (MA1), E48, E63
5	Chordoma	1	E24 (K2)
6	Chronic lymphocytic leukemia	1	E37
7	Colorectal carcinoma	4	E2 (Q1), E36 (N4), E61 (K1), E63
8	Cutaneous squamous carcinoma	1	E44
9	Ependymoma	1	E57 (J16)
10	Ewing sarcoma	1	E10 (E3)
11	Gastric carcinoma	2	E13 (MA1), E45
12	Glioblastoma (See E_)	7	E5 (J10, N3), E21 (AB2), E26 (E2, J13), E27, E31 (J8, J10), E50 (D3), E51 (J16, N2)
13	Liposarcoma	1	E18 (MB4)
14	Liver carcinoma	2	E20, E64 (N4)
15	Lung carcinoma (See E_)	11	E3 (K1), E8 (K1, N4), E12 (A1, H8), E23 (U1), E30, E35 (K1), E43 (K6), E49 (N4), E54 (J13), E63, E67
16	Lymphoma	2	E47 (A3), E53 (N4)
17	Malignant peripheral nerve sheath tumor	1	E70 (H2)
18	Medulloblastoma	2	E6 (A1), E55 (Q1)
19	Melanoma	3	E14 (Q5), E39 (MA1), E41 (MA1, N4)
20	Multiple myeloma	1	E28 (N3)
21	Neuroblastoma	3	E17 (Q2, Q5), E56, E66
22	Ovarian carcinoma	4	E25, E34 (A1, N3, T1), E58 (A5, H3, H8, J16, MB4, N4, Q1), E60 (MA1)
23	Pancreatic ductal carcinoma	2	E42 (E3), E69 (N4)
24	Pituitary neuroendocrine tumor	1	E65
25	Prostate carcinoma	3	E40 (MA1, Q5), E52 (K15, N4), E62 (AB2)
26	Renal carcinoma	3	E19 (J16), E29, E63
27	Synovial sarcoma	1	E46 (Q2)
28	Thyroid carcinoma	1	E19 (J16)
29	Uterine endometrial carcinoma	1	E63

B

KCN Family	Common informative protein abbreviations
KCNH	EAG1 - Ether-A-Go-Go-K+ channel protein 1
	ELK1,2 - EAG Like K+ channel proteins 1,2
	ERG1,3 - EAG Related Gene K+ channel proteins 1,3
KCNJ	Girk3,4 - G protein-activated Inward Rectifier K+ channel proteins 3,4
KCNIP	Kchip1,3 - Kv channel interacting proteins 1,3
KCNE	MiRP - MinK(minimal K+ channel protein (also ISK)) related peptide
	MiRP2,3 - MiRP2,3
KCNT	Slack - Sequence Like A Calcium-activated K+ channel protein (also K channel, Na activated, subfamily member 1)
	Slick - Squence Like Intermediate Conductance K+ channel protein (also Sodium and chloride activated ATP sensitive K+ channel protein)
KCNK	Twik 1,2 - Tandem pore domains in Weak Inward Rectifying K+ channel proteins 1,2
	Task 1,2,5 - Twik-related Acid Sensitive K+ channel proteins 1,2,5
	Thik2 - Tandem pore domain Halothane Inhibited K+ channel protein 2
	Trek1 - Twik-Related K+ channel protein 1
KCNJ	UKATP1 - ATP sensitive inward rectifier K+ channel protein 8

Figure B1. Types of malignancies studied in E1-E70 and informative protein abbreviations for proteins in the KCN family are listed. **(A)** Specific studies are listed for each type of 29 malignancies with their detected KCN DEG. Red underlining indicates the KCN DEG that encode H^+-sensitive proteins. Boxes that correspond with studies of brain, breast, and lung malignancies are color coded, yellow, pink, and blue, respectively. These graphics are also used in the histograms shown in Figures 3 and 4. (**B**) Some of the common protein abbreviations for KCN family members in Figure 3 indicating functional information not explained in the text are included.

Text B1. Potential Interactions of KCN Proteins with H^+-Sensitive G Protein-Coupled Receptors.

Multiple KCN proteins have interactions with four G protein-coupled receptors encoded by *GPR4*, *65*, *68*, and *151* that are among 6 reported to be H^+-sensitive [419-425]. H^+-sensitive proteins encoded by GPR genes are found in many types of tumors [423,424,426,427]. Functional complementation between proteins encoded by *GPR4* and *KCNK5*/TASK2 [427,428,429] and related expression profiles of proteins encoded

by *GPR31*, G*PR151*, *KCNK3*/TASK1, and *KCNK9*/TASK3 have been found in tumors [425]. STRING interactions (Gene Cards, 10/17/2024) of proteins encoded by *GPR4*, *65*, *68*, and*151* as a group included proteins encoded by 9 KCNs, *KCNJ8*, *K1, K2, K4, K5*, *K10*, *K16*, *K17*, and *K18*. Among these, 8 of the 70 studies (E3, 8, 22, 24, 31,35, 61, 68) detected *KCNJ8*, *K1, K2, K5* as DEG. Also, although *GPR39*'s encoded protein is not reported to be H^+-sensitive, it interacts with the four H^+-sensitive proteins encoded by *GPR4*, *65*, *68*, and *132*. *GPR39* is a DEG found in 2 of the 70 studies, E14 [194] and E60 [177], that also detected *KCNQ5* and *KCNMA1*, respectively. The ligand of the protein encoded by *GPR39* is encoded by *GPNMB* [430] and *GPNMB* was a DEG in 3 studies, E26 [213], E29 [158], and E49 [167]. *GPR35*'s protein (also not H^+-sensitive) interacts with *GPR4*'s encoded H^+-sensitive receptor protein. *GPR35* is a DEG in two studies that found *KCNG2* and *KCNE3*, in E20 [211] and E42 [218], respectively. The ligand for *GPR35*'s receptor protein is kynurenic acid [431]. *GPR84*'s protein (also not H^+-sensitive) interacts with *GPR65*'s encoded H^+-sensitive receptor protein. *GPR84* is a DEG from two studies that found *KCNK6* in E11 [174] and *KCNK12* and *KCNU1* in E23 [202]. The ligands for *GPR84*'s receptor protein are medium-chain fatty acids [432]. Thirteen of the14 studies (out of 70) with potential indirect GPR protein sensitivity to H^+ also detected KCN DEG that encode H^+-sensitive proteins. Potentially, KCN DEG encoded proteins in 13 (18.6%) of the E1-E70 studies have indirect involvement with H^+-sensitive G-protein-coupled receptor proteins via STRING interactions (Gene Cards, 10/17/2024) or as described above according to the cited literature. They may function collaboratively with GPR encoded H^+-sensitive proteins in tumors.

References

1. Burger PC, Scheithauer BW. Tumors of the Neuroglia and Choroid Plexus. Tumors of the Central Nervous System. Washington, D.C.: American Registry of Pathology; 2007. p 55-77.
2. Ge L, Hoa NT, Wilson Z, Arismendi-Morillo G, Kong XT, Tajhya RB*, et al.* Big Potassium (BK) ion channels in biology, disease and possible targets for cancer immunotherapy. Int Immunopharmacol **2014**;22:427-43
3. Freshney RI. Defined media and supplements. Table 8.6. Constituents of serum. In: Capes-Davis A, Gregory C, Przyborski S, editors. Culture of Animal Cells. Hoboken, New Jersey: John Wiley & Sons, Inc.; 2016. p 141.
4. Kros JM. Grading of gliomas: the road from eminence to evidence. J Neuropathol Exp Neurol **2011**;70:101-9
5. Puchalski RB, Shah N, Miller J, Dalley R, Nomura SR, Yoon JG*, et al.* An anatomic transcriptional atlas of human glioblastoma. Science **2018**;360:660-3
6. Brat DJ, Castellano-Sanchez AA, Hunter SB, Pecot M, Cohen C, Hammond EH*, et al.* Pseudopalisades in glioblastoma are hypoxic, express extracellular matrix proteases, and are formed by an actively migrating cell population. Cancer Res **2004**;64:920-7
7. Rong Y, Durden DL, Van Meir EG, Brat DJ. 'Pseudopalisading' necrosis in glioblastoma: a familiar morphologic feature that links vascular pathology, hypoxia, and angiogenesis. J Neuropathol Exp Neurol **2006**;65:529-39
8. Chesler M, Kraig RP. Intracellular pH of astrocytes increases rapidly with cortical stimulation. Am J Physiol **1987**;253:R666-70
9. Chesler M, Kraig RP. Intracellular pH transients of mammalian astrocytes. J Neurosci **1989**;9:2011-9
10. Brookes N. Intracellular pH as a regulatory signal in astrocyte metabolism. Glia **1997**;21:64-73
11. Theparambil SM, Weber T, Schmalzle J, Ruminot I, Deitmer JW. Proton Fall or Bicarbonate Rise: Glycolytic Rate in Mouse Astrocytes Is Paved By Intracellular Alkalinization. J Biol Chem **2016**;291:19108-17

12. Vaupel P, Kallinowski F, Okunieff P. Blood flow, oxygen and nutrient supply, and metabolic microenvironment of human tumors: a review. Cancer Res **1989**;49:6449-65
13. Boron WF. Regulation of intracellular pH. Adv Physiol Educ **2004**;28:160-79
14. Andersen AP, Moreira JM, Pedersen SF. Interactions of ion transporters and channels with cancer cell metabolism and the tumour microenvironment. Philos Trans R Soc Lond B Biol Sci **2014**;369:20130098
15. Spugnini EP, Sonveaux P, Stock C, Perez-Sayans M, De Milito A, Avnet S*, et al.* Proton channels and exchangers in cancer. Biochim Biophys Acta **2015**;1848:2715-26
16. Swietach P, Vaughan-Jones RD, Harris AL, Hulikova A. The chemistry, physiology and pathology of pH in cancer. Philos Trans R Soc Lond B Biol Sci **2014**;369:20130099
17. Swietach P, Boedtkjer E, Pedersen SF. How protons pave the way to aggressive cancers. Nat Rev Cancer **2023**;23:825-41
18. McIntyre A, Hulikova A, Ledaki I, Snell C, Singleton D, Steers G*, et al.* Disrupting Hypoxia-Induced Bicarbonate Transport Acidifies Tumor Cells and Suppresses Tumor Growth. Cancer Res **2016**;76:3744-55
19. White KA, Grillo-Hill BK, Barber DL. Cancer cell behaviors mediated by dysregulated pH dynamics at a glance. J Cell Sci **2017**;130:663-9
20. Bhuvaneshwar K, Belouali A, Singh V, Johnson RM, Song L, Alaoui A*, et al.* G-DOC Plus - an integrative bioinformatics platform for precision medicine. BMC Bioinformatics **2016**;17:193
21. Madhavan S, Gusev Y, Harris M, Tanenbaum DM, Gauba R, Bhuvaneshwar K*, et al.* G-DOC: a systems medicine platform for personalized oncology. Neoplasia **2011**;13:771-83
22. Patil V, Pal J, Somasundaram K. Elucidating the cancer-specific genetic alteration spectrum of glioblastoma derived cell lines from whole exome and RNA sequencing. Oncotarget **2015**;6:43452-71
23. Deplazes E, Poger D, Cornell B, Cranfield CG. The effect of H(3)O(+) on the membrane morphology and hydrogen bonding of a phospholipid bilayer. Biophys Rev **2018**;10:1371-6
24. Eigen M, De Maeyer L. Self-dissociation and protonic charge transport in water and ice. Proc R Soc (Lond) A **1958**;247 A.:505-33
25. Johnson DE, Casey JR. Cytosolic H+ microdomain developed around AE1 during AE1-mediated Cl-/HCO3- exchange. J Physiol **2011**;589:1551-69
26. Vaughan-Jones RD, Peercy BE, Keener JP, Spitzer KW. Intrinsic H(+) ion mobility in the rabbit ventricular myocyte. J Physiol **2002**;541:139-58
27. Xie F, Tikhonov DS, Schnell M. Electric nuclear quadrupole coupling reveals dissociation of HCl with a few water molecules. Science **2024**;384:1435-40
28. Grotthuss CJT. Memoire sur la decomposition de l'eau et des corps qu'elle tient en dissolution a l'aide de l'electricite galvanique. Ann Chim **1806**;58:54-74
29. Adelroth P. Preface: Special issue on proton transfer in biological systems. Biochem Biophys Acta **2006**;1757:867-70
30. Cukierman S. Et tu, Grotthuss! and other unfinished stories. Biochim Biophys Acta **2006**;1757:876-85
31. Gutman M, Nachliel E, Friedman R. The mechanism of proton transfer between adjacent sites on the molecular surface. Biochim Biophys Acta **2006**;1757:931-41
32. Mulkidjanian AY, Heberle J, Cherepanov DA. Protons @ interfaces: implications for biological energy conversion. Biochim Biophys Acta **2006**;1757:913-30
33. Ben-Amotz D. Electric buzz in a glass of pure water. Science **2022**;376:800-1
34. Kariev AM, Green ME. Water, Protons, and the Gating of Voltage-Gated Potassium Channels. Membranes (Basel) **2024**;14

35. Horowitz SB, Paine PL. Reference phase analysis of free and bound intracellular solutes. II. Isothermal and isotopic studies of cytoplasmic sodium, potassium, and water. Biophys J **1979**;25:45-62
36. Schornack PA, Gillies RJ. Contributions of cell metabolism and H+ diffusion to the acidic pH of tumors. Neoplasia **2003**;5:135-45
37. Schwab A, Wojnowski L, Gabriel K, Oberleithner H. Oscillating activity of a Ca(2+)-sensitive K+ channel. A prerequisite for migration of transformed Madin-Darby canine kidney focus cells. J Clin Invest **1994**;93:1631-6
38. Schwab A, Nechyporuk-Zloy V, Fabian A, Stock C. Cells move when ions and water flow. Pflugers Arch **2007**;453:421-32
39. Horio Y. Potassium channels of glial cells: distribution and function. Jpn J Pharmacol **2001**;87:1-6
40. Sontheimer H. An unexpected role for ion channels in brain tumor metastasis. Exp Biol Med (Maywood) **2008**;233:779-91
41. Schwab A, Stock C. Ion channels and transporters in tumour cell migration and invasion. Philos Trans R Soc Lond B Biol Sci **2014**;369:20130102
42. Catacuzzeno L, Sforna L, Esposito V, Limatola C, Franciolini F. Ion Channels in Glioma Malignancy. Rev Physiol Biochem Pharmacol **2021**;181:223-67
43. Beckner ME, Chen X, An J, Day BW, Pollack IF. Proteomic characterization of harvested pseudopodia with differential gel electrophoresis and specific antibodies. Lab Invest **2005**;85:316-27
44. Tjaderhane L, Larjava H, Sorsa T, Uitto VJ, Larmas M, Salo T. The activation and function of host matrix metalloproteinases in dentin matrix breakdown in caries lesions. J Dent Res **1998**;77:1622-9
45. Fasciglione GF, Marini S, D'Alessio S, Politi V, Coletta M. pH- and temperature-dependence of functional modulation in metalloproteinases. A comparison between neutrophil collagenase and gelatinases A and B. Biophys J **2000**;79:2138-49
46. Kato Y, Lambert CA, Colige AC, Mineur P, Noel A, Frankenne F*, et al.* Acidic extracellular pH induces matrix metalloproteinase-9 expression in mouse metastatic melanoma cells through the phospholipase D-mitogen-activated protein kinase signaling. J Biol Chem **2005**;280:10938-44
47. Gatenby RA, Gawlinski ET, Gmitro AF, Kaylor B, Gillies RJ. Acid-mediated tumor invasion: a multidisciplinary study. Cancer Res **2006**;66:5216-23
48. Gioia M, Fasciglione GF, Monaco S, Iundusi R, Sbardella D, Marini S*, et al.* pH dependence of the enzymatic processing of collagen I by MMP-1 (fibroblast collagenase), MMP-2 (gelatinase A), and MMP-14 ectodomain. J Biol Inorg Chem **2010**;15:1219-32
49. Pillai SR, Damaghi M, Marunaka Y, Spugnini EP, Fais S, Gillies RJ. Causes, consequences, and therapy of tumors acidosis. Cancer Metastasis Rev **2019**;38:205-22
50. Rohani N, Hao L, Alexis MS, Joughin BA, Krismer K, Moufarrej MN*, et al.* Acidification of Tumor at Stromal Boundaries Drives Transcriptome Alterations Associated with Aggressive Phenotypes. Cancer Res **2019**;79:1952-66
51. Sun H, Zhou Y, Skaro MF, Wu Y, Qu Z, Mao F*, et al.* Metabolic Reprogramming in Cancer Is Induced to Increase Proton Production. Cancer Res **2020**;80:1143-55
52. Buhl M, Hutson T, Missio A, Walton JC. Sulfur and Phosphorus Oxyacid Radicals. J Phys Chem A **2022**;126:760-71
53. Walton JC. Radical-Enhanced Acidity: Why Bicarbonate, Carboxyl, Hydroperoxyl, and Related Radicals Are So Acidic. J Phys Chem A **2017**;121:7761-7
54. Walton JC. Microhydration and the Enhanced Acidity of Free Radicals. Molecules **2018**;23
55. Segal MS, Beem E. Effect of pH, ionic charge, and osmolality on cytochrome c-mediated caspase-3 activity. Am J Physiol Cell Physiol **2001**;281:C1196-204

56. Duffy HS, Ashton AW, O'Donnell P, Coombs W, Taffet SM, Delmar M*, et al.* Regulation of connexin43 protein complexes by intracellular acidification. Circ Res **2004**;94:215-22
57. Hirst-Jensen BJ, Sahoo P, Kieken F, Delmar M, Sorgen PL. Characterization of the pH-dependent interaction between the gap junction protein connexin43 carboxyl terminus and cytoplasmic loop domains. J Biol Chem **2007**;282:5801-13
58. Palacios-Prado N, Briggs SW, Skeberdis VA, Pranevicius M, Bennett MV, Bukauskas FF. pH-dependent modulation of voltage gating in connexin45 homotypic and connexin45/connexin43 heterotypic gap junctions. Proc Natl Acad Sci U S A **2010**;107:9897-902
59. Monterisi S, Michl J, Hulikova A, Koth J, Bridges EM, Hill AE*, et al.* Solute exchange through gap junctions lessens the adverse effects of inactivating mutations in metabolite-handling genes. Elife **2022**;11
60. Ranganathan NS, Srere PA, Linn TC. Comparison of phospho- and dephospho-ATP citrate lyase. Arch Biochem Biophys **1980**;204:52-8
61. Wu T, Jun S, Choi EJ, Sun J, Yang EB, Lee HS*, et al.* 53BP1-ACLY-SLBP-coordinated activation of replication-dependent histone biogenesis maintains genomic integrity. Nucleic Acids Res **2022**;50:1465-83
62. Beckner ME, Fellows-Mayle W, Zhang Z, Agostino NR, Kant JA, Day BW*, et al.* Identification of ATP citrate lyase as a positive regulator of glycolytic function in glioblastomas. Int J Cancer **2010**;126:2282-95
63. Wellen KE, Hatzivassiliou G, Sachdeva UM, Bui TV, Cross JR, Thompson CB. ATP-citrate lyase links cellular metabolism to histone acetylation. Science **2009**;324:1076-80
64. Lazaropoulos MP, Gibb AA, Chapski DJ, Nair AA, Reiter AN, Roy R*, et al.* Nuclear ATP-citrate lyase regulates chromatin-dependent activation and maintenance of the myofibroblast gene program. Nat Cardiovasc Res **2024**;3:869-82
65. Scott JG, Basanta D, Chinnaiyan P, Canoll P, Swanson KR, Anderson AR. Production of 2-hydroxyglutarate by isocitrate dehydrogenase 1-mutated gliomas: an evolutionary alternative to the Warburg shift? Neuro Oncol **2011**;13:1262-4
66. Girault A, Brochiero E. Evidence of K+ channel function in epithelial cell migration, proliferation, and repair. Am J Physiol Cell Physiol **2014**;306:C307-19
67. Boyle Y, Johns TG, Fletcher EV. Potassium Ion Channels in Malignant Central Nervous System Cancers. Cancers (Basel) **2022**;14
68. Cohen NA, Sha Q, Makhina EN, Lopatin AN, Linder ME, Snyder SH*, et al.* Inhibition of an inward rectifier potassium channel (Kir2.3) by G-protein betagamma subunits. J Biol Chem **1996**;271:32301-5
69. Ruppersberg JP. Intracellular regulation of inward rectifier K+ channels. Pflugers Arch **2000**;441:1-11
70. Niemeyer MI, Stutzin A, Sepulveda FV. A voltage-independent K+ conductance activated by cell swelling in Ehrlich cells is modulated by a G-protein-mediated process. Biochim Biophys Acta **2002**;1562:1-5
71. Bedard K, Krause KH. The NOX family of ROS-generating NADPH oxidases: physiology and pathophysiology. Physiol Rev **2007**;87:245-313
72. Hibino H, Inanobe A, Furutani K, Murakami S, Findlay I, Kurachi Y. Inwardly rectifying potassium channels: their structure, function, and physiological roles. Physiol Rev **2010**;90:291-366
73. Sahoo N, Hoshi T, Heinemann SH. Oxidative modulation of voltage-gated potassium channels. Antioxid Redox Signal **2014**;21:933-52
74. Rivera-Aponte DE, Mendez-Gonzalez MP, Rivera-Pagan AF, Kucheryavykh YV, Kucheryavykh LY, Skatchkov SN*, et al.* Hyperglycemia reduces functional expression of astrocytic Kir4.1 channels and glial glutamate uptake. Neuroscience **2015**;310:216-23

75. Wang J, Li Y, Jiang C. MiR-133b contributes to arsenic-induced apoptosis in U251 glioma cells by targeting the hERG channel. J Mol Neurosci **2015**;55:985-94
76. Pegg AE. Functions of Polyamines in Mammals. J Biol Chem **2016**;291:14904-12
77. Cabanos C, Wang M, Han X, Hansen SB. A Soluble Fluorescent Binding Assay Reveals PIP(2) Antagonism of TREK-1 Channels. Cell Rep **2017**;20:1287-94
78. Li D, Xia L, Chen M, Lin C, Wu H, Zhang Y*, et al.* miR-133b, a particular member of myomiRs, coming into playing its unique pathological role in human cancer. Oncotarget **2017**;8:50193-208
79. Verkhratsky A, Nedergaard M. Physiology of Astroglia. Physiol Rev **2018**;98:239-389
80. Bukiya AN, Dopico AM. Regulation of BK Channel Activity by Cholesterol and Its Derivatives. Adv Exp Med Biol **2019**;1115:53-75
81. Burton MJ, Cresser-Brown J, Thomas M, Portolano N, Basran J, Freeman SL*, et al.* Discovery of a heme-binding domain in a neuronal voltage-gated potassium channel. J Biol Chem **2020**;295:13277-86
82. Dudem S, Boon PX, Mullins N, McClafferty H, Shipston MJ, Wilkinson RDA*, et al.* Oxidation modulates LINGO2-induced inactivation of large conductance, Ca(2+)-activated potassium channels. J Biol Chem **2023**;299:102975
83. Dudem S, Large RJ, Kulkarni S, McClafferty H, Tikhonova IG, Sergeant GP*, et al.* LINGO1 is a regulatory subunit of large conductance, Ca(2+)-activated potassium channels. Proc Natl Acad Sci U S A **2020**;117:2194-200
84. Rotko D, Kunz WS, Szewczyk A, Kulawiak B. Signaling pathways targeting mitochondrial potassium channels. Int J Biochem Cell Biol **2020**;125:105792
85. Abbott GW. Control of Biophysical and Pharmacological Properties of Potassium Channels by Ancillary Subunits. Handb Exp Pharmacol **2021**;267:445-80
86. Abbott GW. Kv Channel Ancillary Subunits: Where Do We Go from Here? Physiology (Bethesda) **2022**;37:0
87. North KC, Zhang M, Singh AK, Zaytseva D, Slayden AV, Bukiya AN*, et al.* Cholesterol Inhibition of Slo1 Channels Is Calcium-Dependent and Can Be Mediated by Either High-Affinity Calcium-Sensing Site in the Slo1 Cytosolic Tail. Mol Pharmacol **2022**;101:132-43
88. Kim SS, Bae Y, Kwon O, Kwon SH, Seo JB, Hwang EM*, et al.* beta-COP Regulates TWIK1/TREK1 Heterodimeric Channel-Mediated Passive Conductance in Astrocytes. Cells **2022**;11
89. Pardo LA. Voltage-Gated Potassium Channels Beyond the Action Potential. Bioelectricity **2022**;4:117-25
90. Vaithianathan T, Schneider EH, Bukiya AN, Dopico AM. Cholesterol and PIP(2) Modulation of BK(Ca) Channels. Adv Exp Med Biol **2023**;1422:217-43
91. Huang X, He Y, Dubuc AM, Hashizume R, Zhang W, Reimand J*, et al.* EAG2 potassium channel with evolutionarily conserved function as a brain tumor target. Nat Neurosci **2015**;18:1236-46
92. Santos R, Ursu O, Gaulton A, Bento AP, Donadi RS, Bologa CG*, et al.* A comprehensive map of molecular drug targets. Nat Rev Drug Discov **2017**;16:19-34
93. Hutchings CJ, Colussi P, Clark TG. Ion channels as therapeutic antibody targets. MAbs **2019**;11:265-96
94. Weise-Cross L, Resta TC, Jernigan NL. Redox Regulation of Ion Channels and Receptors in Pulmonary Hypertension. Antioxid Redox Signal **2019**;31:898-915
95. Wang Y, Qi H, Liu Y, Duan C, Liu X, Xia T*, et al.* The double-edged roles of ROS in cancer prevention and therapy. Theranostics **2021**;11:4839-57
96. Park JK, Kim YC, Sim JH, Choi MY, Choi W, Hwang KK*, et al.* Regulation of membrane excitability by intracellular pH (pHi) changers through Ca2+-activated K+ current (BK channel) in single smooth muscle cells from rabbit basilar artery. Pflugers Arch **2007**;454:307-19

97. Lewandowska J, Kalenik B, Wrzosek A, Szewczyk A. Redox Regulation of Mitochondrial Potassium Channels Activity. Antioxidants (Basel) **2024**;13
98. Lee YM, Kim BJ, Chun YS, So I, Choi H, Kim MS*, et al.* NOX4 as an oxygen sensor to regulate TASK-1 activity. Cell Signal **2006**;18:499-507
99. Michl J, White B, Monterisi S, Bodmer WF, Swietach P. Phenotypic screen of sixty-eight colorectal cancer cell lines identifies CEACAM6 and CEACAM5 as markers of acid resistance. Proc Natl Acad Sci U S A **2024**;121:e2319055121
100. Selivanov VA, Zeak JA, Roca J, Cascante M, Trucco M, Votyakova TV. The role of external and matrix pH in mitochondrial reactive oxygen species generation. J Biol Chem **2008**;283:29292-300
101. Barar J, Omidi Y. Dysregulated pH in Tumor Microenvironment Checkmates Cancer Therapy. Bioimpacts **2013**;3:149-62
102. Damaghi M, Wojtkowiak JW, Gillies RJ. pH sensing and regulation in cancer. Front Physiol **2013**;4:370
103. Vrbka L, Vondrasek J, Jagoda-Cwiklik B, Vacha R, Jungwirth P. Quantification and rationalization of the higher affinity of sodium over potassium to protein surfaces. Proc Natl Acad Sci U S A **2006**;103:15440-4
104. Tansel B. Significance of thermodynamic and physical characteristics on permeation of ions during membrane separation: Hydrated radius, hydration free energy and viscous effects. Separation and Purification Technology **2012**;86:119-26
105. Danchin A, Nikel PI. Why Nature Chose Potassium. J Mol Evol **2019**;87:271-88
106. Kopec W, Kopfer DA, Vickery ON, Bondarenko AS, Jansen TLC, de Groot BL*, et al.* Direct knock-on of desolvated ions governs strict ion selectivity in K(+) channels. Nat Chem **2018**;10:813-20
107. Jing Z, Rackers JA, Pratt LR, Liu C, Rempe SB, Ren P. Thermodynamics of ion binding and occupancy in potassium channels. Chem Sci **2021**;12:8920-30
108. Lam CK, de Groot BL. Ion Conduction Mechanisms in Potassium Channels Revealed by Permeation Cycles. J Chem Theory Comput **2023**;19:2574-89
109. Collins KD. Charge density-dependent strength of hydration and biological structure. Biophys J **1997**;72:65-76
110. Nagy IZ, Lustyik G, Nagy VZ, Zarandi B, Bertoni-Freddari C. Intracellular Na+:K+ ratios in human cancer cells as revealed by energy dispersive x-ray microanalysis. J Cell Biol **1981**;90:769-77
111. Leslie TK, James AD, Zaccagna F, Grist JT, Deen S, Kennerley A*, et al.* Sodium homeostasis in the tumour microenvironment. Biochim Biophys Acta Rev Cancer **2019**;1872:188304
112. Allu AS, Tiriveedhi V. Cancer Salt Nostalgia. Cells **2021**;10
113. Bortner CD, Hughes FM, Jr., Cidlowski JA. A primary role for K+ and Na+ efflux in the activation of apoptosis. J Biol Chem **1997**;272:32436-42
114. Pietrzak M, Meyerhoff ME. Determination of potassium in red blood cells using unmeasured volumes of whole blood and combined sodium/potassium-selective membrane electrode measurements. Anal Chem **2009**;81:5961-5
115. Martinez-Valverde T, Vidal-Jorge M, Montoya N, Sanchez-Guerrero A, Manrique S, Munar F*, et al.* Brain microdialysis as a tool to explore the ionic profile of the brain extracellular space in neurocritical patients: a methodological approach and feasibility study. J Neurotrauma **2015**;32:7-16
116. Eil R, Vodnala SK, Clever D, Klebanoff CA, Sukumar M, Pan JH*, et al.* Ionic immune suppression within the tumour microenvironment limits T cell effector function. Nature **2016**;537:539-43
117. Lehmann HP, Henry JB. Appendix 4, Table A4-4. Whole Blood, Serum, and Plasma Chemistry. In: Henry JB, editor. Clinical Diagnosis and Management by Laboratory Methods. Philadelphia: W.B. Saunders; 1996. p 1450-4.

118. Ghosh S, Yang R, Duraki D, Zhu J, Kim JE, Jabeen M*, et al.* Plasma Membrane Channel TRPM4 Mediates Immunogenic Therapy-Induced Necrosis. Cancer Res **2023**;83:3115-30
119. Oliver D, Baukrowitz T, Fakler B. Polyamines as gating molecules of inward-rectifier K+ channels. Eur J Biochem **2000**;267:5824-9
120. Hopp L, Lasker N, Bamforth R, Aviv A. Characterization of Na(+)-K+ homeostasis of cultured human skin fibroblasts in the presence and absence of fetal bovine serum. J Cell Physiol **1992**;151:427-32
121. Abdullah NA, Hirata M, Matsumoto K, Aizawa H, Inoue R, Hamano S*, et al.* Contraction and depolarization induced by fetal bovine serum in airway smooth muscle. Am J Physiol **1994**;266:L528-35
122. Marton LJ, Heby O, Levin VA, Lubich WP, Crafts DC, Wilson CB. The relationship of polyamines in cerebrospinal fluid to the presence of central nervous system tumors. Cancer Res **1976**;36:973-7
123. Miska J, Rashidi A, Lee-Chang C, Gao P, Lopez-Rosas A, Zhang P*, et al.* Polyamines drive myeloid cell survival by buffering intracellular pH to promote immunosuppression in glioblastoma. Sci Adv **2021**;7
124. Monsorno K, Buckinx A, Paolicelli RC. Microglial metabolic flexibility: emerging roles for lactate. Trends Endocrinol Metab **2022**;33:186-95
125. Augustynek B, Kudin AP, Bednarczyk P, Szewczyk A, Kunz WS. Hemin inhibits the large conductance potassium channel in brain mitochondria: a putative novel mechanism of neurodegeneration. Exp Neurol **2014**;257:70-5
126. Bailey CS, Moldenhauer HJ, Park SM, Keros S, Meredith AL. KCNMA1-linked channelopathy. J Gen Physiol **2019**;151:1173-89
127. Zhao Y, Wang D, Xu T, Liu P, Cao Y, Wang Y*, et al.* Bladder cancer cells re-educate TAMs through lactate shuttling in the microfluidic cancer microenvironment. Oncotarget **2015**;6:39196-210
128. Zhang L, Li S. Lactic acid promotes macrophage polarization through MCT-HIF1alpha signaling in gastric cancer. Exp Cell Res **2020**;388:111846
129. Zhou HC, Xin-Yan Y, Yu WW, Liang XQ, Du XY, Liu ZC*, et al.* Lactic acid in macrophage polarization: The significant role in inflammation and cancer. Int Rev Immunol **2022**;41:4-18
130. Liebig C, Ayala G, Wilks JA, Berger DH, Albo D. Perineural invasion in cancer: a review of the literature. Cancer **2009**;115:3379-91
131. Bakst RL, Wong RJ. Mechanisms of Perineural Invasion. J Neurol Surg B Skull Base **2016**;77:96-106
132. Narayan P, Flynn J, Zhang Z, Gillespie EF, Mueller B, Xu AJ*, et al.* Perineural invasion as a risk factor for locoregional recurrence of invasive breast cancer. Sci Rep **2021**;11:12781
133. Hosoya K, Wakahara M, Ikeda K, Umekita Y. Perineural Invasion Predicts Unfavorable Prognosis in Patients With Invasive Breast Cancer. Cancer Diagn Progn **2023**;3:208-14
134. Beckner ME, Fellows-Mayle W, Agostino NR, Gobbel GT, Pollack IF. Tumor markers in pseudopodia for invasive migration. In: Swenson LI, editor. Progress in Tumor Marker Research. New York: Nova Science Publishers, Inc.; 2007. p 43-66.
135. Beckner ME, Gobbel GT, Abounader R, Burovic F, Agostino NR, Laterra J*, et al.* Glycolytic glioma cells with active glycogen synthase are sensitive to PTEN and inhibitors of PI3K and gluconeogenesis. Lab Invest **2005**;85:1457-70
136. Beckner ME, Zhang Z, Agostino NR, Day BW, Pollack IF. Albumin marks pseudopodia of astrocytoma cells responding to hepatocyte growth factor or serum. Lab Invest **2006**;86:1103-14
137. Silverman JF, Frable WJ. The use of the diff-quik stain in the immediate interpretation of fine-needle aspiration biopsies. Diagn Cytopathol **1990**;6:366-9
138. Eagle H. Amino acid metabolism in mammalian cell cultures. Science **1959**;130:432-7

139. Clark MJ, Homer N, O'Connor BD, Chen Z, Eskin A, Lee H*, et al.* U87MG decoded: the genomic sequence of a cytogenetically aberrant human cancer cell line. PLoS Genet **2010**;6:e1000832
140. Clark MJ, Homer N, O'Connor BD, Chen Z, Eskin A, Lee H*, et al.* Correction: U87MG Decoded: The Genomic Sequence of a Cytogenetically Aberrant Human Cancer Cell Line. PLoS Genet **2018**;14:e1007392
141. Becker HM. Carbonic anhydrase IX and acid transport in cancer. Br J Cancer **2020**;122:157-67
142. Noor SI, Jamali S, Ames S, Langer S, Deitmer JW, Becker HM. A surface proton antenna in carbonic anhydrase II supports lactate transport in cancer cells. Elife **2018**;7
143. Cheng J, Wen J, Wang N, Wang C, Xu Q, Yang Y. Ion Channels and Vascular Diseases. Arterioscler Thromb Vasc Biol **2019**;39:e146-e56
144. Crepalde MA, Faria-Campos AC, Campos SV. Modeling and analysis of cell membrane systems with probabilistic model checking. BMC Genomics **2011**;12 Suppl 4:S14
145. Sajic JL, Langthaler S, Baumgartner C. Creating a novel mathematical model of the Kv10.1 ion channel and controlling channel activity with nanoelectromechanical systems. Applied Sciences **2022**;12
146. Sun X, Lee HC, Lu T. Sorbs2 Deficiency and Vascular BK Channelopathy in Diabetes. Circ Res **2024**;134:858-71
147. Wulff H, Castle NA. Therapeutic potential of KCa3.1 blockers: an overview of recent advances, and promising trends. Expert Reviews Clinical Pharmacology **2010**;3:385-96
148. Zaika OL, Mamenko M, Palygin O, Boukelmoune N, Staruschenko A, Pochynyuk O. Direct inhibition of basolateral Kir4.1/5.1 and Kir4.1 channels in the cortical collecting duct by dopamine. Am J Physiol Renal Physiol **2013**;305:F1277-87
149. Fournier PA, Fairchild TJ, Ferreira LD, Brau L. Post-exercise muscle glycogen repletion in the extreme: effect of food absence and active recovery. J Sports Sci Med **2004**;3:139-46
150. Bangsbo J, Gollnick PD, Graham TE, Saltin B. Substrates for muscle glycogen synthesis in recovery from intense exercise in man. J Physiol **1991**;434:423-40
151. Talmadge RJ, Scheide JI, Silverman H. Glycogen synthesis from lactate in a chronically active muscle. J Appl Physiol (1985) **1989**;66:2231-8
152. Hydrean C, Ghosh A, Nallin M, Ghosh BK. Interrelationship of carbohydrate metabolism and alkaline phosphatase synthesis in Bacillus licheniformis 749/c. J Biol Chem **1977**;252:6806-12
153. Tucci V, Isles AR, Kelsey G, Ferguson-Smith AC, Erice Imprinting G. Genomic Imprinting and Physiological Processes in Mammals. Cell **2019**;176:952-65
154. Berlin C, Cottard F, Willmann D, Urban S, Tirier SM, Marx L*, et al.* KMT9 Controls Stemness and Growth of Colorectal Cancer. Cancer Res **2022**;82:210-20
155. Contreras-Espinosa L, Alcaraz N, De La Rosa-Velazquez IA, Diaz-Chavez J, Cabrera-Galeana P, Rebollar-Vega R*, et al.* Transcriptome Analysis Identifies GATA3-AS1 as a Long Noncoding RNA Associated with Resistance to Neoadjuvant Chemotherapy in Locally Advanced Breast Cancer Patients. J Mol Diagn **2021**;23:1306-23
156. Nargund AM, Xu C, Mandoli A, Okabe A, Chen GB, Huang KK*, et al.* Chromatin Rewiring by Mismatch Repair Protein MSH2 Alters Cell Adhesion Pathways and Sensitivity to BET Inhibition in Gastric Cancer. Cancer Res **2022**;82:2538-51
157. Pine AR, Cirigliano SM, Singhania R, Nicholson J, da Silva B, Leslie CS*, et al.* Microenvironment-Driven Dynamic Chromatin Changes in Glioblastoma Recapitulate Early Neural Development at Single-Cell Resolution. Cancer Res **2023**;83:1581-95
158. Yu Z, Lv Y, Su C, Lu W, Zhang R, Li J*, et al.* Integrative Single-Cell Analysis Reveals Transcriptional and Epigenetic Regulatory Features of Clear Cell Renal Cell Carcinoma. Cancer Res **2023**;83:700-19

159. Zhu Q, Zhang C, Qu T, Lu X, He X, Li W*, et al.* MNX1-AS1 Promotes Phase Separation of IGF2BP1 to Drive c-Myc-Mediated Cell-Cycle Progression and Proliferation in Lung Cancer. Cancer Res **2022**;82:4340-58
160. Guetta-Terrier C, Karambizi D, Akosman B, Zepecki JP, Chen JS, Kamle S*, et al.* Chi3l1 Is a Modulator of Glioma Stem Cell States and a Therapeutic Target in Glioblastoma. Cancer Res **2023**;83:1984-99
161. Mohan DR, Borges KS, Finco I, LaPensee CR, Rege J, Solon AL*, et al.* beta-Catenin-Driven Differentiation Is a Tissue-Specific Epigenetic Vulnerability in Adrenal Cancer. Cancer Res **2023**;83:2123-41
162. Abruzzo LV, Barron LL, Anderson K, Newman RJ, Wierda WG, O'Brien S*, et al.* Identification and validation of biomarkers of IgV(H) mutation status in chronic lymphocytic leukemia using microfluidics quantitative real-time polymerase chain reaction technology. J Mol Diagn **2007**;9:546-55
163. Emmons MF, Bennett RL, Riva A, Gupta K, Carvalho L, Zhang C*, et al.* HDAC8-mediated inhibition of EP300 drives a transcriptional state that increases melanoma brain metastasis. Nat Commun **2023**;14:7759
164. Newman AC, Kemp AJ, Drabsch Y, Behrends C, Wilkinson S. Autophagy acts through TRAF3 and RELB to regulate gene expression via antagonism of SMAD proteins. Nat Commun **2017**;8:1537
165. Min J, Vega PN, Engevik AC, Williams JA, Yang Q, Patterson LM*, et al.* Heterogeneity and dynamics of active Kras-induced dysplastic lineages from mouse corpus stomach. Nat Commun **2019**;10:5549
166. Banito A, Li X, Laporte AN, Roe JS, Sanchez-Vega F, Huang CH*, et al.* The SS18-SSX Oncoprotein Hijacks KDM2B-PRC1.1 to Drive Synovial Sarcoma. Cancer Cell **2018**;33:527-41 e8
167. Pan Y, Han H, Hu H, Wang H, Song Y, Hao Y*, et al.* KMT2D deficiency drives lung squamous cell carcinoma and hypersensitivity to RTK-RAS inhibition. Cancer Cell **2023**;41:88-105 e8
168. Chapuy B, McKeown MR, Lin CY, Monti S, Roemer MG, Qi J*, et al.* Discovery and characterization of super-enhancer-associated dependencies in diffuse large B cell lymphoma. Cancer Cell **2013**;24:777-90
169. Beddows I, Fan H, Heinze K, Johnson BK, Leonova A, Senz J*, et al.* Cell State of Origin Impacts Development of Distinct Endometriosis-Related Ovarian Carcinoma Histotypes. Cancer Res **2024**;84:26-38
170. Shih AH, Jiang Y, Meydan C, Shank K, Pandey S, Barreyro L*, et al.* Mutational cooperativity linked to combinatorial epigenetic gain of function in acute myeloid leukemia. Cancer Cell **2015**;27:502-15
171. Veschi V, Liu Z, Voss TC, Ozbun L, Gryder B, Yan C*, et al.* Epigenetic siRNA and Chemical Screens Identify SETD8 Inhibition as a Therapeutic Strategy for p53 Activation in High-Risk Neuroblastoma. Cancer Cell **2017**;31:50-63
172. da Silva LS, Mancano BM, de Paula FE, Dos Reis MB, de Almeida GC, Matsushita M*, et al.* Expression of GNAS, TP53, and PTEN Improves the Patient Prognostication in Sonic Hedgehog (SHH) Medulloblastoma Subgroup. J Mol Diagn **2020**;22:957-66
173. East P, Kelly GP, Biswas D, Marani M, Hancock DC, Creasy T*, et al.* RAS oncogenic activity predicts response to chemotherapy and outcome in lung adenocarcinoma. Nat Commun **2022**;13:5632
174. Ishizawa J, Nakamaru K, Seki T, Tazaki K, Kojima K, Chachad D*, et al.* Predictive Gene Signatures Determine Tumor Sensitivity to MDM2 Inhibition. Cancer Res **2018**;78:2721-31
175. Wang XQ, Wang XQ, Hsu A, Goytain A, Ng TLT, Nielsen TO. A Rapid and Cost-Effective Gene Expression Assay for the Diagnosis of Well-Differentiated and Dedifferentiated Liposarcomas. J Mol Diagn **2021**;23:274-84

176. Wang LB, Karpova A, Gritsenko MA, Kyle JE, Cao S, Li Y*, et al.* Proteogenomic and metabolomic characterization of human glioblastoma. Cancer Cell **2021**;39:509-28 e20
177. Soragni A, Janzen DM, Johnson LM, Lindgren AG, Thai-Quynh Nguyen A, Tiourin E*, et al.* A Designed Inhibitor of p53 Aggregation Rescues p53 Tumor Suppression in Ovarian Carcinomas. Cancer Cell **2016**;29:90-103
178. Mello SS, Valente LJ, Raj N, Seoane JA, Flowers BM, McClendon J*, et al.* A p53 Super-tumor Suppressor Reveals a Tumor Suppressive p53-Ptpn14-Yap Axis in Pancreatic Cancer. Cancer Cell **2017**;32:460-73 e6
179. Dong L, Lu D, Chen R, Lin Y, Zhu H, Zhang Z*, et al.* Proteogenomic characterization identifies clinically relevant subgroups of intrahepatic cholangiocarcinoma. Cancer Cell **2022**;40:70-87 e15
180. Zhang H, Christensen CL, Dries R, Oser MG, Deng J, Diskin B*, et al.* CDK7 Inhibition Potentiates Genome Instability Triggering Anti-tumor Immunity in Small Cell Lung Cancer. Cancer Cell **2020**;37:37-54 e9
181. Schwab A, Siddiqui A, Vazakidou ME, Napoli F, Bottcher M, Menchicchi B*, et al.* Polyol Pathway Links Glucose Metabolism to the Aggressiveness of Cancer Cells. Cancer Res **2018**;78:1604-18
182. Zhang Y, Cruickshanks N, Yuan F, Wang B, Pahuski M, Wulfkuhle J*, et al.* Targetable T-type Calcium Channels Drive Glioblastoma. Cancer Res **2017**;77:3479-90
183. Halvorsen SC, Benita Y, Hopton M, Hoppe B, Gunnlaugsson HO, Korgaonkar P*, et al.* Transcriptional Profiling Supports the Notochordal Origin of Chordoma and Its Dependence on a TGFB1-TBXT Network. Am J Pathol **2023**;193:532-47
184. Sahu SK, Tiwari N, Pataskar A, Zhuang Y, Borisova M, Diken M*, et al.* FBXO32 promotes microenvironment underlying epithelial-mesenchymal transition via CtBP1 during tumour metastasis and brain development. Nat Commun **2017**;8:1523
185. Verfaillie A, Imrichova H, Atak ZK, Dewaele M, Rambow F, Hulselmans G*, et al.* Decoding the regulatory landscape of melanoma reveals TEADS as regulators of the invasive cell state. Nat Commun **2015**;6:6683
186. Wu LMN, Deng Y, Wang J, Zhao C, Wang J, Rao R*, et al.* Programming of Schwann Cells by Lats1/2-TAZ/YAP Signaling Drives Malignant Peripheral Nerve Sheath Tumorigenesis. Cancer Cell **2018**;33:292-308 e7
187. Haider S, McIntyre A, van Stiphout RG, Winchester LM, Wigfield S, Harris AL*, et al.* Genomic alterations underlie a pan-cancer metabolic shift associated with tumour hypoxia. Genome Biol **2016**;17:140
188. Zhang D, Park D, Zhong Y, Lu Y, Rycaj K, Gong S*, et al.* Stem cell and neurogenic gene-expression profiles link prostate basal cells to aggressive prostate cancer. Nat Commun **2016**;7:10798
189. Ni Y, Schmidt KR, Werner BA, Koenig JK, Guldner IH, Schnepp PM*, et al.* Death effector domain-containing protein induces vulnerability to cell cycle inhibition in triple-negative breast cancer. Nat Commun **2019**;10:2860
190. Wang Z, Sun D, Chen YJ, Xie X, Shi Y, Tabar V*, et al.* Cell Lineage-Based Stratification for Glioblastoma. Cancer Cell **2020**;38:366-79 e8
191. Zhang Z, Karthaus WR, Lee YS, Gao VR, Wu C, Russo JW*, et al.* Tumor Microenvironment-Derived NRG1 Promotes Antiandrogen Resistance in Prostate Cancer. Cancer Cell **2020**;38:279-96 e9
192. Cheung WK, Zhao M, Liu Z, Stevens LE, Cao PD, Fang JE*, et al.* Control of alveolar differentiation by the lineage transcription factors GATA6 and HOPX inhibits lung adenocarcinoma metastasis. Cancer Cell **2013**;23:725-38
193. Kelenis DP, Rodarte KE, Kollipara RK, Pozo K, Choudhuri SP, Spainhower KB*, et al.* Inhibition of Karyopherin beta1-Mediated Nuclear Import Disrupts Oncogenic Lineage-Defining Transcription Factor Activity in Small Cell Lung Cancer. Cancer Res **2022**;82:3058-73

194. Pozniak J, Nsengimana J, Laye JP, O'Shea SJ, Diaz JMS, Droop AP*, et al.* Genetic and Environmental Determinants of Immune Response to Cutaneous Melanoma. Cancer Res **2019**;79:2684-96
195. Van de Velde LA, Allen EK, Crawford JC, Wilson TL, Guy CS, Russier M*, et al.* Neuroblastoma Formation Requires Unconventional CD4 T Cells and Arginase-1-Dependent Myeloid Cells. Cancer Res **2021**;81:5047-59
196. Cai L, DeBerardinis RJ, Xie Y, Minna JD, Xiao G. A Comparative Study of Neuroendocrine Heterogeneity in Small Cell Lung Cancer and Neuroblastoma. Mol Cancer Res **2023**;21:795-807
197. Kawauchi D, Robinson G, Uziel T, Gibson P, Rehg J, Gao C*, et al.* A mouse model of the most aggressive subgroup of human medulloblastoma. Cancer Cell **2012**;21:168-80
198. Topham C, Tighe A, Ly P, Bennett A, Sloss O, Nelson L*, et al.* MYC Is a Major Determinant of Mitotic Cell Fate. Cancer Cell **2015**;28:129-40
199. Alam A, Levanduski E, Denz P, Villavicencio HS, Bhatta M, Alhorebi L*, et al.* Fungal mycobiome drives IL-33 secretion and type 2 immunity in pancreatic cancer. Cancer Cell **2022**;40:153-67 e11
200. Altwegg KA, Viswanadhapalli S, Mann M, Chakravarty D, Krishnan S, Liu Z*, et al.* A First-in-Class Inhibitor of ER Coregulator PELP1 Targets ER+ Breast Cancer. Cancer Res **2022**;82:3830-44
201. Guieze R, Liu VM, Rosebrock D, Jourdain AA, Hernandez-Sanchez M, Martinez Zurita A*, et al.* Mitochondrial Reprogramming Underlies Resistance to BCL-2 Inhibition in Lymphoid Malignancies. Cancer Cell **2019**;36:369-84 e13
202. Roh W, Geffen Y, Cha H, Miller M, Anand S, Kim J*, et al.* High-Resolution Profiling of Lung Adenocarcinoma Identifies Expression Subtypes with Specific Biomarkers and Clinically Relevant Vulnerabilities. Cancer Res **2022**;82:3917-31
203. Vidal SJ, Rodriguez-Bravo V, Quinn SA, Rodriguez-Barrueco R, Lujambio A, Williams E*, et al.* A targetable GATA2-IGF2 axis confers aggressiveness in lethal prostate cancer. Cancer Cell **2015**;27:223-39
204. Alothman SJ, Kang K, Liu X, Krawczyk E, Azhar RI, Hu R*, et al.* Characterization of transcriptome diversity and in vitro behavior of primary human high-risk breast cells. Sci Rep **2022**;12:6159
205. Chen R, Khatri P, Mazur PK, Polin M, Zheng Y, Vaka D*, et al.* A meta-analysis of lung cancer gene expression identifies PTK7 as a survival gene in lung adenocarcinoma. Cancer Res **2014**;74:2892-902
206. Darmanis S, Sloan SA, Croote D, Mignardi M, Chernikova S, Samghababi P*, et al.* Single-Cell RNA-Seq Analysis of Infiltrating Neoplastic Cells at the Migrating Front of Human Glioblastoma. Cell Rep **2017**;21:1399-410
207. de Jong JJ, Narayan VM, Cronican AA, Gupta S, van Leenders GJLH, Boormans JL*, et al.* Gene expression profiling of muscle-invasive bladder cancer with secondary variant histology. Am J Clin Pathol **2021**;156:895-905
208. Harlow ML, Maloney N, Roland J, Guillen Navarro MJ, Easton MK, Kitchen-Goosen SM*, et al.* Lurbinectedin Inactivates the Ewing Sarcoma Oncoprotein EWS-FLI1 by Redistributing It within the Nucleus. Cancer Res **2016**;76:6657-68
209. Scheidmann MC, Castro-Giner F, Strittmatter K, Krol I, Paasinen-Sohns A, Scherrer R*, et al.* An In Vivo CRISPR Screen Identifies Stepwise Genetic Dependencies of Metastatic Progression. Cancer Res **2022**;82:681-94
210. Xu Q, Chen J, Ni S, Tan C, Xu M, Dong L*, et al.* Pan-cancer transcriptome analysis reveals a gene expression signature for the identification of tumor tissue origin. Mod Pathol **2016**;29:546-56
211. Zhang S, Zhou YF, Cao J, Burley SK, Wang HY, Zheng XFS. mTORC1 Promotes ARID1A Degradation and Oncogenic Chromatin Remodeling in Hepatocellular Carcinoma. Cancer Res **2021**;81:5652-65

212. Khlebus E, Vuttaradhi VK, Welte T, Khurana N, Celestino J, Beird HC*, et al.* Comparative Tumor Microenvironment Analysis of Primary and Recurrent Ovarian Granulosa Cell Tumors. Mol Cancer Res **2023**;21:483-94
213. Mirzaei R, D'Mello C, Liu M, Nikolic A, Kumar M, Visser F*, et al.* Single-Cell Spatial Analysis Identifies Regulators of Brain Tumor-Initiating Cells. Cancer Res **2023**;83:1725-41
214. Yao L, Wang JT, Jayasinghe RG, O'Neal J, Tsai CF, Rettig MP*, et al.* Single-Cell Discovery and Multiomic Characterization of Therapeutic Targets in Multiple Myeloma. Cancer Res **2023**;83:1214-33
215. Roda N, Cossa A, Hillje R, Tirelli A, Ruscitto F, Cheloni S*, et al.* A Rare Subset of Primary Tumor Cells with Concomitant Hyperactivation of Extracellular Matrix Remodeling and dsRNA-IFN1 Signaling Metastasizes in Breast Cancer. Cancer Res **2023**;83:2155-70
216. Restaino AC, Walz A, Vermeer SJ, Barr J, Kovacs A, Fettig RR*, et al.* Functional neuronal circuits promote disease progression in cancer. Sci Adv **2023**;9:eade4443
217. Song Y, Deng Z, Sun H, Zhao Y, Zhao R, Cheng J*, et al.* Predicting tumor repopulation through the gene panel derived from radiation resistant colorectal cancer cells. J Transl Med **2023**;21:390
218. Zhou X, An J, Kurilov R, Brors B, Hu K, Peccerella T*, et al.* Persister cell phenotypes contribute to poor patient outcomes after neoadjuvant chemotherapy in PDAC. Nat Cancer **2023**;4:1362-81
219. Inman GJ, Wang J, Nagano A, Alexandrov LB, Purdie KJ, Taylor RG*, et al.* The genomic landscape of cutaneous SCC reveals drivers and a novel azathioprine associated mutational signature. Nat Commun **2018**;9:3667
220. Pandey GK, Mitra S, Subhash S, Hertwig F, Kanduri M, Mishra K*, et al.* The risk-associated long noncoding RNA NBAT-1 controls neuroblastoma progression by regulating cell proliferation and neuronal differentiation. Cancer Cell **2014**;26:722-37
221. Witt H, Mack SC, Ryzhova M, Bender S, Sill M, Isserlin R*, et al.* Delineation of two clinically and molecularly distinct subgroups of posterior fossa ependymoma. Cancer Cell **2011**;20:143-57
222. Neou M, Villa C, Armignacco R, Jouinot A, Raffin-Sanson ML, Septier A*, et al.* Pangenomic Classification of Pituitary Neuroendocrine Tumors. Cancer Cell **2020**;37:123-34 e5
223. Fukumoto T, Umakoshi H, Iwahashi N, Ogasawara T, Yokomoto-Umakoshi M, Kaneko H*, et al.* Steroids-producing nodules: a two-layered adrenocortical nodular structure as a precursor lesion of cortisol-producing adenoma. EBioMedicine **2024**;103:105087
224. Papier K, Atkins JR, Tong TYN, Gaitskell K, Desai T, Ogamba CF*, et al.* Identifying proteomic risk factors for cancer using prospective and exome analyses of 1463 circulating proteins and risk of 19 cancers in the UK Biobank. Nat Commun **2024**;15:4010
225. Smith-Byrne K, Hedman A, Dimitriou M, Desai T, Sokolov AV, Schioth HB*, et al.* Identifying therapeutic targets for cancer among 2074 circulating proteins and risk of nine cancers. Nat Commun **2024**;15:3621
226. Suchak SK, Baloyianni NV, Perkinton MS, Williams RJ, Meldrum BS, Rattray M. The 'glial' glutamate transporter, EAAT2 (Glt-1) accounts for high affinity glutamate uptake into adult rodent nerve endings. J Neurochem **2003**;84:522-32
227. Al Awabdh S, Gupta-Agarwal S, Sheehan DF, Muir J, Norkett R, Twelvetrees AE*, et al.* Neuronal activity mediated regulation of glutamate transporter GLT-1 surface diffusion in rat astrocytes in dissociated and slice cultures. Glia **2016**;64:1252-64
228. Mai D, Chen R, Wang J, Zheng J, Zhang X, Qu S. Critical amino acids in the TM2 of EAAT2 are essential for membrane-bound localization, substrate binding, transporter function and anion currents. J Cell Mol Med **2021**;25:2530-48
229. Molenaar RJ. Ion channels in glioblastoma. ISRN Neurol **2011**;2011:590249
230. Pedersen SF, Stock C. Ion channels and transporters in cancer: pathophysiology, regulation, and clinical potential. Cancer Res **2013**;73:1658-61

231. Huang X, Jan LY. Targeting potassium channels in cancer. J Cell Biol **2014**;206:151-62
232. Pardo LA, Stuhmer W. The roles of K(+) channels in cancer. Nat Rev Cancer **2014**;14:39-48
233. Comes N, Serrano-Albarras A, Capera J, Serrano-Novillo C, Condom E, Ramon YCS*, et al.* Involvement of potassium channels in the progression of cancer to a more malignant phenotype. Biochim Biophys Acta **2015**;1848:2477-92
234. Prevarskaya N, Skryma R, Shuba Y. Ion Channels in Cancer: Are Cancer Hallmarks Oncochannelopathies? Physiol Rev **2018**;98:559-621
235. Iorio J, Petroni G, Duranti C, Lastraioli E. Potassium and Sodium Channels and the Warburg Effect: Biophysical Regulation of Cancer Metabolism. Bioelectricity **2019**;1:188-200
236. Girault A, Ahidouch A, Ouadid-Ahidouch H. Roles for Ca(2+) and K(+) channels in cancer cells exposed to the hypoxic tumour microenvironment. Biochim Biophys Acta Mol Cell Res **2020**;1867:118644
237. Petho Z, Najder K, Carvalho T, McMorrow R, Todesca LM, Rugi M*, et al.* pH-Channeling in Cancer: How pH-Dependence of Cation Channels Shapes Cancer Pathophysiology. Cancers (Basel) **2020**;12
238. Ganser K, Klumpp L, Bischof H, Lukowski R, Eckert F, Huber SM. Potassium Channels in Cancer. Handb Exp Pharmacol **2021**;267:253-75
239. Verkhratsky A, Parpura V. Physiology of Astroglia: Channels, Receptors, Transporters, Ion Signaling, and Gliotransmission. Verkhratsky A, Parpura V, editors. store.morganclaypool.com: Morgan & Claypool Publishers; 2015.
240. Lopatin AN, Makhina EN, Nichols CG. The mechanism of inward rectification of potassium channels: "long-pore plugging" by cytoplasmic polyamines. J Gen Physiol **1995**;106:923-55
241. Taura J, Kircher DM, Gameiro-Ros I, Slesinger PA. Comparison of K(+) Channel Families. Handb Exp Pharmacol **2021**;267:1-49
242. Beckner ME. A roadmap for potassium buffering/dispersion via the glial network of the CNS. Neurochem Int **2020**;136:104727
243. Schroder W, Hinterkeuser S, Seifert G, Schramm J, Jabs R, Wilkin GP*, et al.* Functional and molecular properties of human astrocytes in acute hippocampal slices obtained from patients with temporal lobe epilepsy. Epilepsia **2000**;41 Suppl 6:S181-4
244. Larson VA, Mironova Y, Vanderpool KG, Waisman A, Rash JE, Agarwal A*, et al.* Oligodendrocytes control potassium accumulation in white matter and seizure susceptibility. Elife **2018**;7
245. Song S, Luo L, Sun B, Sun D. Roles of glial ion transporters in brain diseases. Glia **2020**;68:472-94
246. Aronica E, Gorter JA, Jansen GH, Leenstra S, Yankaya B, Troost D. Expression of connexin 43 and connexin 32 gap-junction proteins in epilepsy-associated brain tumors and in the perilesional epileptic cortex. Acta Neuropathol **2001**;101:449-59
247. Caltabiano R, Torrisi A, Condorelli D, Albanese V, Lanzafame S. High levels of connexin 43 mRNA in high grade astrocytomas. Study of 32 cases with in situ hybridization. Acta Histochem **2010**;112:529-35
248. McClenaghan C, Schewe M, Aryal P, Carpenter EP, Baukrowitz T, Tucker SJ. Polymodal activation of the TREK-2 K2P channel produces structurally distinct open states. J Gen Physiol **2016**;147:497-505
249. Woo J, Jun YK, Zhang YH, Nam JH, Shin DH, Kim SJ. Identification of critical amino acids in the proximal C-terminal of TREK-2 K(+) channel for activation by acidic pH(i) and ATP-dependent inhibition. Pflugers Arch **2018**;470:327-37
250. Lee J, Kang M, Kim S, Chang I. Structural and molecular insight into the pH-induced low-permeability of the voltage-gated potassium channel Kv1.2 through dewetting of the water cavity. PLoS Comput Biol **2020**;16:e1007405

251. Claydon TW, Boyett MR, Sivaprasadarao A, Ishii K, Owen JM, O'Beirne HA*, et al.* Inhibition of the K+ channel kv1.4 by acidosis: protonation of an extracellular histidine slows the recovery from N-type inactivation. J Physiol **2000**;526 Pt 2:253-64
252. Li X, Bett GC, Jiang X, Bondarenko VE, Morales MJ, Rasmusson RL. Regulation of N- and C-type inactivation of Kv1.4 by pHo and K+: evidence for transmembrane communication. Am J Physiol Heart Circ Physiol **2003**;284:H71-80
253. Abbott GW, Butler MH, Goldstein SA. Phosphorylation and protonation of neighboring MiRP2 sites: function and pathophysiology of MiRP2-Kv3.4 potassium channels in periodic paralysis. FASEB J **2006**;20:293-301
254. Kazmierczak M, Zhang X, Chen B, Mulkey DK, Shi Y, Wagner PG*, et al.* External pH modulates EAG superfamily K+ channels through EAG-specific acidic residues in the voltage sensor. J Gen Physiol **2013**;141:721-35
255. Mao J, Li L, McManus M, Wu J, Cui N, Jiang C. Molecular determinants for activation of G-protein-coupled inward rectifier K+ (GIRK) channels by extracellular acidosis. J Biol Chem **2002**;277:46166-71
256. Mao J, Wu J, Chen F, Wang X, Jiang C. Inhibition of G-protein-coupled inward rectifying K+ channels by intracellular acidosis. J Biol Chem **2003**;278:7091-8
257. Wu J, Xu H, Yang Z, Wang Y, Mao J, Jiang C. Protons activate homomeric Kir6.2 channels by selective suppression of the long and intermediate closures. J Membr Biol **2002**;190:105-16
258. Cui N, Wu J, Xu H, Wang R, Rojas A, Piao H*, et al.* A threonine residue (Thr71) at the intracellular end of the M1 helix plays a critical role in the gating of Kir6.2 channels by intracellular ATP and protons. J Membr Biol **2003**;192:111-22
259. Maksaev G, Brundl-Jirout M, Stary-Weinzinger A, Zangerl-Plessl EM, Lee SJ, Nichols CG. Subunit gating resulting from individual protonation events in Kir2 channels. Nat Commun **2023**;14:4538
260. Meuth SG, Kleinschnitz C, Broicher T, Austinat M, Braeuninger S, Bittner S*, et al.* The neuroprotective impact of the leak potassium channel TASK1 on stroke development in mice. Neurobiol Dis **2009**;33:1-11
261. Buckler KJ. TASK channels in arterial chemoreceptors and their role in oxygen and acid sensing. Pflugers Arch **2015**;467:1013-25
262. Decher N, Maier M, Dittrich W, Gassenhuber J, Bruggemann A, Busch AE*, et al.* Characterization of TASK-4, a novel member of the pH-sensitive, two-pore domain potassium channel family. FEBS Lett **2001**;492:84-9
263. Bales CE, Durfee GR. Part I: Cytologic Techniques. In: Koss LG, editor. Diagnostic Cytology and Its Histopathologic Bases. Philadelphia: J.B. Lippincott Company; 1992. p 1484-6.
264. Folstad L, Look M, Pallavicini M. A polycarbonate filter technique for collection of sorted cells. Cytometry **1982**;3:64-5
265. Druzhkova I, Lukina M, Dudenkova V, Ignatova N, Snopova L, Gavrina A*, et al.* Tracing of intracellular pH in cancer cells in response to Taxol treatment. Cell Cycle **2021**;20:1540-51
266. Lemasters JJ. Molecular mechanisms of cell death. In: Coleman WB, Tsongalis GJ, editors. Molecular Pathology, The Molecular Basis of Disease. Burlington, MA: Academic Press; 2009. p 3-24.
267. Lemasters JJ. Molecular Mechanisms of Cell Death. In: Coleman WB, Tsongalis GJ, editors. Molecular Pathology, The Molecular Basis of Human Disease. Cambridge, MA: Academic Press; 2018. p 1-24.
268. Green DR. Nonapoptotic cell death pathways. Cell Death, Apoptosis and Other Means to an End. Cold Spring Harbor, NY: Cold Spring Harbor Laboratory Press; 2018. p 135.

269. Gow IF, Thomson J, Davidson J, Shennan DB. The effect of a hyposmotic shock and purinergic agonists on K+(Rb+) efflux from cultured human breast cancer cells. Biochim Biophys Acta **2005**;1712:52-61
270. Nakada T. The Molecular Mechanisms of Neural Flow Coupling: A New Concept. J Neuroimaging **2015**;25:861-5
271. Li C, Voth GA. A quantitative paradigm for water-assisted proton transport through proteins and other confined spaces. Proc Natl Acad Sci U S A **2021**;118
272. Drew D, Boudker O. Ion and lipid orchestration of secondary active transport. Nature **2024**;626:963-74
273. Persi E, Duran-Frigola M, Damaghi M, Roush WR, Aloy P, Cleveland JL*, et al.* Systems analysis of intracellular pH vulnerabilities for cancer therapy. Nat Commun **2018**;9:2997
274. Russell S, Xu L, Kam Y, Abrahams D, Ordway B, Lopez AS*, et al.* Proton export upregulates aerobic glycolysis. BMC Biol **2022**;20:163
275. Swietach P, Spitzer KW, Vaughan-Jones RD. pH-Dependence of extrinsic and intrinsic H(+)-ion mobility in the rat ventricular myocyte, investigated using flash photolysis of a caged-H(+) compound. Biophys J **2007**;92:641-53
276. Barron T, Yalcin B, Su M, Byun YG, Gavish A, Shamardani K*, et al.* GABAergic neuron-to-glioma synapses in diffuse midline gliomas. Nature **2025**;639:1060-8
277. Garofano L, Migliozzi S, Oh YT, D'Angelo F, Najac RD, Ko A*, et al.* Pathway-based classification of glioblastoma uncovers a mitochondrial subtype with therapeutic vulnerabilities. Nat Cancer **2021**;2:141-56
278. Xia J, Wang H, Li S, Wu Q, Sun L, Huang H*, et al.* Ion channels or aquaporins as novel molecular targets in gastric cancer. Mol Cancer **2017**;16:54
279. Kurzeder C, Nguyen-Strauli BD, Krol I, Ring A, Castro-Giner F, Nuesch M*, et al.* Digoxin for reduction of circulating tumor cell cluster size in metastatic breast cancer: a proof-of-concept trial. Nat Med **2025**;31
280. Moriyama T, Kataoka H, Seguchi K, Tsubouchi H, Koono M. Effects of hepatocyte growth factor (HGF) on human glioma cells in vitro: HGF acts as a motility factor in glioma cells. Int J Cancer **1996**;66:678-85
281. Yamamoto S, Wakimoto H, Aoyagi M, Hirakawa K, Hamada H. Modulation of motility and proliferation of glioma cells by hepatocyte growth factor. Jpn J Cancer Res **1997**;88:564-77
282. Yuan S, Almagro J, Fuchs E. Beyond genetics: driving cancer with the tumour microenvironment behind the wheel. Nat Rev Cancer **2024**;24:274-86
283. Baumann F, Leukel P, Doerfelt A, Beier CP, Dettmer K, Oefner PJ*, et al.* Lactate promotes glioma migration by TGF-beta2-dependent regulation of matrix metalloproteinase-2. Neuro Oncol **2009**;11:368-80
284. Hirschhaeuser F, Sattler UG, Mueller-Klieser W. Lactate: a metabolic key player in cancer. Cancer Res **2011**;71:6921-5
285. Seliger C, Leukel P, Moeckel S, Jachnik B, Lottaz C, Kreutz M*, et al.* Lactate-modulated induction of THBS-1 activates transforming growth factor (TGF)-beta2 and migration of glioma cells in vitro. PLoS One **2013**;8:e78935
286. Ward C, Meehan J, Gray ME, Murray AF, Argyle DJ, Kunkler IH*, et al.* The impact of tumour pH on cancer progression: strategies for clinical intervention. Explor Target Antitumor Ther **2020**;1:71-100
287. Zhou R, Tang X, Wang Y. Emerging strategies to investigate the biology of early cancer. Nat Rev Cancer **2024**;24:850-66
288. Putnam RW, Roos A, Wilding TJ. Properties of the intracellular pH-regulating systems of frog skeletal muscle. J Physiol **1986**;381:205-19

289. Fraser SP, Pardo LA. Ion channels: functional expression and therapeutic potential in cancer. Colloquium on Ion Channels and Cancer. EMBO Rep **2008**;9:512-5
290. Lang F, Stournaras C. Ion channels in cancer: future perspectives and clinical potential. Philos Trans R Soc Lond B Biol Sci **2014**;369:20130108
291. Martina M. Ion channel screening: advances in technologies and analysis. Front Pharmacol **2012**;3:86
292. Bretschneider F, Wrisch A, Lehmann-Horn F, Grissmer S. External tetraethylammonium as a molecular caliper for sensing the shape of the outer vestibule of potassium channels. Biophys J **1999**;76:2351-60
293. Somodi S, Hajdu P, Gaspar R, Panyi G, Varga Z. Effects of changes in extracellular pH and potassium concentration on Kv1.3 inactivation. Eur Biophys J **2008**;37:1145-56
294. Somodi S, Varga Z, Hajdu P, Starkus JG, Levy DI, Gaspar R*, et al.* pH-dependent modulation of Kv1.3 inactivation: role of His399. Am J Physiol Cell Physiol **2004**;287:C1067-76
295. Steidl JV, Yool AJ. Differential sensitivity of voltage-gated potassium channels Kv1.5 and Kv1.2 to acidic pH and molecular identification of pH sensor. Mol Pharmacol **1999**;55:812-20
296. Jager H, Grissmer S. Regulation of a mammalian Shaker-related potassium channel, hKv1.5, by extracellular potassium and pH. FEBS Lett **2001**;488:45-50
297. Kehl SJ, Eduljee C, Kwan DC, Zhang S, Fedida D. Molecular determinants of the inhibition of human Kv1.5 potassium currents by external protons and Zn(2+). J Physiol **2002**;541:9-24
298. Trapani JG, Korn SJ. Effect of external pH on activation of the Kv1.5 potassium channel. Biophys J **2003**;84:195-204
299. Zhang S, Kurata HT, Kehl SJ, Fedida D. Rapid induction of P/C-type inactivation is the mechanism for acid-induced K+ current inhibition. J Gen Physiol **2003**;121:215-25
300. Fedida D, Zhang S, Kwan DC, Eduljee C, Kehl SJ. Synergistic inhibition of the maximum conductance of Kv1.5 channels by extracellular K+ reduction and acidification. Cell Biochem Biophys **2005**;43:231-42
301. Wang S, Ding WG, Bai JY, Toyoda F, Wei MJ, Matsuura H. Regulation of human cardiac Kv1.5 channels by extracellular acidification. Pflugers Arch **2016**;468:1885-94
302. Tipparaju SM, Barski OA, Srivastava S, Bhatnagar A. Catalytic mechanism and substrate specificity of the beta-subunit of the voltage-gated potassium channel. Biochemistry **2008**;47:8840-54
303. Raph SM, Bhatnagar A, Nystoriak MA. Biochemical and physiological properties of K(+) channel-associated AKR6A (Kvbeta) proteins. Chem Biol Interact **2019**;305:21-7
304. Singarayar S, Bursill J, Wyse K, Bauskin A, Wu W, Vandenberg J*, et al.* Extracellular acidosis modulates drug block of Kv4.3 currents by flecainide and quinidine. J Cardiovasc Electrophysiol **2003**;14:641-50
305. Singarayar S, Singleton C, Tie H, Wyse K, Bursill J, Bauskin A*, et al.* Effects of components of ischemia on the Kv4.3 current stably expressed in Chinese hamster ovary cells. J Mol Cell Cardiol **2002**;34:197-207
306. Saegusa N, Garg V, Spitzer KW. Modulation of ventricular transient outward K(+) current by acidosis and its effects on excitation-contraction coupling. Am J Physiol Heart Circ Physiol **2013**;304:H1680-96
307. Heitzmann D, Grahammer F, von Hahn T, Schmitt-Graff A, Romeo E, Nitschke R*, et al.* Heteromeric KCNE2/KCNQ1 potassium channels in the luminal membrane of gastric parietal cells. J Physiol **2004**;561:547-57
308. Heitzmann D, Koren V, Wagner M, Sterner C, Reichold M, Tegtmeier I*, et al.* KCNE beta subunits determine pH sensitivity of KCNQ1 potassium channels. Cell Physiol Biochem **2007**;19:21-32

309. Heitzmann D, Warth R. No potassium, no acid: K+ channels and gastric acid secretion. Physiology (Bethesda) **2007**;22:335-41
310. Abbott GW, Roepke TK. KCNE2 and gastric cancer: bench to bedside. Oncotarget **2016**;7:17286-7
311. Engevik AC, Kaji I, Goldenring JR. The Physiology of the Gastric Parietal Cell. Physiol Rev **2020**;100:573-602
312. Terlau H, Ludwig J, Steffan R, Pongs O, Stuhmer W, Heinemann SH. Extracellular Mg2+ regulates activation of rat eag potassium channel. Pflugers Arch **1996**;432:301-12
313. Anumonwo JM, Horta J, Delmar M, Taffet SM, Jalife J. Proton and zinc effects on HERG currents. Biophys J **1999**;77:282-98
314. Berube J, Chahine M, Daleau P. Modulation of HERG potassium channel properties by external pH. Pflugers Arch **1999**;438:419-22
315. Jiang M, Dun W, Tseng GN. Mechanism for the effects of extracellular acidification on HERG-channel function. Am J Physiol **1999**;277:H1283-92
316. Jo SH, Youm JB, Kim I, Lee CO, Earm YE, Ho WK. Blockade of HERG channels expressed in Xenopus oocytes by external H+. Pflugers Arch **1999**;438:23-9
317. Terai T, Furukawa T, Katayama Y, Hiraoka M. Effects of external acidosis on HERG current expressed in Xenopus oocytes. J Mol Cell Cardiol **2000**;32:11-21
318. Vereecke J, Carmeliet E. The effect of external pH on the delayed rectifying K+ current in cardiac ventricular myocytes. Pflugers Arch **2000**;439:739-51
319. Zhou Q, Bett GC. Regulation of the voltage-insensitive step of HERG activation by extracellular pH. Am J Physiol Heart Circ Physiol **2010**;298:H1710-8
320. Van Slyke AC, Cheng YM, Mafi P, Allard CR, Hull CM, Shi YP*, et al.* Proton block of the pore underlies the inhibition of hERG cardiac K+ channels during acidosis. Am J Physiol Cell Physiol **2012**;302:C1797-806
321. Shi YP, Cheng YM, Van Slyke AC, Claydon TW. External protons destabilize the activated voltage sensor in hERG channels. Eur Biophys J **2014**;43:59-69
322. Shi YP, Thouta S, Cheng YM, Claydon TW. Extracellular protons accelerate hERG channel deactivation by destabilizing voltage sensor relaxation. J Gen Physiol **2019**;151:231-46
323. Shi YP, Thouta S, Claydon TW. Modulation of hERG K(+) Channel Deactivation by Voltage Sensor Relaxation. Front Pharmacol **2020**;11:139
324. Wilson SL, Dempsey CE, Hancox JC, Marrion NV. Identification of a proton sensor that regulates conductance and open time of single hERG channels. Sci Rep **2019**;9:19825
325. Ukachukwu CU, Jimenez-Vazquez EN, Jain A, Jones DK. hERG1 channel subunit composition mediates proton inhibition of rapid delayed rectifier potassium current (I(Kr)) in cardiomyocytes derived from hiPSCs. J Biol Chem **2023**;299:102778
326. Shi W, Wang HS, Pan Z, Wymore RS, Cohen IS, McKinnon D*, et al.* Cloning of a mammalian elk potassium channel gene and EAG mRNA distribution in rat sympathetic ganglia. J Physiol **1998**;511 (Pt 3):675-82
327. Sala-Rabanal M, Nichols CG. Inward rectifying potassium channels. In: Zheng J, Trudeau MC, editors. Handbook of Ion Channels. Boca Raton, FL: CRC Press; 2015. p 241-60.
328. Davies NW. Modulation of ATP-sensitive K+ channels in skeletal muscle by intracellular protons. Nature **1990**;343:375-7
329. Davies NW, Standen NB, Stanfield PR. The effect of intracellular pH on ATP-dependent potassium channels of frog skeletal muscle. J Physiol **1992**;445:549-68
330. Vivaudou M, Forestier C. Modification by protons of frog skeletal muscle KATP channels: effects on ion conduction and nucleotide inhibition. J Physiol **1995**;486 (Pt 3):629-45

331. Forestier C, Pierrard J, Vivaudou M. Mechanism of action of K channel openers on skeletal muscle KATP channels. Interactions with nucleotides and protons. J Gen Physiol **1996**;107:489-502
332. Santa N, Kitazono T, Ago T, Ooboshi H, Kamouchi M, Wakisaka M*, et al.* ATP-sensitive potassium channels mediate dilatation of basilar artery in response to intracellular acidification in vivo. Stroke **2003**;34:1276-80
333. Butt AM, Kalsi A. Inwardly rectifying potassium channels (Kir) in central nervous system glia: a special role for Kir4.1 in glial functions. J Cell Mol Med **2006**;10:33-44
334. Shuck ME, Piser TM, Bock JH, Slightom JL, Lee KS, Bienkowski MJ. Cloning and characterization of two K+ inward rectifier (Kir) 1.1 potassium channel homologs from human kidney (Kir1.2 and Kir1.3). J Biol Chem **1997**;272:586-93
335. Yang Z, Jiang C. Opposite effects of pH on open-state probability and single channel conductance of kir4.1 channels. J Physiol **1999**;520 Pt 3:921-7
336. Xu H, Yang Z, Cui N, Giwa LR, Abdulkadir L, Patel M*, et al.* Molecular determinants for the distinct pH sensitivity of Kir1.1 and Kir4.1 channels. Am J Physiol Cell Physiol **2000**;279:C1464-71
337. Xu H, Cui N, Yang Z, Qu Z, Jiang C. Modulation of kir4.1 and kir5.1 by hypercapnia and intracellular acidosis. J Physiol **2000**;524 Pt 3:725-35
338. Tucker SJ, Imbrici P, Salvatore L, D'Adamo MC, Pessia M. pH dependence of the inwardly rectifying potassium channel, Kir5.1, and localization in renal tubular epithelia. J Biol Chem **2000**;275:16404-7
339. Tanemoto M, Kittaka N, Inanobe A, Kurachi Y. In vivo formation of a proton-sensitive K+ channel by heteromeric subunit assembly of Kir5.1 with Kir4.1. J Physiol **2000**;525 Pt 3:587-92
340. Yang Z, Xu H, Cui N, Qu Z, Chanchevalap S, Shen W*, et al.* Biophysical and molecular mechanisms underlying the modulation of heteromeric Kir4.1-Kir5.1 channels by CO2 and pH. J Gen Physiol **2000**;116:33-45
341. Pessia M, Imbrici P, D'Adamo MC, Salvatore L, Tucker SJ. Differential pH sensitivity of Kir4.1 and Kir4.2 potassium channels and their modulation by heteropolymerisation with Kir5.1. J Physiol **2001**;532:359-67
342. Hibino H, Fujita A, Iwai K, Yamada M, Kurachi Y. Differential assembly of inwardly rectifying K+ channel subunits, Kir4.1 and Kir5.1, in brain astrocytes. J Biol Chem **2004**;279:44065-73
343. Sepulveda FV, Pablo Cid L, Teulon J, Niemeyer MI. Molecular aspects of structure, gating, and physiology of pH-sensitive background K2P and Kir K+-transport channels. Physiol Rev **2015**;95:179-217
344. Hughes BA, Swaminathan A. Modulation of the Kir7.1 potassium channel by extracellular and intracellular pH. Am J Physiol Cell Physiol **2008**;294:C423-31
345. Lesage F, Guillemare E, Fink M, Duprat F, Lazdunski M, Romey G*, et al.* TWIK-1, a ubiquitous human weakly inward rectifying K+ channel with a novel structure. EMBO J **1996**;15:1004-11
346. Lesage F, Lazdunski M. Molecular and functional properties of two-pore-domain potassium channels. Am J Physiol Renal Physiol **2000**;279:F793-801
347. Rajan S, Plant LD, Rabin ML, Butler MH, Goldstein SA. Sumoylation silences the plasma membrane leak K+ channel K2P1. Cell **2005**;121:37-47
348. Feliciangeli S, Chatelain FC, Bichet D, Lesage F. The family of K2P channels: salient structural and functional properties. J Physiol **2015**;593:2587-603
349. Turney TS, Li V, Brohawn SG. Structural Basis for pH-gating of the K(+) channel TWIK1 at the selectivity filter. Nat Commun **2022**;13:3232
350. Chatelain FC, Gilbert N, Bichet D, Jauch A, Feliciangeli S, Lesage F*, et al.* Mechanistic basis of the dynamic response of TWIK1 ionic selectivity to pH. Nat Commun **2024**;15:3849

351. Maingret F, Patel AJ, Lesage F, Lazdunski M, Honore E. Mechano- or acid stimulation, two interactive modes of activation of the TREK-1 potassium channel. J Biol Chem **1999**;274:26691-6
352. Honore E, Maingret F, Lazdunski M, Patel AJ. An intracellular proton sensor commands lipid- and mechano-gating of the K(+) channel TREK-1. EMBO J **2002**;21:2968-76
353. Cohen A, Ben-Abu Y, Hen S, Zilberberg N. A novel mechanism for human K2P2.1 channel gating. Facilitation of C-type gating by protonation of extracellular histidine residues. J Biol Chem **2008**;283:19448-55
354. Sandoz G, Douguet D, Chatelain F, Lazdunski M, Lesage F. Extracellular acidification exerts opposite actions on TREK1 and TREK2 potassium channels via a single conserved histidine residue. Proc Natl Acad Sci U S A **2009**;106:14628-33
355. Ryoo K, Park JY. Two-pore Domain Potassium Channels in Astrocytes. Exp Neurobiol **2016**;25:222-32
356. Nasr N, Faucherre A, Borsotto M, Heurteaux C, Mazella J, Jopling C*, et al.* Identification and characterization of two zebrafish Twik related potassium channels, Kcnk2a and Kcnk2b. Sci Rep **2018**;8:15311
357. Luo Y, Huang L, Liao P, Jiang R. Contribution of Neuronal and Glial Two-Pore-Domain Potassium Channels in Health and Neurological Disorders. Neural Plast **2021**;2021:8643129
358. Duprat F, Lesage F, Fink M, Reyes R, Heurteaux C, Lazdunski M. TASK, a human background K+ channel to sense external pH variations near physiological pH. EMBO J **1997**;16:5464-71
359. Millar JA, Barratt L, Southan AP, Page KM, Fyffe RE, Robertson B*, et al.* A functional role for the two-pore domain potassium channel TASK-1 in cerebellar granule neurons. Proc Natl Acad Sci U S A **2000**;97:3614-8
360. Torborg CL, Berg AP, Jeffries BW, Bayliss DA, McBain CJ. TASK-like conductances are present within hippocampal CA1 stratum oriens interneuron subpopulations. J Neurosci **2006**;26:7362-7
361. Shvetsova AA, Lazarenko VS, Gaynullina DK, Tarasova OS, Schubert R. TWIK-Related Acid-Sensitive Potassium Channels (TASK-1) Emerge as Contributors to Tone Regulation in Renal Arteries at Alkaline pH. Front Physiol **2022**;13:895863
362. Reyes R, Duprat F, Lesage F, Fink M, Salinas M, Farman N*, et al.* Cloning and expression of a novel pH-sensitive two pore domain K+ channel from human kidney. J Biol Chem **1998**;273:30863-9
363. Morton MJ, Abohamed A, Sivaprasadarao A, Hunter M. pH sensing in the two-pore domain K+ channel, TASK2. Proc Natl Acad Sci U S A **2005**;102:16102-6
364. Gonczi M, Szentandrassy N, Johnson IT, Heagerty AM, Weston AH. Investigation of the role of TASK-2 channels in rat pulmonary arteries; pharmacological and functional studies following RNA interference procedures. Br J Pharmacol **2006**;147:496-505
365. Niemeyer MI, Cid LP, Pena-Munzenmayer G, Sepulveda FV. Separate gating mechanisms mediate the regulation of K2P potassium channel TASK-2 by intra- and extracellular pH. J Biol Chem **2010**;285:16467-75
366. Zuniga L, Marquez V, Gonzalez-Nilo FD, Chipot C, Cid LP, Sepulveda FV*, et al.* Gating of a pH-sensitive K(2P) potassium channel by an electrostatic effect of basic sensor residues on the selectivity filter. PLoS One **2011**;6:e16141
367. Cid LP, Roa-Rojas HA, Niemeyer MI, Gonzalez W, Araki M, Araki K*, et al.* TASK-2: a K2P K(+) channel with complex regulation and diverse physiological functions. Front Physiol **2013**;4:198
368. Bustos D, Bedoya M, Ramirez D, Concha G, Zuniga L, Decher N*, et al.* Elucidating the Structural Basis of the Intracellular pH Sensing Mechanism of TASK-2 K(2)P Channels. Int J Mol Sci **2020**;21
369. Khoubza L, Gilbert N, Kim EJ, Chatelain FC, Feliciangeli S, Abelanet S*, et al.* Alkaline-sensitive two-pore domain potassium channels form functional heteromers in pancreatic beta-cells. J Biol Chem **2022**;298:102447

370. Chavez RA, Gray AT, Zhao BB, Kindler CH, Mazurek MJ, Mehta Y*, et al.* TWIK-2, a new weak inward rectifying member of the tandem pore domain potassium channel family. J Biol Chem **1999**;274:7887-92
371. Patel AJ, Maingret F, Magnone V, Fosset M, Lazdunski M, Honore E. TWIK-2, an inactivating 2P domain K+ channel. J Biol Chem **2000**;275:28722-30
372. Rinne S, Schick F, Vowinkel K, Schutte S, Krasel C, Kauferstein S*, et al.* Potassium channel TASK-5 forms functional heterodimers with TASK-1 and TASK-3 to break its silence. Nat Commun **2024**;15:7548
373. Cook DL, Ikeuchi M, Fujimoto WY. Lowering of pHi inhibits Ca2+-activated K+ channels in pancreatic B-cells. Nature **1984**;311:269-71
374. Christensen O, Zeuthen T. Maxi K+ channels in leaky epithelia are regulated by intracellular Ca2+, pH and membrane potential. Pflugers Arch **1987**;408:249-59
375. Kume H, Takagi K, Satake T, Tokuno H, Tomita T. Effects of intracellular pH on calcium-activated potassium channels in rabbit tracheal smooth muscle. J Physiol **1990**;424:445-57
376. Peers C, Green FK. Inhibition of Ca(2+)-activated K+ currents by intracellular acidosis in isolated type I cells of the neonatal rat carotid body. J Physiol **1991**;437:589-602
377. Schubert R, Krien U, Gagov H. Protons inhibit the BK(Ca) channel of rat small artery smooth muscle cells. J Vasc Res **2001**;38:30-8
378. Avdonin V, Tang XD, Hoshi T. Stimulatory action of internal protons on Slo1 BK channels. Biophys J **2003**;84:2969-80
379. Brelidze TI, Magleby KL. Protons block BK channels by competitive inhibition with K+ and contribute to the limits of unitary currents at high voltages. J Gen Physiol **2004**;123:305-19
380. Raingo J, Rebolledo A, Grassi de Gende AO, Sanz N, Tommasi J, Milesi V. pH effects on high conductance Ca2+-activated K+ channels (BK(Ca)) in human internal mammary artery smooth muscle cells. Life Sci **2005**;77:1993-2003
381. Petroff E, Snitsarev V, Gong H, Abboud FM. Acid sensing ion channels regulate neuronal excitability by inhibiting BK potassium channels. Biochem Biophys Res Commun **2012**;426:511-5
382. Petroff EY, Price MP, Snitsarev V, Gong H, Korovkina V, Abboud FM*, et al.* Acid-sensing ion channels interact with and inhibit BK K+ channels. Proc Natl Acad Sci U S A **2008**;105:3140-4
383. Hou S, Horrigan FT, Xu R, Heinemann SH, Hoshi T. Comparative effects of H+ and Ca2+ on large-conductance Ca2+- and voltage-gated Slo1 K+ channels. Channels (Austin) **2009**;3:249-58
384. Yang H, Cui J. BK channels. In: Zheng J, Trudeau MC, editors. Handbook of Ion Channels. Boca Raton, FL: CRC Press; 2015. p 227-39.
385. Guarina L, Vandael DH, Carabelli V, Carbone E. Low pH(o) boosts burst firing and catecholamine release by blocking TASK-1 and BK channels while preserving Cav1 channels in mouse chromaffin cells. J Physiol **2017**;595:2587-609
386. Zhou Y, Xia XM, Lingle CJ. BK channel inhibition by strong extracellular acidification. Elife **2018**;7
387. Dopico AM, Bukiya AN, Jaggar JH. Calcium- and voltage-gated BK channels in vascular smooth muscle. Pflugers Arch **2018**;470:1271-89
388. Sancho M, Kyle BD. The Large-Conductance, Calcium-Activated Potassium Channel: A Big Key Regulator of Cell Physiology. Front Physiol **2021**;12:750615
389. Yang CT, Zeng XH, Xia XM, Lingle CJ. Interactions between beta subunits of the KCNMB family and Slo3: beta4 selectively modulates Slo3 expression and function. PLoS One **2009**;4:e6135
390. Wen D, Cornelius RJ, Yuan Y, Sansom SC. Regulation of BK-alpha expression in the distal nephron by aldosterone and urine pH. Am J Physiol Renal Physiol **2013**;305:F463-76
391. Wen D, Cornelius RJ, Rivero-Hernandez D, Yuan Y, Li H, Weinstein AM*, et al.* Relation between BK-alpha/beta4-mediated potassium secretion and ENaC-mediated sodium reabsorption. Kidney Int **2014**;86:139-45

392. Wang B, Wang-France J, Li H, Sansom SC. Furosemide reduces BK-alphabeta4-mediated K(+) secretion in mice on an alkaline high-K(+) diet. Am J Physiol Renal Physiol **2019**;316:F341-F50
393. Al-Qusairi L, Ferdaus MZ, Pham TD, Li D, Grimm PR, Zapf AM*, et al.* Dietary anions control potassium excretion: it is more than a poorly absorbable anion effect. Am J Physiol Renal Physiol **2023**;325:F377-F93
394. Goodchild SJ, Lamy C, Seutin V, Marrion NV. Inhibition of K(Ca)2.2 and K(Ca)2.3 channel currents by protonation of outer pore histidine residues. J Gen Physiol **2009**;134:295-308
395. Srivastava S, Li Z, Ko K, Choudhury P, Albaqumi M, Johnson AK*, et al.* Histidine phosphorylation of the potassium channel KCa3.1 by nucleoside diphosphate kinase B is required for activation of KCa3.1 and CD4 T cells. Mol Cell **2006**;24:665-75
396. Kee JM, Muir TW. Chasing phosphohistidine, an elusive sibling in the phosphoamino acid family. ACS Chem Biol **2012**;7:44-51
397. Kalagiri R, Hunter T. The many ways that nature has exploited the unusual structural and chemical properties of phosphohistidine for use in proteins. Biochem J **2021**;478:3575-96
398. Ning J, Sala M, Reina J, Kalagiri R, Hunter T, McCullough BS. Histidine Phosphorylation: Protein Kinases and Phosphatases. Int J Mol Sci **2024**;25
399. Yamane T, Furukawa T, Horikawa S, Hiraoka M. External pH regulates the slowly activating potassium current IsK expressed in Xenopus oocytes. FEBS Lett **1993**;319:229-32
400. Freeman LC, Lippold JJ, Mitchell KE. Glycosylation influences gating and pH sensitivity of I(sK). J Membr Biol **2000**;177:65-79
401. Unsold B, Kerst G, Brousos H, Hubner M, Schreiber R, Nitschke R*, et al.* KCNE1 reverses the response of the human K+ channel KCNQ1 to cytosolic pH changes and alters its pharmacology and sensitivity to temperature. Pflugers Arch **2000**;441:368-78
402. Peretz A, Schottelndreier H, Aharon-Shamgar LB, Attali B. Modulation of homomeric and heteromeric KCNQ1 channels by external acidification. J Physiol **2002**;545:751-66
403. Roepke TK, King EC, Purtell K, Kanda VA, Lerner DJ, Abbott GW. Genetic dissection reveals unexpected influence of beta subunits on KCNQ1 K+ channel polarized trafficking in vivo. FASEB J **2011**;25:727-36
404. Dixit G, Dabney-Smith C, Lorigan GA. The membrane protein KCNQ1 potassium ion channel: Functional diversity and current structural insights. Biochim Biophys Acta Biomembr **2020**;1862:183148
405. Abbott GW. KCNQs: Ligand- and Voltage-Gated Potassium Channels. Front Physiol **2020**;11:583
406. Prole DL, Lima PA, Marrion NV. Mechanisms underlying modulation of neuronal KCNQ2/KCNQ3 potassium channels by extracellular protons. J Gen Physiol **2003**;122:775-93
407. Mehrdel B, Villalba-Galea CA. Effect of a sensing charge mutation on the deactivation of KV7.2 channels. J Gen Physiol **2024**;156
408. Jensen HS, Callo K, Jespersen T, Jensen BS, Olesen SP. The KCNQ5 potassium channel from mouse: a broadly expressed M-current like potassium channel modulated by zinc, pH, and volume changes. Brain Res Mol Brain Res **2005**;139:52-62
409. Ruffin VA, Gu XQ, Zhou D, Douglas RM, Sun X, Trouth CO*, et al.* The sodium-activated potassium channel Slack is modulated by hypercapnia and acidosis. Neuroscience **2008**;151:410-8
410. Ruffin VA, Salameh AI, Boron WF, Parker MD. Intracellular pH regulation by acid-base transporters in mammalian neurons. Front Physiol **2014**;5:43
411. Kaczmarek LK. Slack, Slick and Sodium-Activated Potassium Channels. ISRN Neurosci **2013**;2013
412. Kaczmarek LK, Aldrich RW, Chandy KG, Grissmer S, Wei AD, Wulff H. International Union of Basic and Clinical Pharmacology. C. Nomenclature and Properties of Calcium-Activated and Sodium-Activated Potassium Channels. Pharmacol Rev **2017**;69:1-11

413. Schreiber M, Wei A, Yuan A, Gaut J, Saito M, Salkoff L. Slo3, a novel pH-sensitive K+ channel from mammalian spermatocytes. J Biol Chem **1998**;273:3509-16
414. Zhang X, Zeng X, Lingle CJ. Slo3 K+ channels: voltage and pH dependence of macroscopic currents. J Gen Physiol **2006**;128:317-36
415. Zhang X, Zeng X, Xia XM, Lingle CJ. pH-regulated Slo3 K+ channels: properties of unitary currents. J Gen Physiol **2006**;128:301-15
416. Navarro B, Kirichok Y, Clapham DE. KSper, a pH-sensitive K+ current that controls sperm membrane potential. Proc Natl Acad Sci U S A **2007**;104:7688-92
417. Leonetti MD, Yuan P, Hsiung Y, Mackinnon R. Functional and structural analysis of the human SLO3 pH- and voltage-gated K+ channel. Proc Natl Acad Sci U S A **2012**;109:19274-9
418. Brenker C, Zhou Y, Muller A, Echeverry FA, Trotschel C, Poetsch A*, et al.* The Ca2+-activated K+ current of human sperm is mediated by Slo3. Elife **2014**;3:e01438
419. Ludwig MG, Vanek M, Guerini D, Gasser JA, Jones CE, Junker U*, et al.* Proton-sensing G-protein-coupled receptors. Nature **2003**;425:93-8
420. Weiss KT, Fante M, Kohl G, Schreml J, Haubner F, Kreutz M*, et al.* Proton-sensing G protein-coupled receptors as regulators of cell proliferation and migration during tumor growth and wound healing. Exp Dermatol **2017**;26:127-32
421. Hosford PS, Mosienko V, Kishi K, Jurisic G, Seuwen K, Kinzel B*, et al.* CNS distribution, signalling properties and central effects of G-protein coupled receptor 4. Neuropharmacology **2018**;138:381-92
422. Mashiko M, Kurosawa A, Tani Y, Tsuji T, Takeda S. GPR31 and GPR151 are activated under acidic conditions. J Biochem **2019**;166:317-22
423. Klatt W, Wallner S, Brochhausen C, Stolwijk JA, Schreml S. Expression profiles of proton-sensing G-protein coupled receptors in common skin tumors. Sci Rep **2020**;10:15327
424. Sisignano M, Fischer MJM, Geisslinger G. Proton-Sensing GPCRs in Health and Disease. Cells **2021**;10
425. Forch A, Wallner S, Zeman F, Ettl T, Brochhausen C, Schreml S. Expression of Proton-Sensitive GPR31, GPR151, TASK1 and TASK3 in Common Skin Tumors. Cells **2021**;11
426. Imenez Silva PH, Camara NO, Wagner CA. Role of proton-activated G protein-coupled receptors in pathophysiology. Am J Physiol Cell Physiol **2022**;323:C400-C14
427. Imenez Silva PH, Wagner CA. Physiological relevance of proton-activated GPCRs. Pflugers Arch **2022**;474:487-504
428. Kumar NN, Velic A, Soliz J, Shi Y, Li K, Wang S*, et al.* PHYSIOLOGY. Regulation of breathing by CO(2) requires the proton-activated receptor GPR4 in retrotrapezoid nucleus neurons. Science **2015**;348:1255-60
429. Guyenet PG, Bayliss DA. Neural Control of Breathing and CO2 Homeostasis. Neuron **2015**;87:946-61
430. Ramadoss S, Qin J, Tao B, Thomas NE, Cao E, Wu R*, et al.* Bone-marrow macrophage-derived GPNMB protein binds to orphan receptor GPR39 and plays a critical role in cardiac repair. Nat Cardiovasc Res **2024**;3:1356-73
431. Wang J, Simonavicius N, Wu X, Swaminath G, Reagan J, Tian H*, et al.* Kynurenic acid as a ligand for orphan G protein-coupled receptor GPR35. J Biol Chem **2006**;281:22021-8
432. Wang J, Wu X, Simonavicius N, Tian H, Ling L. Medium-chain fatty acids as ligands for orphan G protein-coupled receptor GPR84. J Biol Chem **2006**;281:34457-64

Disclaimer: The statements and opinions are those of the author. The author disclaims responsibility for any injury to people or property resulting from any ideas, methods, instructions, products, or publications cited in the content.

FullTBLB1DEGalphaAZ

1	E21	A2M	41	E43	ADAM19
2	E65	AAK1	42	E28	ADAM28
3	E54	AATK	43	E49	Adam8
4	E1	AB113AP	44	E45	Adam9
5	E50	ABCA1	45	E49	Adamdec1
6	E54	ABCA12	46	E14	ADAMTS15
7	E48	ABCB10	47	E1	ADAMTS2
8	E69	Abcb1a	48	E21	ADAMTS4
9	E70	Abcc3	49	E26	Adarb1
10	E31	ABCD1	50	E26	Adcy1
11	E9	ABHD11	51	E4	ADCY2
12	E58	AC004019.18	52	E26	Adcy5
13	E14	AC012501.3	53	E4	ADCY6
14	E58	AC079602.1	54	E4	ADCY8
15	E25	AC092162.1	55	E62	ADCY9
16	E33	ACAA2	56	E34	ADCYAP1
17	E21	ACACA	57	E5	ADCYAP1R1
18	E24	ACAN	58	E27	ADD2
19	E69	Ace	59	E21	ADGRG1
20	E20	ACSM1	60	E34	ADIPOR2
21	E2	ACSM3	61	E15	ADORA2A
22	E29	ACTA2	62	E38	ADRA1D
23	E1	ACTA2	63	E2	ADRA2A
24	E43	ACTA2	64	E52	ADRA2A
25	E66	ACTA2	65	E40	AEBP1
26	E45	Actb	66	E30	AFAP1-AS1
27	E4	ACTC1	67	E2	Afap1l1
28	E1	ACTG2	68	E25	AFAP1L1
29	E21	ACTG2	69	E23	AFAP1L2
30	E43	ACTG2	70	E14	AFMID
31	E4	ACTN2	71	E21	AGAP2
32	E16	ACTR3	72	E57	AGBL2
33	E35	ACTR3	73	E20	AGFG2
34	E59	Actr3b	74	E50	AGO2
35	E1	ACVR2A	75	E14	AGO3
36	E70	Acvrl1	76	E58	AGPAT9
37	E38	ADAM12	77	E2	AGR3
38	E39	ADAM12	78	E42	AGR3
39	E21	ADAM19	79	E31	AGRN
40	E38	ADAM19	80	E34	AGT

81	E51	AGT	
82	E34	AGTR1	
83	E70	Agtr1	
84	E26	Ahl1	
85	E21	AHRR	
86	E37	AICDA	
87	E54	AICDA	
88	E21	AIFM1	
89	E23	AIM2	
90	E14	AJ239322.1	
91	E70	Ak1	
92	E70	Ak5	
93	E15	AK8	
94	E37	AKAP12	
95	E38	AKAP12	
96	E31	AKAP13	
97	E16	AKR1B1	
98	E45	Akr1b10	
99	E45	Akr1b3	
100	E45	Akr1b8	
101	E23	AKR1C2	
102	E42	AKR1C3	
103	E23	AKR1C4	
104	E35	AKT3	
105	E52	AL354984.1	
106	E21	ALDH18A1	
107	E54	ALDH1A1	
108	E20	ALDH1A2	
109	E49	Aldh1a2	
110	E54	ALDH1A2	
111	E1	ALDH1A3	
112	E69	Aldh1a3	
113	E57	ALDH1L1	
114	E21	ALDH3B1	
115	E44	ALG3	
116	E2	ALMS1	
117	E43	ALOX5AP	
118	E64	ALOX5AP	
119	E54	ALPPL2	
120	E21	AMDHD2	
121	E55	Amhr2	
122	E11	AMIG02	

123	E13	AMN	
124	E58	AMOT	
125	E20	AMOTL2	
126	E70	Amotl2	
127	E2	ANGPT2	
128	E1	ANGPTL2	
129	E29	ANGPTL4	
130	E33	ANGPTL4	
131	E43	ANGPTL4	
132	E69	Angptl4	
133	E65	ANGPTL7	
134	E20	ANKRD1	
135	E31	ANKRD46	
136	E20	ANKRD7	
137	E63	ANLN	
138	E70	Anln	
139	E66	ANP32B	
140	E41	ANTXR2	
141	E56	ANTXR2	
142	E41	ANXA1	
143	E70	Anxa1	
144	E49	Anxa10	
145	E69	Anxa10	
146	E42	ANXA13	
147	E60	ANXA13	
148	E37	ANXA2	
149	E45	Anxa2	
150	E70	Anxa3	
151	E29	ANXA4	
152	E16	ANXA6	
153	E21	ANXA6	
154	E40	ANXA8L2	
155	E22	ANXA9	
156	E58	AOC1	
157	E58	AP001626.1	
158	E44	AP2M1	
159	E48	APBA2	
160	E66	APC2	
161	E32	APCDD1	
162	E56	APCDD1	
163	E34	APLN	
164	E37	APOBEC3G	
165	E26	Apod	

166	E1	APOE	
167	E14	APOE	
168	E21	APOE	
169	E59	Apoe	
170	E14	APOL3	
171	E2	APP	
172	E2	AQP1	
173	E51	AQP1	
174	E59	Aqp1	
175	E25	AQP3	
176	E8	AQP3	
177	E22	AQP3	
178	E58	AQP3	
179	E51	AQP4	
180	E54	AR	
181	E65	AR	
182	E70	Arap3	
183	E21	ARC	
184	E51	ARC	
185	E52	AREG	
186	E35	ARF4	
187	E43	ARF4	
188	E21	ARFGEF3	
189	E1	ARHGAP20	
190	E35	ARHGAP20	
191	E1	ARHGAP24	
192	E40	ARHGAP25	
193	E58	ARHGAP26	
194	E43	ARHGDIB	
195	E3	ARHGEF16	
196	E27	ARHGEF26-AS1	
197	E67	Arid5b	
198	E41	ARL4C	
199	E14	ARL4C	
200	E4	ARL6IP5	
201	E1	ARMH4	
202	E23	ARNTL2	
203	E38	ARNTL2	
204	E7	ARRB1	
205	E62	ARRDC3	
206	E31	ARSG	
207	E58	ARSI	
208	E65	ARX	

209	E31	ASAH1	
210	E20	ASAP1	
211	E12	ASCL1	
212	E17	ASCL1	
213	E35	ASCL1	
214	E65	ASCL1	
215	E2	ASCL2	
216	E46	ASCL2	
217	E15	ASIC4	
218	E54	ASNS	
219	E2	ASPM	
220	E17	ATCAY	
221	E60	ATF3	
222	E35	ATG14	
223	E60	ATM	
224	E66	ATN1	
225	E26	Atp1a2	
226	E4	ATP1A2	
227	E5	ATP1A2	
228	E51	ATP1A2	
229	E29	ATP1B1	
230	E19	ATP1B1	
231	E51	ATP1B2	
232	E15	ATP2B1	
233	E58	ATP2C2	
234	E66	ATP5D	
235	E70	Atp6v0e1	
236	E48	ATP6V1C1	
237	E42	ATP7B	
238	E25	AURKA	
239	E67	Auts2	
240	E58	AVPI1	
241	E34	AVPR2	
242	E68	AXIN2	
243	E41	AXL	
244	E14	B2M	
245	E67	B2m	
246	E21	B4GALT5	
247	E33	B4GALT5	
248	E54	B4GALT6	
249	E41	BAALC	
250	E42	BACE2	
251	E56	BACE2	

252	E22	BAG1	
253	E13	BAIAP2L1	
254	E42	BAIAP2L2	
255	E63	BAIAP2L2	
256	E55	Bambi	
257	E62	BANF1	
258	E37	BANK1	
259	E56	BANK1	
260	E46	BARX2	
261	E23	BATF3	
262	E60	BBC3(PUMA)	
263	E59	BC064078	
264	E26	Bc1	
265	E60	BCAM	
266	E14	BCAN	
267	E35	BCAR3	
268	E60	BCAS3	
269	E63	BCAT1	
270	E21	BCAT2	
271	E20	BCL11A	
272	E12	BCL2	
273	E22	BCL2	
274	E35	BCL2	
275	E1	BCL3	
276	E2	BCL7A	
277	E14	BCL7A	
278	E37	BCL7A	
279	E46	BCOR	
280	E66	BCORL1	
281	E65	BEND2	
282	E14	BEND3	
283	E14	BEND6	
284	E26	Bgn	
285	E21	BHLHE40	
286	E20	BICC1	
287	E58	BICC1	
288	E1	BIK	
289	E49	Birc3	
290	E60	BIRC3	
291	E20	BIRC5	
292	E63	BIRC5	
293	E14	BIRC7	
294	E39	BIRC7	

295	E3	BLNK	
296	E15	BLVRA	
297	E38	BMP2	
298	E41	BMP2	
299	E49	Bmp2	
300	E60	BMP4	
301	E5	BMP7	
302	E56	BMX	
303	E40	BNC1	
304	E29	BNIP3	
305	E16	BNIP3	
306	E66	BOLA2B	
307	E15	BRAF	
308	E2	BRCA2	
309	E66	BRD4	
310	E34	BRN3A	
311	E15	BRSK2	
312	E33	BSG	
313	E11	BSLC18A2	
314	E41	BST1	
315	E67	Bst2	
316	E11	BTBD11	
317	E54	BTG2	
318	E60	BTG2	
319	E66	BTG2	
320	E53	BTK	
321	E15	BTN2A2	
322	E42	BTNL8	
323	E54	C10orf10	
324	E58	C10orf99	
325	E65	C11orf87	
326	E14	C11orf96	
327	E23	C12orf39	
328	E23	C12orf56	
329	E41	C12orf75	
330	E29	C15orf48	
331	E23	C15orf48	
332	E41	C16orf45	
333	E40	C16orf74	
334	E43	C17orf91	
335	E14	C1orf115	
336	E66	C1orf173	
337	E21	C1orf95	

338	E34	C1QBP	
339	E58	C1QC	
340	E56	C1QTNF1	
341	E23	C20orf70	
342	E58	C2CD4B	
343	E34	C3AR1	
344	E54	C4orf34	
345	E45	C5orf51	
346	E11	C6orf192	
347	E58	C9orf152	
348	E29	CA12	
349	E19	CA12	
350	E21	CA14	
351	E42	CA2	
352	E29	CA9	
353	E58	CACNA1A	
354	E4	CACNA1B	
355	E34	CACNA1C	
356	E4	CACNA1E	
357	E11	CACNA2D3	
358	E58	CACNB1	
359	E3	CACNB3	
360	E28	CADM1	
361	E29	CADM1	
362	E41	CADM1	
363	E41	CADM4	
364	E58	CADPS	
365	E23	CALB1	
366	E57	CALB1	
367	E26	Calb2	
368	E52	CALCA	
369	E60	CALD1	
370	E21	CALM1	
371	E50	CALM1	
372	E31	CALM3	
373	E30	CALML3-AS1	
374	E26	Calml4	
375	E42	CALML4	
376	E62	CALU	
377	E51	CAMK2B	
378	E58	CAMK4	
379	E26	Campk2a	
380	E16	CAP1	

381	E21	CAPN5	
382	E59	Car2	
383	E60	CARD10	
384	E26	Cartpt	
385	E34	CASK	
386	E59	Casp1	
387	E37	CASP3	
388	E44	CASP4	
389	E20	CAT	
390	E23	CATSPER1	
391	E66	CATSPERD	
392	E28	CAV1	
393	E41	CAV1	
394	E60	CAV1	
395	E20	CAVIN2	
396	E50	CBL	
397	E45	Cbr1	
398	E45	Cbr3	
399	E60	CBS	
400	E31	CBX5	
401	E2	CC2D2A	
402	E20	CCDC114	
403	E26	Ccdc136	
404	E26	Ccdc153	
405	E2	CCDC18	
406	E54	CCDC33	
407	E54	CCDC46	
408	E66	CCDC85B	
409	E60	CCDN1	
410	E26	Cck	
411	E11	CCL1	
412	E49	Ccl20	
413	E22	CCND1	
414	E35	CCND1	
415	E45	Ccnd1	
416	E37	CCND2	
417	E45	Ccnd2	
418	E65	CCND2	
419	E53	CCND3	
420	E35	CCNE1	
421	E60	CCNE2	
422	E21	CCNG1	
423	E33	CCNL1	

424	E66	CCNL2	
425	E28	CCR10	
426	E18	CCT2	
427	E41	CD163L1	
428	E14	CD163L1	
429	E28	CD19	
430	E28	CD22	
431	E53	CD22	
432	E28	CD24	
433	E58	CD247	
434	E23	CD274	
435	E53	CD36	
436	E28	CD38	
437	E54	CD4	
438	E28	CD40	
439	E13	CD44	
440	E45	Cd44	
441	E34	CD55	
442	E29	CD68	
443	E23	CD70	
444	E28	CD79A	
445	E28	CD79B	
446	E37	CD86	
447	E23	CD8A	
448	E41	CD96	
449	E11	CD99	
450	E23	CDA	
451	E14	CDC16	
452	E20	CDC20	
453	E63	CDC20	
454	E21	CDC25B	
455	E2	CDC42EP1	
456	E60	CDC42EP3	
457	E2	CDCA7	
458	E14	CDCA7	
459	E2	CDCA71	
460	E50	CDCP1	
461	E16	CDH1	
462	E39	CDH13	
463	E40	CDH13	
464	E41	CDH13	
465	E14	CDH13	
466	E42	CDH17	

467	E16	CDH2	
468	E43	CDH2	
469	E15	CDH7	
470	E39	CDK14	
471	E20	CDK18	
472	E14	CDK2	
473	E18	CDK4	
474	E39	CDK5R1	
475	E63	CDK6	
476	E65	CDK6	
477	E10	CDKN1A	
478	E43	CDKN1A	
479	E66	CDKN1A	
480	E67	Cdkn1a	
481	E60	CDKN1A(p21)	
482	E65	CDKN1B	
483	E18	CDKN2A	
484	E46	CDKN2A/B	
485	E63	CDKN2C	
486	E2	CDO1	
487	E46	CDX2	
488	E64	CEACAM5	
489	E11	CEBPD	
490	E33	CEBPD	
491	E14	CECR5	
492	E31	CELF1	
493	E56	CELF6	
494	E45	Cend1	
495	E2	CENPF	
496	E63	CENPF	
497	E36	CENPH	
498	E31	CEP126	
499	E2	CEP192	
500	E58	CEP44	
501	E14	CEP68	
502	E43	CES1	
503	E54	CES1	
504	E59	Ces2g	
505	E35	CFLAR	
506	E11	CFR	
507	E52	CGA	
508	E43	CGB1	
509	E43	CGB5	

510	E52	CHAC1	
511	E58	CHDC2	
512	E60	CHECK1	
513	E17	CHGA	
514	E17	CHGB	
515	E54	CHGB	
516	E56	CHODL	
517	E52	CHRNA2	
518	E17	CHRNA3	
519	E58	CHRNA5	
520	E14	CHRNA9	
521	E27	CHST11	
522	E56	CHST15	
523	E54	CIITA	
524	E59	Cish	
525	E2	CIT	
526	E26	Cit	
527	E25	CITED1	
528	E2	CKAP2	
529	E16	CKAP4	
530	E33	CKB	
531	E51	CKB	
532	E42	CKMT1A	
533	E44	CKMT2	
534	E61	CLASPIN	
535	E41	CLCF1	
536	E56	CLCF1	
537	E21	CLCN7	
538	E26	Cldn11	
539	E7	CLDN3	
540	E13	CLDN4	
541	E59	Clec12a	
542	E11	CLEC4D	
543	E58	CLEC4E	
544	E59	Clec7a	
545	E37	CLECSF2	
546	E26	Clic6	
547	E66	CLIP3	
548	E14	CLN6	
549	E4	CLN8	
550	E31	CLOCK	
551	E62	CLSTN1	
552	E45	Clu	

553	E29	CMBL	
554	E67	Cmklr1	
555	E11	CMTM8	
556	E56	CMTM8	
557	E51	CNGA3	
558	E1	CNN1	
559	E21	CNN2	
560	E2	CNN3	
561	E16	CNN3	
562	E18	CNOT2	
563	E26	Cnp	
564	E35	CNTF	
565	E5	CNTN1	
566	E40	CNTNAP3B	
567	E37	COBLL1	
568	E26	Col11a1	
569	E26	Col11a2	
570	E39	COL13A1	
571	E41	COL13A1	
572	E1	COL16A1	
573	E40	COL17A1	
574	E33	COL18A1	
575	E26	Col19a2	
576	E43	COL22A1	
577	E1	COL23A1	
578	E58	COL26A1	
579	E24	COL2A1	
580	E26	Col2a1	
581	E43	COL4A1	
582	E57	COL4A1	
583	E63	COL4A3	
584	E21	COL4A3BP	
585	E58	COL4A4	
586	E40	COL4A6	
587	E43	COL5A1	
588	E3	COL5A2	
589	E33	COL6A1	
590	E60	COL6A1	
591	E33	COL6A2	
592	E14	COL8A1	
593	E26	Col9a1	
594	E1	COL9A2	
595	E58	COLCA1	

596	E31	COP1	
597	E11	COTL1	
598	E61	COX4L1	
599	E61	COX7B	
600	E61	COX7C	
601	E59	Cp	
602	E29	CP	
603	E20	CPA2	
604	E11	CPA3	
605	E31	CPD	
606	E33	CPE	
607	E26	Cplx2	
608	E18	CPM	
609	E2	CPN1	
610	E20	CPS1	
611	E23	CPS1	
612	E11	CR1	
613	E45	Creg1	
614	E34	CRHR1	
615	E20	CRIM1	
616	E41	CRIP2	
617	E54	CRISPLD2	
618	E37	CRY1	
619	E23	CSAG2	
620	E1	CSDC2	
621	E33	CSDE1	
622	E67	Csf1	
623	E38	CSF2	
624	E49	Csf2	
625	E23	CSF2	
626	E11	CSF2RB	
627	E38	CSF3	
628	E40	CSMD2	
629	E15	CSNK1A1L	
630	E15	CSNK2A	
631	E24	CSPG4	
632	E51	CSPG5	
633	E26	Csrp1	
634	E43	CSRP1	
635	E41	CSRP2	
636	E33	CST3	
637	E38	CTBP1	
638	E58	CTD-2114J12.1	

639	E65	CTD-2192J16.22	
640	E25	CTD-2303H24.2	
641	E66	CTDNEP1	
642	E18	CTDSP2	
643	E20	CTGF	
644	E43	CTGF	
645	E17	CTNNA2	
646	E13	CTNNB1	
647	E50	CTNNB1	
648	E37	CTPS	
649	E21	CTSA	
650	E37	CTSB	
651	E42	CTSE	
652	E11	CTSH	
653	E49	Ctss	
654	E43	CTXN1	
655	E65	CUX2	
656	E21	CX3CL1	
657	E17	CXADR	
658	E58	CXADR	
659	E66	CXADR	
660	E8	CXCL1	
661	E38	CXCL1	
662	E49	Cxcl10	
663	E67	Cxcl10	
664	E8	CXCL2	
665	E20	CXCL8	
666	E38	CXCR1	
667	E32	CYB5A	
668	E41	CYB5R2	
669	E13	CYBA	
670	E47	CYBB	
671	E38	CYGB	
672	E11	CYorf15A	
673	E32	CYP11B1	
674	E32	CYP11B2	
675	E32	CYP17A1	
676	E29	CYP1B1	
677	E57	CYP1B1	
678	E18	CYP27B1	
679	E38	CYP27B1	
680	E42	CYP2C18	
681	E58	CYP2C18	

682	E58	CYP2C19	
683	E45	Cyp2c70	
684	E2	CYP2E1	
685	E42	CYP2S1	
686	E47	CYP2U1	
687	E58	CYP4B1	
688	E63	CYP4B1	
689	E66	CYP4F2	
690	E66	CYP4F3	
691	E25	CYPP19A1	
692	E20	CYR61	
693	E41	CYR61	
694	E67	Cyr61	
695	E58	CYS1	
696	E65	DACH2	
697	E14	DAP	
698	E14	DAPK1	
699	E58	DAPK1	
700	E65	DAPK1	
701	E2	DAPK2	
702	E17	DBH	
703	E31	DBP	
704	E58	DCAF12L1	
705	E23	DCBLD2	
706	E25	DCC	
707	E28	DCC	
708	E58	DCDC2	
709	E2	DCTD	
710	E63	DDB2	
711	E66	DDB2	
712	E17	DDC	
713	E42	DDC	
714	E54	DDIT3	
715	E33	DDIT4	
716	E52	DDIT4	
717	E54	DDIT4	
718	E26	Ddn	
719	E65	DDR2	
720	E67	Ddx60	
721	E33	DEAF1	
722	E48	DEDD	
723	E29	DEFB1	
724	E31	DENND6A	

725	E16	DFNA5	
726	E30	DGCR5	
727	E38	DHRS2	
728	E11	DHRS3	
729	E59	Diap2	
730	E14	DIAPH2-AS1	
731	E47	DIRAS1	
732	E31	DIXDC1	
733	E41	DKK1	
734	E52	DKK1	
735	E60	DKK1	
736	E1	DKK3	
737	E40	DKK3	
738	E43	DKK3	
739	E40	DLC1	
740	E14	DLG3	
741	E17	DLK1	
742	E40	DLK2	
743	E12	DLL1	
744	E14	DLL3	
745	E56	DLX5	
746	E63	DLX5	
747	E58	DLX6	
748	E58	DLX6-AS1	
749	E37	DMD	
750	E2	DMPK	
751	E65	DMRT2	
752	E65	DMRT3	
753	E65	DMRTA1	
754	E65	DMRTA2	
755	E59	Dnahc8	
756	E58	DNAJC22	
757	E17	DNAJC6	
758	E66	DNHD1	
759	E31	DNLZ	
760	E49	Dnmbp	
761	E4	DNMT3B	
762	E58	DNMT3B	
763	E41	DOCK5	
764	E55	Dock9	
765	E42	DOK4	
766	E27	DOK5	
767	E42	DPCR1	

768	E28	DPEP1	
769	E20	DPF3	
770	E37	DPP4	
771	E51	DPP6	
772	E4	DPPA4	
773	E62	DPYSL3	
774	E43	DPYSL4	
775	E60	DRAM1	
776	E66	DRAM1	
777	E67	Dram1	
778	E38	DRAS1	
779	E41	DRD2	
780	E27	DSCR8	
781	E13	DST	
782	E2	DTL	
783	E21	DTNA	
784	E58	DUOX2	
785	E38	DUSP10	
786	E67	Dusp2	
787	E4	DUSP4	
788	E8	DUSP4	
789	E8	DUSP5	
790	E67	Dusp5	
791	E59	Dusp6	
792	E52	DUX4L8	
793	E52	DUX4L9	
794	E26	Dynlrb2	
795	E18	DYRK2	
796	E27	DYSF	
797	E54	DYSF	
798	E56	DYSF	
799	E5	ECHDC2	
800	E1	ECRG4	
801	E26	Ecrg4	
802	E20	ECT2	
803	E63	ECT2	
804	E66	EDA2R	
805	E60	EDN2	
806	E28	EDNRB	
807	E17	EEF1A2	
808	E43	EEF1A2	
809	E56	EFCAB4A	
810	E20	EFHB	

811	E57	EFHB	
812	E65	EFHD1	
813	E46	EFNA2/3	
814	E7	EFNB1	
815	E27	EGFEM1P	
816	E24	EGFLAM	
817	E50	EGFR	
818	E51	EGFR	
819	E29	EGLN3	
820	E24	EGR1	
821	E21	EGR1	
822	E21	EGR2	
823	E60	EGR2	
824	E21	EGR3	
825	E2	EHF	
826	E54	EIF4EBP1	
827	E58	ELAPOR1	
828	E17	ELAVL2	
829	E17	ELAVL3	
830	E17	ELAVL4	
831	E29	ELF3	
832	E1	ELF3	
833	E46	ELFN2/3	
834	E38	ELK3	
835	E2	ELL3	
836	E57	ELMOD1	
837	E59	Elovl7	
838	E54	EMID1	
839	E55	Emid1	
840	E59	Emilin2	
841	E41	EML1	
842	E20	EMP2	
843	E16	EMP3	
844	E67	Emp3	
845	E15	EMR1	
846	E59	Emr1	
847	E46	EN2	
848	E59	Enah	
849	E26	Enc	
850	E26	Enc1	
851	E2	ENGASE	
852	E54	ENOX1	
853	E24	ENPP1	

854	E26	Enpp2	
855	E1	ENPP2	
856	E58	ENPP3	
857	E11	ENTPD1	
858	E15	ENTPD1	
859	E6	EOMES	
860	E50	EPB41	
861	E1	EPCAM	
862	E8	EPHA2	
863	E64	EPHA2	
864	E43	EPHB1	
865	E27	EPHB2	
866	E3	EPHB2	
867	E49	Ephb2	
868	E2	EPHB3	
869	E41	EPHB3	
870	E38	EPN3	
871	E59	Epx	
872	E14	ERAP1	
873	E50	ERBB2	
874	E60	ERBB4	
875	E8	EREG	
876	E49	Ereg	
877	E54	EREG	
878	E7	ERF	
879	E40	ERG	
880	E2	ERI2	
881	E26	Ermn	
882	E58	ERN2	
883	E56	ERP27	
884	E21	ERRFI1	
885	E41	ERRFI1	
886	E2	ESAM	
887	E2	ESPL1	
888	E50	ESR1	
889	E58	ESR1	
890	E65	ESR1	
891	E34	ETV1	
892	E49	Etv1	
893	E31	ETV4	
894	E20	ETV5	
895	E37	ETV5	
896	E49	Etv5	

897	E46	EVX1	
898	E27	EXOC6B	
899	E16	EXT1	
900	E58	EYA2	
901	E57	EYA4	
902	E23	F2	
903	E44	F2R	
904	E39	F2RL1	
905	E23	F7	
906	E14	FABP5	
907	E29	FABP6	
908	E51	FABP7	
909	E2	FADS1	
910	E8	FAM107B	
911	E50	FAM129B	
912	E26	Fam131a	
913	E17	FAM163A	
914	E2	FAM171A1	
915	E14	FAM180B	
916	E5	FAM181B	
917	E26	Fam183b	
918	E14	FAM3C2	
919	E62	FAM49B	
920	E14	FAM69B	
921	E14	FAM69C	
922	E38	FAM83A	
923	E42	FAM83E	
924	E41	FAM83G	
925	E35	FAM83H	
926	E58	FAR2P1	
927	E40	FAT3	
928	E1	FBLN7	
929	E65	FBN3	
930	E55	Fbx17	
931	E31	FBXL17	
932	E56	FBXL21	
933	E31	FBXL3	
934	E58	FBXO17	
935	E38	FBXO32	
936	E23	FBXO32	
937	E43	FBXO32	
938	E56	FBXO43	
939	E58	FBXO8	

940	E28	FCER2	
941	E59	Fcgr2b	
942	E10	FCGRT	
943	E33	FCGRT	
944	E28	FCRL1	
945	E28	FCRL2	
946	E28	FCRL5	
947	E65	FEV	
948	E41	FEZ1	
949	E67	Ffar2	
950	E38	FFRMT1	
951	E11	FGD5	
952	E4	FGF17	
953	E46	FGF18	
954	E46	FGF19	
955	E4	FGF2	
956	E39	FGF2	
957	E60	FGF2	
958	E46	FGF3	
959	E65	FGF5	
960	E4	FGF8	
961	E46	FGF8	
962	E21	FGFBP3	
963	E37	FGFR1	
964	E5	FGFR3	
965	E40	FGFR3	
966	E46	FGFR3	
967	E51	FGFR3	
968	E58	FGFR3	
969	E2	FGFR4	
970	E18	FGFR4	
971	E58	FGFR4	
972	E15	FGFRL1	
973	E37	FGL2	
974	E67	Fgl2	
975	E2	FHDC1	
976	E40	FHL1	
977	E29	FHL2	
978	E15	FITM10	
979	E40	FJX1	
980	E41	FJX1	
981	E21	FLCN	
982	E54	FLG	

983	E16	FLNA	
984	E41	FLNB	
985	E43	FLNC	
986	E40	FLRT2	
987	E34	FLRT3	
988	E41	FLT1	
989	E54	FLT3	
990	E56	FLT4	
991	E26	Fmod	
992	E1	FMOD	
993	E16	FN1	
994	E33	FN1	
995	E44	FNDC3B	
996	E15	FOCAD	
997	E26	Folr1	
998	E67	Fos	
999	E41	FOSL1	
1000	E54	FOSL1	
1001	E10	FOSL2	
1002	E16	FOSL2	
1003	E66	FOSL2	
1004	E34	FOXA2	
1005	E35	FOXA2	
1006	E42	FOXA3	
1007	E54	FOXD1	
1008	E19	FOXE1S	
1009	E41	FOXF1	
1010	E4	FOXH1	
1011	E40	FOXI1	
1012	E26	Foxj1	
1013	E54	FOXJ1	
1014	E65	FOXL2	
1015	E62	FOXM1	
1016	E31	FOXO3	
1017	E8	FOXQ1	
1018	E41	FREM2	
1019	E60	FRMD4A	
1020	E43	FRMD6	
1021	E66	FRMPD2	
1022	E14	FRMPD4	
1023	E18	FRS2	
1024	E20	FSCN1	
1025	E63	FSCN1	

1026	E39	FST	
1027	E43	FST	
1028	E27	FTCDNL1	
1029	E45	Fth1	
1030	E66	FTX	
1031	E1	FUT3	
1032	E20	FUT5	
1033	E37	FUT8	
1034	E63	FUT8	
1035	E31	FUT9	
1036	E5	FXYD1	
1037	E51	FXYD1	
1038	E29	FXYD2	
1039	E43	FXYD5	
1040	E65	FXYD7	
1041	E58	FYB	
1042	E46	FZD10	
1043	E42	FZD5	
1044	E15	FZD6	
1045	E2	FZD7	
1046	E21	FZD7	
1047	E50	GAB1	
1048	E58	GABARAPL1	
1049	E31	GABBR1	
1050	E65	GABBR1	
1051	E67	Gabbr1	
1052	E15	GABBR2	
1053	E31	GABPA	
1054	E49	Gabra3	
1055	E55	Gabra5	
1056	E51	GABRB1	
1057	E4	GABRB3	
1058	E34	GABRG1	
1059	E4	GABRP	
1060	E58	GABRP	
1061	E54	GADD45A	
1062	E60	GADD45B	
1063	E60	GADD45G	
1064	E17	GAL	
1065	E43	GAL	
1066	E42	GAL3ST1	
1067	E62	GALNT7	
1068	E17	GAP43	

1069	E14	GAPDHS	
1070	E34	GARS	
1071	E54	GARS	
1072	E51	GAS1	
1073	E63	GAS2L3	
1074	E41	GAS7	
1075	E59	Gas7	
1076	E59	Gata1	
1077	E59	Gata2	
1078	E62	GATA2	
1079	E65	GATA2	
1080	E17	GATA3	
1081	E65	GATA3	
1082	E42	GATA6	
1083	E54	GATA6	
1084	E11	GCA	
1085	E20	GCLC	
1086	E45	Gclc	
1087	E45	Gclm	
1088	E42	GCNT3	
1089	E45	Gcnt3	
1090	E58	GCNT3	
1091	E17	GDAP1L1	
1092	E59	Gdf10	
1093	E8	GDF15	
1094	E52	GDF15	
1095	E63	GDF15	
1096	E66	GDF15	
1097	E4	GDF3	
1098	E35	GDF3	
1099	E25	GDF6	
1100	E7	GDPD3	
1101	E1	GEM	
1102	E38	GEM	
1103	E59	Gem	
1104	E26	Gfap	
1105	E37	GFI1	
1106	E49	Gfpt2	
1107	E22	GFRA1	
1108	E41	GFRA1	
1109	E35	GGCX	
1110	E20	GGH	
1111	E63	GGH	

1112	E45	Ggt6	
1113	E58	GGT6	
1114	E54	GGTLC1	
1115	E11	GIMAP1	
1116	E40	GIMAP8	
1117	E2	GINS1	
1118	E38	GJB2	
1119	E15	GK5	
1120	E2	GKN3	
1121	E31	GLCCI1	
1122	E21	GLDC	
1123	E41	GLI2	
1124	E16	GLIPR1	
1125	E21	GLIPR1	
1126	E43	GLIPR1	
1127	E43	GLIPR2	
1128	E58	GLRX	
1129	E63	GLS	
1130	E45	Glt28d2	
1131	E26	Glul	
1132	E59	Gm14005	
1133	E45	Gm34240	
1134	E26	Gm42418	
1135	E42	GMDS	
1136	E48	GMDS	
1137	E62	GNA12	
1138	E56	GNAO1	
1139	E66	GNAO1	
1140	E4	GNG13	
1141	E17	GNG3	
1142	E17	GNG4	
1143	E23	GNG4	
1144	E26	Gng7	
1145	E11	GNPDA1	
1146	E61	GNPDA1	
1147	E63	GOLGA2B	
1148	E56	GOLGA7B	
1149	E62	GOPC	
1150	E8	GOS2	
1151	E32	GOS2	
1152	E11	GP1BA	
1153	E59	Gp5	
1154	E42	GPA33	

1155	E1	GPC3	
1156	E64	GPD2	
1157	E54	GPM6A	
1158	E26	Gpnmb	
1159	E29	GPNMB	
1160	E49	Gpnmb	
1161	E58	GPR111	
1162	E59	Gpr141	
1163	E31	GPR155	
1164	E28	GPR160	
1165	E41	GPR176	
1166	E31	GPR180	
1167	E20	GPR35	
1168	E42	GPR35	
1169	E14	GPR39	
1170	E60	GPR39	
1171	E56	GPR56	
1172	E11	GPR84	
1173	E23	GPR84	
1174	E15	GPR85	
1175	E54	GPR87	
1176	E26	Gpr88	
1177	E58	GPR97	
1178	E21	GPRC5B	
1179	E28	GPRC5D	
1180	E63	GPT2	
1181	E42	GPX2	
1182	E19	GPX3	
1183	E58	GPX3	
1184	E33	GPX4	
1185	E58	GR1A2	
1186	E54	GRB10	
1187	E59	Grb10	
1188	E58	GRB14	
1189	E50	GRB2	
1190	E2	GRB7	
1191	E43	GREM1	
1192	E17	GRIA2	
1193	E66	GRIA2	
1194	E4	GRIA4	
1195	E34	GRID1	
1196	E34	GRID2	
1197	E39	GRIM2	

1198	E4	GRIN2B	
1199	E12	GRIP1	
1200	E10	GRK5	
1201	E54	GRRP1	
1202	E14	GS1-257G1.1	
1203	E55	Gsn	
1204	E37	GSS	
1205	E45	Gsta3	
1206	E45	Gstm1	
1207	E45	Gstm3	
1208	E31	GTF2I	
1209	E14	GYG2	
1210	E58	GZMA	
1211	E23	GZMB	
1212	E58	GZMB	
1213	E31	H2AFX	
1214	E66	H1F0	
1215	E67	H2-D1	
1216	E67	H2-Dma	
1217	E67	H2-Q4	
1218	E26	Hap1	
1219	E38	HAS2	
1220	E2	HAUS4	
1221	E58	HAVCR1	
1222	E49	Hbegf	
1223	E67	Hbegf	
1224	E31	HBP1	
1225	E57	HCN1	
1226	E67	HD-K1	
1227	E23	HEPACAM2	
1228	E42	HEPH	
1229	E38	HEPHL1	
1230	E43	HERPUD1	
1231	E31	HES1	
1232	E33	HES1	
1233	E67	Hes1	
1234	E46	HES2/3/5	
1235	E37	HFE	
1236	E42	HHLA2	
1237	E5	HIF3A	
1238	E65	HIF3A	
1239	E29	HILPDA	
1240	E2	HIRIP3	

1241	E66	HIST1H1E	
1242	E43	HIST1H2BD	
1243	E43	HIST1H2BK	
1244	E37	HIST2H2AA	
1245	E43	HIST2H2AA3	
1246	E66	HK2	
1247	E42	HKDC1	
1248	E14	HLA-B	
1249	E14	HLA-C	
1250	E15	HLA-DMA	
1251	E54	HLA-DMB	
1252	E54	HLA-DPA1	
1253	E4	HMGA2	
1254	E18	HMGA2	
1255	E40	HMGA2	
1256	E54	HMGA2	
1257	E65	HMGA2	
1258	E66	HMGCS1	
1259	E63	HMMR	
1260	E46	HMX1/2	
1261	E11	HNRPLL	
1262	E58	HOMER2	
1263	E54	HOPX	
1264	E30	HOXA11-AS	
1265	E65	HOXB5	
1266	E23	HOXD11	
1267	E23	HOXD13	
1268	E26	Hpcal4	
1269	E56	HPCAL4	
1270	E54	HPN	
1271	E37	HPRT1	
1272	E22	HR	
1273	E41	HRH1	
1274	E5	HRSP12	
1275	E39	HS3ST3A1	
1276	E21	HSD17B14	
1277	E52	HSD17B14	
1278	E42	HSD17B2	
1279	E66	HSD17B7	
1280	E32	HSD3B2	
1281	E21	HSF4	
1282	E66	HSPA5	
1283	E11	HSPA6	

1284	E31	HSPB1	
1285	E11	HSPC159	
1286	E65	HTR1E	
1287	E58	HTR3A	
1288	E28	HVCN1	
1289	E21	IARS2	
1290	E17	ICA1	
1291	E31	ICA1	
1292	E60	ICAM1	
1293	E67	Icam1	
1294	E67	Icosl	
1295	E59	Id1	
1296	E19	ID4	
1297	E49	Ida	
1298	E45	Idh1	
1299	E53	IDH2	
1300	E66	IDI1	
1301	E8	IER3	
1302	E41	IER3	
1303	E54	IER3	
1304	E60	IER3	
1305	E31	IER5	
1306	E67	Ifi30	
1307	E59	Ifitm1	
1308	E26	Ifitm3	
1309	E2	IFITM3	
1310	E67	Ifitm3	
1311	E7	IGDCC3	
1312	E58	IGDCC3	
1313	E34	IGF1	
1314	E59	Igf1r	
1315	E34	IGF2	
1316	E62	IGF2	
1317	E66	IGF2	
1318	E4	IGF2BP1	
1319	E23	IGF2BP1	
1320	E4	IGF2BP2	
1321	E4	IGF2BP3	
1322	E11	IGF2R	
1323	E34	IGF2R	
1324	E59	Igfals	
1325	E29	IGFBP1	
1326	E29	IGFBP3	

1327	E21	IGFBP3	
1328	E38	IGFBP3	
1329	E60	IGFBP3	
1330	E19	IGFBP7	
1331	E40	IGFBP7	
1332	E43	IGFBP7	
1333	E60	IGFBP7	
1334	E29	IGKC	
1335	E29	IGLC2	
1336	E14	IGSF11	
1337	E58	IGSF9	
1338	E41	IL11	
1339	E43	IL11	
1340	E54	IL11	
1341	E11	IL15	
1342	E1	IL17B	
1343	E15	IL18R1	
1344	E11	IL18RAP	
1345	E40	IL1A	
1346	E38	IL1B	
1347	E14	IL1B	
1348	E49	Il1b	
1349	E54	IL1B	
1350	E54	IL1R2	
1351	E10	IL1RAP	
1352	E15	IL1RAPL1	
1353	E25	IL1RL1	
1354	E49	Il1rl2	
1355	E58	IL20RA	
1356	E54	IL2RB	
1357	E43	IL32	
1358	E40	IL33	
1359	E49	Il33	
1360	E38	IL36G	
1361	E15	IL4	
1362	E28	IL5RA	
1363	E24	IL6R	
1364	E8	IL8	
1365	E43	IL8	
1366	E1	ILDR1	
1367	E2	ILF3	
1368	E37	ILK	
1369	E2	IMPDH2	

1370	E38	INHBA	
1371	E54	INHBE	
1372	E66	INPP5D	
1373	E66	INSIG1	
1374	E25	INSL3	
1375	E23	INSLA4	
1376	E12	INSM1	
1377	E65	IPO11	
1378	E1	IRAG1	
1379	E33	IRF1	
1380	E7	IRF2	
1381	E60	IRF5	
1382	E49	Irf8	
1383	E67	Irf8	
1384	E35	IRS2	
1385	E65	IRX2	
1386	E31	IRX3	
1387	E67	Isg15	
1388	E67	Isg20	
1389	E17	ISL1	
1390	E65	ISL1	
1391	E25	ISM1	
1392	E20	ITCB2	
1393	E33	ITGA10	
1394	E8	ITGA2	
1395	E15	ITGA2	
1396	E39	ITGA2	
1397	E41	ITGA2	
1398	E49	Itga2	
1399	E64	ITGA2	
1400	E59	Itga2b	
1401	E64	ITGA2B	
1402	E43	ITGA5	
1403	E21	ITGA7	
1404	E28	ITGA8	
1405	E59	Itga9	
1406	E58	ITGAD	
1407	E34	ITGAM	
1408	E59	Itgam	
1409	E24	ITGB1	
1410	E13	ITGB1	
1411	E49	Itgb2	
1412	E38	ITGB3	

1413	E67	Itgb3	
1414	E33	ITGB4	
1415	E64	ITGB6	
1416	E41	ITGB8	
1417	E39	IVNS1ABP	
1418	E42	IYD	
1419	E38	JAG1	
1420	E40	JAG2	
1421	E50	JAK2	
1422	E1	JAM2	
1423	E40	JAM3	
1424	E56	JPH2	
1425	E17	JPH4	
1426	E33	JUNB	
1427	E67	Junb	
1428	E38	KAL1	
1429	E5	KAT2B	
1430	E27	KAZN	
1431	E6	KCNA1	
1432	E12	KCNA1	
1433	E34	KCNA1	
1434	E47	KCNA3	
1435	E58	KCNA5	
1436	E21	KCNAB2	
1437	E62	KCNAB2	
1438	E12	KCNB2	
1439	E26	Kcnc2	
1440	E34	KCNC3	
1441	E58	KCNC3	
1442	E65	KCND1	
1443	E50	KCND3	
1444	E26	Kcne2	
1445	E2	KCNE3	
1446	E10	KCNE3	
1447	E42	KCNE3	
1448	E27	KCNE4	
1449	E7	KCNF1	
1450	E56	KCNF1	
1451	E37	KCNG1	
1452	E43	KCNG1	
1453	E58	KCNG1	
1454	E20	KCNG2	
1455	E12	KCNG3	

1456	E9	KCNH1	
1457	E58	KCNH3	
1458	E45	Kcnh7	
1459	E12	KCNH8	
1460	E58	KCNH8	
1461	E51	KCNIP1	
1462	E65	KCNIP3	
1463	E5	KCNJ10	
1464	E31	KCNJ10	
1465	E26	Kcnj13	
1466	E54	KCNJ13	
1467	E19	KCNJ16	
1468	E51	KCNJ16	
1469	E57	KCNJ16	
1470	E58	KCNJ16	
1471	E32	KCNJ5	
1472	E31	KCNJ8	
1473	E48	KCNJ9	
1474	E3	KCNK1	
1475	E8	KCNK1	
1476	E35	KCNK1	
1477	E61	KCNK1	
1478	E23	KCNK12	
1479	E63	KCNK12	
1480	E9	KCNK15	
1481	E22	KCNK15	
1482	E52	KCNK15	
1483	E24	KCNK2	
1484	E16	KCNK3	
1485	E22	KCNK5	
1486	E11	KCNK6	
1487	E43	KCNK6	
1488	E13	KCNMA1	
1489	E38	KCNMA1	
1490	E39	KCNMA1	
1491	E40	KCNMA1	
1492	E41	KCNMA1	
1493	E60	KCNMA1	
1494	E25	KCNMB1	
1495	E1	KCNMB1	
1496	E12	KCNMB2	
1497	E34	KCNMB2	
1498	E67	Kcnmb2	

1499	E27	KCNMB2-AS1	
1500	E44	KCNMB3	
1501	E18	KCNMB4	
1502	E58	KCNMB4	
1503	E51	KCNN2	
1504	E28	KCNN3	
1505	E4	KCNN3	
1506	E5	KCNN3	
1507	E34	KCNN3	
1508	E8	KCNN4	
1509	E36	KCNN4	
1510	E41	KCNN4	
1511	E49	Kcnn4	
1512	E52	KCNN4	
1513	E53	KCNN4	
1514	E58	KCNN4	
1515	E64	KCNN4	
1516	E2	KCNQ1	
1517	E55	Kcnq1	
1518	E58	KCNQ1	
1519	E29	KCNQ1OT1	
1520	E33	KCNQ1OT1	
1521	E66	KCNQ1OT1	
1522	E17	KCNQ2	
1523	E46	KCNQ2	
1524	E59	Kcnq3	
1525	E14	KCNQ5	
1526	E17	KCNQ5	
1527	E40	KCNQ5	
1528	E30	KCNQ5-IT1	
1529	E34	KCNS1	
1530	E34	KCNS3	
1531	E34	KCNT1	
1532	E15	KCNT2	
1533	E23	KCNU1	
1534	E46	KDM2B	
1535	E30	KDM4A-AS1	
1536	E66	KDM6B	
1537	E67	Kdm6b	
1538	E6	KHBRBS2	
1539	E38	KIAA1644	
1540	E2	KIF12	
1541	E2	KIF20A	

1542	E17	KIF21A	
1543	E65	KIF21B	
1544	E14	KIF3B	
1545	E40	KIRREL	
1546	E34	KISS1	
1547	E59	Kit	
1548	E26	Kl	
1549	E59	Klf1	
1550	E33	KLF10	
1551	E67	Klf10	
1552	E31	KLF12	
1553	E66	KLF16	
1554	E67	Klf6	
1555	E17	KLHL13	
1556	E21	KLHL24	
1557	E21	KLHL4	
1558	E52	KLK13	
1559	E23	KLK14	
1560	E37	KLK2	
1561	E15	KLRK1	
1562	E10	KMO	
1563	E64	KRAS	
1564	E22	KRT15	
1565	E60	KRT17	
1566	E45	Krt18	
1567	E24	KRT19	
1568	E29	KRT19	
1569	E22	KRT19	
1570	E60	KRT19	
1571	E45	Krt222	
1572	E58	KRT23	
1573	E7	KRT5	
1574	E54	KRT6A	
1575	E54	KRT6B	
1576	E38	KRT76	
1577	E45	Krt8	
1578	E38	KRTAP19	
1579	E58	LAMA1	
1580	E57	LAMA2	
1581	E56	LAMA4	
1582	E33	LAMA5	
1583	E33	LAMB2	
1584	E41	LAMB3	

1585	E54	LAMC2	
1586	E20	LAMP5	
1587	E37	LASS6	
1588	E59	Lass6	
1589	E28	LAX1	
1590	E54	LBH	
1591	E26	Lbp	
1592	E31	LBR	
1593	E53	LCK	
1594	E65	LCN12	
1595	E21	LCNL1	
1596	E2	LCP1	
1597	E43	LCP1	
1598	E29	LDHA	
1599	E55	Ldha	
1600	E66	LDLR	
1601	E67	Ldlr	
1602	E37	LDOC1	
1603	E2	LECT2	
1604	E32	LEF1	
1605	E55	Lef1	
1606	E4	LEFTY1	
1607	E4	LEFTY2	
1608	E27	LEKR1	
1609	E34	LEP	
1610	E34	LEPR	
1611	E31	LFNG	
1612	E26	Lgals1	
1613	E16	LGALS1	
1614	E29	LGALS3	
1615	E59	Lgals3	
1616	E42	LGALS4	
1617	E51	LGI1	
1618	E2	LGR5	
1619	E36	LGR5	
1620	E57	LGR6	
1621	E25	LHCGR	
1622	E59	Lhfpl2	
1623	E46	LHX3	
1624	E65	LHX3	
1625	E46	LHX3/4	
1626	E49	Lif	
1627	E54	LIF	

1628	E60	LIF	
1629	E67	Lif	
1630	E8	LIF	
1631	E1	LIFR	
1632	E15	LIMK2	
1633	E1	LIMS2	
1634	E4	LIN28A	
1635	E65	LIN28B	
1636	E14	LINC00282	
1637	E14	LINC00348	
1638	E30	LINC00511	
1639	E25	LINC00607	
1640	E29	LINC00626	
1641	E27	LINC00886	
1642	E66	LINC01021	
1643	E25	LINC01116	
1644	E58	LINC01132	
1645	E29	LINC01320	
1646	E14	LINC01531	
1647	E58	LINC01671	
1648	E58	LINC02532	
1649	E52	LINC02683	
1650	E26	Lingo1	
1651	E57	LINGO2	
1652	E21	LIPG	
1653	E1	LIPH	
1654	E2	LIPT2	
1655	E5	LMO3	
1656	E51	LMO3	
1657	E1	LMOD1	
1658	E65	LMX1A	
1659	E43	LOC100132564	
1660	E23	LOC100190940	
1661	E24	LOC100192378	
1662	E66	LOC729966	
1663	E17	LONRF2	
1664	E16	LOXL2	
1665	E39	LOXL2	
1666	E41	LOXL2	
1667	E65	LPA	
1668	E34	LPAR3	
1669	E21	LPCAT1	
1670	E31	LPGAT1	

1671	E37	LPL	
1672	E43	LPXN	
1673	E11	LRG1	
1674	E2	LRIG1	
1675	E15	LRP11	
1676	E21	LRP4	
1677	E14	LRPPRC	
1678	E41	LRRC15	
1679	E31	LRRC4	
1680	E56	LRRN2	
1681	E17	LRRN3	
1682	E52	LRRTM1	
1683	E58	LRRTM1	
1684	E17	LRRTM2	
1685	E28	LSAMP	
1686	E28	LSR	
1687	E21	LSS	
1688	E54	LTB	
1689	E38	LTB	
1690	E60	LTBP1	
1691	E40	LTBP2	
1692	E33	LTBP3	
1693	E24	LUM	
1694	E45	Ly6a	
1695	E7	LY6D	
1696	E33	LY6E	
1697	E50	LYN	
1698	E42	LYZ	
1699	E54	LZTFL1	
1700	E66	LZTS1	
1701	E17	MAB21L2	
1702	E26	Mag	
1703	E26	Mal	
1704	E13	MAL2	
1705	E57	MAL2	
1706	E14	MAMDC2-AS1	
1707	E66	MAMDC4	
1708	E11	MANEAL	
1709	E17	MAOA	
1710	E1	MAOB	
1711	E44	MAP1B	
1712	E43	MAP1LC3A	
1713	E60	MAP2K6	

1714	E15	MAP3K14	
1715	E58	MAP3K15	
1716	E56	MAP3K5	
1717	E64	MAP3K5	
1718	E64	MAP3K6	
1719	E16	MAP4K4	
1720	E14	MAP6D1	
1721	E50	MAPK1	
1722	E59	Mapk13	
1723	E50	MAPK14	
1724	E38	MAPK6	
1725	E21	MAPT	
1726	E56	MARCH4	
1727	E16	MARCKS	
1728	E54	MARK1	
1729	E14	MARS2	
1730	E2	MARVELD1	
1731	E27	MAST4	
1732	E31	MAZ	
1733	E1	MB	
1734	E14	MBD5	
1735	E59	Mc5r	
1736	E62	MCFD2	
1737	E26	Mcm2	
1738	E60	MCM2	
1739	E2	MCM8	
1740	E59	Mcpt8	
1741	E59	Mdga1	
1742	E48	MDH1	
1743	E18	MDM2	
1744	E2	MECOM	
1745	E26	Mef2c	
1746	E1	MEF2C	
1747	E59	Mefv	
1748	E1	MEG3	
1749	E26	Melat1	
1750	E52	MEP1A	
1751	E14	MESDC1	
1752	E7	MESP1	
1753	E23	MET	
1754	E59	Met	
1755	E62	MET	
1756	E67	Met	

1757	E18	METTL1	
1758	E18	METTL21B	
1759	E66	METTL7A	
1760	E21	METTL7B	
1761	E21	MFGE8	
1762	E58	MFSD2A	
1763	E59	Mfsd2b	
1764	E14	MGAT4C	
1765	E26	Mia	
1766	E22	MICB	
1767	E2	MIF	
1768	E30	MIR205HG	
1769	E30	MIR31HG	
1770	E65	MKX	
1771	E51	MLC1	
1772	E25	MLK4	
1773	E23	MLLT11	
1774	E1	MLPH	
1775	E11	MLT11	
1776	E29	MME	
1777	E44	MMP1	
1778	E56	MMP1	
1779	E64	MMP1	
1780	E38	MMP1	
1781	E38	MMP10	
1782	E44	MMP10	
1783	E49	Mmp10	
1784	E24	MMP14	
1785	E40	MMP3	
1786	E54	MMP7	
1787	E58	MMP7	
1788	E38	MMP9	
1789	E59	Mmrn1	
1790	E65	MNX1	
1791	E46	MNX1	
1792	E30	MNX1-AS1	
1793	E58	MOB1B	
1794	E26	Mobp	
1795	E26	Mog	
1796	E31	MORC3	
1797	E11	MOSC2	
1798	E57	MOXD1	
1799	E13	MPDZ	

1800	E59	Mpl	
1801	E2	MPP3	
1802	E2	MPZL1	
1803	E3	MPZL1	
1804	E15	MPZL2	
1805	E21	MRC2	
1806	E40	MRC2	
1807	E14	MREG	
1808	E24	MRGPRX3	
1809	E14	MRPL24	
1810	E7	MRPL4	
1811	E31	MRPS33	
1812	E45	Mrps35	
1813	E28	MS4A1	
1814	E58	MS4A7	
1815	E64	MSLN	
1816	E66	MSMO1	
1817	E21	MSN	
1818	E43	MSN	
1819	E63	MSN	
1820	E15	MSR1	
1821	E40	MSRB3	
1822	E43	MT1A	
1823	E25	MT1F	
1824	E43	MT1X	
1825	E26	Mt2	
1826	E43	MT2A	
1827	E21	MT-CYB	
1828	E63	MTHFD2	
1829	E52	MTND4P12	
1830	E58	MTRNR2L12	
1831	E1	MUC1	
1832	E7	MUC1	
1833	E42	MUC13	
1834	E42	MUC17	
1835	E41	MUC5B	
1836	E58	MUC6	
1837	E40	MUM1L1	
1838	E21	MVD	
1839	E23	MYBL1	
1840	E14	MYC	
1841	E35	MYC	
1842	E61	MYC	

1843	E17	MYCN	
1844	E25	MYH11	
1845	E1	MYH11	
1846	E38	MYH16	
1847	E21	MYH9	
1848	E1	MYL9	
1849	E1	MYLK	
1850	E65	MYO18B	
1851	E42	MYO1A	
1852	E2	MYO1B	
1853	E59	Myo1d	
1854	E1	MYO5B	
1855	E1	MYO5C	
1856	E42	MYO7B	
1857	E21	MYRF	
1858	E18	MYRFL	
1859	E17	MYT2L	
1860	E21	NAB2	
1861	E4	NANOG	
1862	E49	Nap1l2	
1863	E26	Nap1l5	
1864	E2	NAPEPLD	
1865	E33	NARF	
1866	E14	NAV2	
1867	E12	NCAM1	
1868	E66	NCAM-AS1	
1869	E5	NCAN	
1870	E17	NCAN	
1871	E51	NCAN	
1872	E14	NCL	
1873	E14	NCOA3	
1874	E26	Ndn	
1875	E8	NDRG1	
1876	E63	NDRG1	
1877	E26	Ndrg2	
1878	E38	NDRG4	
1879	E51	NDRG4	
1880	E29	NDUFA4L2	
1881	E66	NDUFB9	
1882	E33	NEAT1	
1883	E56	NEBL	
1884	E37	NEDD9	
1885	E34	NEFH	

1886	E17	NEFL	
1887	E17	NEFM	
1888	E41	NEGR1	
1889	E25	NELL2	
1890	E57	NELL2	
1891	E15	NEO1	
1892	E60	NEO1	
1893	E51	NES	
1894	E21	NEU1	
1895	E65	NEUROD1	
1896	E65	NEUROD4	
1897	E34	NF1	
1898	E35	NF1B	
1899	E24	NFAT5	
1900	E31	NFAT5	
1901	E2	NFIA	
1902	E31	NFIA	
1903	E58	NFIA	
1904	E12	NFIB	
1905	E58	NFIB	
1906	E33	NFIC	
1907	E66	NFIC	
1908	E66	NFIX	
1909	E50	NFKB1	
1910	E8	NFKBIZ	
1911	E31	NFKBIZ	
1912	E41	NGEF	
1913	E49	Ngf	
1914	E1	NGFR	
1915	E40	NGFR	
1916	E62	NGRN	
1917	E31	NHEJ1	
1918	E58	NID2	
1919	E60	NID2	
1920	E15	NINJ1	
1921	E25	NIPAL1	
1922	E56	NIPAL1	
1923	E40	NIPAL4	
1924	E23	NKG7	
1925	E19	NKX2-1	
1926	E35	NKX2-1	
1927	E65	NKX2-2	
1928	E52	NKX3-1	

1929	E46	NKX6-2	
1930	E4	NLGN4X	
1931	E4	NLGN4Y	
1932	E43	NLRP1	
1933	E67	Nlrp3	
1934	E29	NMB	
1935	E17	NMNAT2	
1936	E41	NMNAT2	
1937	E34	NMU	
1938	E60	NMU	
1939	E56	NNAT	
1940	E29	NNMT	
1941	E2	NOD1	
1942	E4	NODAL	
1943	E14	NOP56	
1944	E2	NOTCH1	
1945	E60	NOTCH1	
1946	E66	NOTCH1	
1947	E66	NOTCH3	
1948	E40	NOTCH4	
1949	E59	Nov	
1950	E66	NOVA2	
1951	E21	NPC2	
1952	E65	NPHS1	
1953	E34	NPPA	
1954	E43	NPTX1	
1955	E65	NPTX1	
1956	E26	Nptxr	
1957	E19	NPY1R	
1958	E34	NPY1R	
1959	E34	NPY2R	
1960	E65	NR0B1	
1961	E51	NR2E1	
1962	E2	NR2E3	
1963	E33	NR2F1	
1964	E7	NR4A1	
1965	E67	Nr4a2	
1966	E67	Nr4a3	
1967	E65	NR5A1	
1968	E62	NRBF2	
1969	E31	NRCAM	
1970	E44	NREP	
1971	E40	NRG1	

1972	E59	Nrg1	
1973	E54	NRG2	
1974	E26	Nrgn	
1975	E58	NRGN	
1976	E42	NRIL2	
1977	E26	Nrip3	
1978	E10	NROB1	
1979	E39	NRP1	
1980	E41	NRP1	
1981	E14	NRP1	
1982	E21	NRP2	
1983	E17	NRSN1	
1984	E41	NRXN3	
1985	E60	NT5E	
1986	E34	NTF3	
1987	E25	NTM	
1988	E39	NTM	
1989	E41	NTN4	
1990	E46	NTNG2	
1991	E46	NTSR1	
1992	E51	NTSR2	
1993	E34	NUCB1	
1994	E33	NUCB2	
1995	E34	NUCB2	
1996	E37	NUDT1	
1997	E45	Nupr1	
1998	E60	ODC1	
1999	E58	OGDHL	
2000	E26	Olfm1	
2001	E22	OLFM1	
2002	E58	OLFM2	
2003	E54	OPN1SW	
2004	E41	OPRD1	
2005	E66	OPRM1	
2006	E16	OPTN	
2007	E15	OR4K2	
2008	E1	ORAI1	
2009	E2	ORC1	
2010	E39	OSMR	
2011	E1	OSR1	
2012	E20	OSR1	
2013	E46	OTX2	
2014	E11	OVOS2	

2015	E26	Oxt	
2016	E37	P2RX1	
2017	E28	P2RX5	
2018	E67	P2ry2	
2019	E55	P4ha2	
2020	E47	PAG1	
2021	E2	PAICS	
2022	E37	PAK1	
2023	E62	PAK4	
2024	E2	PALB2	
2025	E21	PALLD	
2026	E54	PALM	
2027	E43	PAPPA	
2028	E11	PAPSS2	
2029	E42	PAQR8	
2030	E28	PARM1	
2031	E43	PAT1	
2032	E46	PAX2	
2033	E51	PAX6	
2034	E4	PAX7	
2035	E29	PAX8	
2036	E31	PBX1	
2037	E66	PCBP2	
2038	E60	PCCA	
2039	E41	PCDH1	
2040	E21	PCDH1	
2041	E65	PCDH17	
2042	E1	PCDH18	
2043	E31	PCDH9	
2044	E66	PCDHGC3	
2045	E60	PCNA	
2046	E23	PCSK1	
2047	E49	Pcsk1n	
2048	E66	PCSK1N	
2049	E26	Pde10a	
2050	E55	Pde11a	
2051	E58	PDE11A	
2052	E26	Pde1b	
2053	E38	PDE2A	
2054	E65	PDE3A	
2055	E2	PDE3B	
2056	E67	Pde4b	
2057	E1	PDGFA	

2058	E21	PDGFA	
2059	E21	PDGFB	
2060	E39	PDGFC	
2061	E43	PDGFC	
2062	E26	Pdp1	
2063	E50	PDP1	
2064	E40	PDPN	
2065	E60	PDRG1	
2066	E29	PDZK1IP1	
2067	E16	PEA15	
2068	E31	PEA15	
2069	E49	Peg3	
2070	E26	Penk	
2071	E67	Per1	
2072	E28	PERP	
2073	E43	PFKFB4	
2074	E16	PFKP	
2075	E37	PFKP	
2076	E44	PFN2	
2077	E58	PGBD5	
2078	E54	PGC	
2079	E11	PGCP	
2080	E66	PGF	
2081	E58	PGR	
2082	E17	PHACTR3	
2083	E63	PHGDH	
2084	E66	PHGDH	
2085	E10	PHLDA1	
2086	E45	Phlda1	
2087	E54	PHLDA1	
2088	E8	PHLDA2	
2089	E41	PHLDA2	
2090	E17	PHOX2A	
2091	E17	PHOX2B	
2092	E58	PI3	
2093	E2	PICALM	
2094	E66	PIDD	
2095	E34	PIEZO2	
2096	E49	Pigr	
2097	E50	PIK3C2B	
2098	E62	PIP4K2A	
2099	E52	PIP5K1B	
2100	E58	PIP5K1B	

2101	E65	PITX2	
2102	E1	PKD1	
2103	E65	PKD1L1	
2104	E21	PKDCC	
2105	E58	PKHD1	
2106	E55	Pkp4	
2107	E9	PLA2G10	
2108	E20	PLA2G4E	
2109	E11	PLAG1	
2110	E57	PLAG1	
2111	E65	PLAGL1	
2112	E33	PLAT	
2113	E64	PLAT	
2114	E49	Plau	
2115	E54	PLAU	
2116	E64	PLAU	
2117	E67	Plau	
2118	E38	PLAU	
2119	E8	PLAUR	
2120	E13	PLAUR	
2121	E41	PLAUR	
2122	E43	PLAUR	
2123	E49	Plaur	
2124	E2	PLCE1	
2125	E47	PLCL2	
2126	E52	PLCXD3	
2127	E29	PLEKHA1	
2128	E54	PLEKHA4	
2129	E14	PLEKHS1	
2130	E58	PLEKHS1	
2131	E67	Plk2	
2132	E16	PLOD2	
2133	E26	Plp1	
2134	E65	PLP1	
2135	E1	PLPP1	
2136	E28	PLPP5	
2137	E67	Plscr1	
2138	E31	PLTP	
2139	E39	PLXNC1	
2140	E25	PMAIP1	
2141	E60	PMAIP1(NOXA)	
2142	E26	Pmch	
2143	E41	PMEPA1	

2144	E43	PMEPA1	
2145	E16	PML	
2146	E35	PNMA2	
2147	E51	PNOC	
2148	E67	Pnp	
2149	E31	PODXL	
2150	E42	POF18	
2151	E2	POLD1	
2152	E2	POLE	
2153	E2	POLI	
2154	E66	POLR2A	
2155	E44	POLR2H	
2156	E62	POM121	
2157	E23	POPDC3	
2158	E1	POSTN	
2159	E19	POSTN	
2160	E65	POU1F1	
2161	E38	POU2F2	
2162	E31	POU3F2	
2163	E51	POU3F2	
2164	E19	POU3F3	
2165	E31	POU3F3	
2166	E4	POU5F1	
2167	E50	PPARG	
2168	E2	PPAT	
2169	E49	Ppbp	
2170	E13	PPL	
2171	E5	PPMiK	
2172	E38	PPP1CB	
2173	E1	PPP1R14A	
2174	E31	PPP1R14C	
2175	E49	Ppp1R15a	
2176	E67	Ppp1r15a	
2177	E26	Ppp1r1b	
2178	E58	PPP1R3B	
2179	E26	Ppp1r9b	
2180	E62	PPP2R1B	
2181	E58	PPP2R2C	
2182	E41	PRDM1	
2183	E27	PRDM16	
2184	E65	PRDM8	
2185	E45	Prdx6	
2186	E2	PRELP	

2187	E41	PRICKLE2	
2188	E60	PRIM1	
2189	E58	PRKAG2-AS1	
2190	E47	PRKAR2B	
2191	E24	PRKCB	
2192	E26	Prkcd	
2193	E27	PRKCE	
2194	E50	PRKD1	
2195	E59	Prkd2	
2196	E49	Prkg2	
2197	E5	PRODH	
2198	E66	PRODH	
2199	E7	PROM1	
2200	E11	PROS1	
2201	E54	PROS1	
2202	E12	PROX1	
2203	E66	PRR12	
2204	E66	PRR36	
2205	E1	PRRX1	
2206	E41	PRSS23	
2207	E59	Prss34	
2208	E31	PRTG	
2209	E48	PSAT1	
2210	E54	PSAT1	
2211	E63	PSAT1	
2212	E26	Psd	
2213	E5	PSD2	
2214	E67	Psmb9	
2215	E44	PSMD2	
2216	E55	Pstpip2	
2217	E60	PSTPIP2	
2218	E6	PTEN	
2219	E26	Ptgds	
2220	E21	PTGDS	
2221	E67	Ptger4	
2222	E60	PTGES(PIG12)	
2223	E52	PTGFR	
2224	E65	PTGFR	
2225	E49	Ptgs2	
2226	E34	PTH1R	
2227	E58	PTHLH	
2228	E3	PTK7	
2229	E50	PTPN1	

2230	E50	PTPN12	
2231	E50	PTPN21	
2232	E66	PTPN23	
2233	E50	PTPN6	
2234	E13	PTPRC	
2235	E1	PTPRE	
2236	E15	PTPRE	
2237	E67	Ptpre	
2238	E50	PTPRJ	
2239	E27	PTPRK	
2240	E11	PTPRN2	
2241	E2	PTPRO	
2242	E1	PTPRT	
2243	E31	PTPRZ1	
2244	E36	PTRH1	
2245	E58	PVR	
2246	E66	PVRL4	
2247	E30	PVT1	
2248	E66	PVT1	
2249	E13	PXN	
2250	E35	PXN	
2251	E42	PZDP3	
2252	E11	QPCT	
2253	E21	QPRT	
2254	E1	QRICH2	
2255	E2	QSOX2	
2256	E16	RAB11FIP5	
2257	E35	RAB12	
2258	E17	RAB33A	
2259	E11	RAB34	
2260	E14	RAB38	
2261	E54	RAB3B	
2262	E56	RAB3C	
2263	E16	RAB6IP1	
2264	E35	RAC1	
2265	E61	RAD51	
2266	E26	Ramp3	
2267	E34	RAMP3	
2268	E56	RAMP3	
2269	E44	RAP2B	
2270	E59	Rapgef3	
2271	E47	RAPGEF5	
2272	E22	RAPGEFL1	

2273	E59	Raph1	
2274	E66	RAPH1	
2275	E26	Rarres2	
2276	E29	RARRES2	
2277	E2	RASA3	
2278	E26	Rasd2	
2279	E42	RASEF	
2280	E58	RASGRF1	
2281	E59	Rasgrf2	
2282	E51	RASGRP1	
2283	E2	RASL11B	
2284	E2	RASSF4	
2285	E59	Rassf4	
2286	E66	RAVER1	
2287	E46	RAX	
2288	E65	RAX2	
2289	E22	RBBP8	
2290	E58	RBBP8NL	
2291	E14	RBFA	
2292	E56	RBFOX1	
2293	E60	RBL1	
2294	E6	RBM24	
2295	E17	RBMS3	
2296	E58	RBP7	
2297	E12	RBPJ	
2298	E24	RCAN3	
2299	E25	RCAN3	
2300	E58	RCAN3	
2301	E10	RCOR	
2302	E55	Rcvm	
2303	E14	RDH13	
2304	E21	RDH5	
2305	E67	Rel	
2306	E34	RELN	
2307	E57	RELN	
2308	E21	RENBP	
2309	E66	RERE	
2310	E26	Resp18	
2311	E12	RET	
2312	E15	RET	
2313	E22	RET	
2314	E31	REXO1	
2315	E65	RFX4	

2316	E33	RGCC	
2317	E2	RGMB	
2318	E49	Rgs16	
2319	E20	RGS17	
2320	E60	RGS2	
2321	E17	RGS4	
2322	E56	RGS7	
2323	E26	Rgs9	
2324	E14	RGS9	
2325	E2	RHOBTB3	
2326	E33	RHOBTB3	
2327	E13	RHOU	
2328	E1	RHPN2	
2329	E31	RIBC1	
2330	E4	RIMS1	
2331	E67	Ripk1	
2332	E64	RIPK3	
2333	E14	RLBP1	
2334	E34	RLN1	
2335	E52	RLN1	
2336	E31	RND2	
2337	E67	Rnf144b	
2338	E21	RNF145	
2339	E2	RNF32	
2340	E58	RNF39	
2341	E66	RNU1-1	
2342	E38	ROBO4	
2343	E41	ROBO4	
2344	E57	ROPN1L	
2345	E65	RORB	
2346	E25	RP1	
2347	E25	RP11-141M1.3	
2348	E65	RP11-192H23.4	
2349	E65	RP11-362F19.1	
2350	E58	RP11-392E22.10	
2351	E58	RP11-392E22.12	
2352	E21	RP11-644F5.10	
2353	E65	RP11-701P16.2	
2354	E14	RP11-79H23.3	
2355	E14	RP13-631K18.2	
2356	E25	RP1-78014.1	
2357	E66	RP3-326I13.1	
2358	E65	RP5-842K16.1	

2359	E51	RPH3A	
2360	E48	RPIA	
2361	E65	RPL21	
2362	E65	RPL37	
2363	E65	RPLP0	
2364	E38	RPLPOP2	
2365	E60	RPRM	
2366	E65	RPS16	
2367	E44	RPS23	
2368	E65	RPS23	
2369	E19	RPS4Y1	
2370	E65	RPS5	
2371	E60	RRAD	
2372	E54	RRM2	
2373	E66	RRM2B	
2374	E24	RRN3P3	
2375	E65	RRS1	
2376	E67	Rsad2	
2377	E26	Rsph1	
2378	E65	RSPO2	
2379	E32	RSPO3	
2380	E66	RTL1	
2381	E11	RTN1	
2382	E17	RTN1	
2383	E21	RTN1	
2384	E44	RTP4	
2385	E3	RUNX1	
2386	E35	RUNX1	
2387	E58	RUNX3	
2388	E34	RXFP1	
2389	E65	RXRG	
2390	E65	RYR1	
2391	E51	RYR3	
2392	E23	S100A2	
2393	E60	S100A2	
2394	E64	S100A2	
2395	E58	S100A3	
2396	E64	S100A4	
2397	E8	S100A6	
2398	E38	S100A6	
2399	E38	S100A9	
2400	E58	S100A9	
2401	E59	S1pr1	

2402	E60	SAA1(PIG4)	
2403	E5	SALLA	
2404	E35	SAMD4A	
2405	E44	SAMD9	
2406	E5	SAMD9L	
2407	E67	Samhd1	
2408	E11	SAMSN1	
2409	E60	SARDH	
2410	E5	SASH1	
2411	E59	Satb1	
2412	E46	SATB2	
2413	E66	SBK1	
2414	E50	SCAMP3	
2415	E60	SCARA3	
2416	E24	SCARA5	
2417	E43	SCARNA13	
2418	E43	SCARNA8	
2419	E61	SCC1	
2420	E45	Scd2	
2421	E35	SCFD2	
2422	E34	SCG2	
2423	E54	SCG2	
2424	E17	SCG5	
2425	E43	SCG5	
2426	E49	Scg5	
2427	E58	SCGB1D2	
2428	E58	SCGB2A1	
2429	E16	SCHIP1	
2430	E52	SCIN	
2431	E59	Scin	
2432	E60	SCL4A10	
2433	E52	SCML4	
2434	E12	SCN3A	
2435	E17	SCN3A	
2436	E26	Scn4b	
2437	E4	SCN5A	
2438	E34	SCN7A	
2439	E28	SDC1	
2440	E8	SDC4	
2441	E67	Sdc4	
2442	E41	SDK1	
2443	E58	SDK2	
2444	E59	Sdpr	

2445	E14	SEC24D	
2446	E2	SECTM1B	
2447	E15	SELP	
2448	E54	SELPLG	
2449	E41	SEMA3B	
2450	E44	SEMA3C	
2451	E63	SEMA3C	
2452	E59	Sema4a	
2453	E42	SEMA4G	
2454	E21	SEMA7A	
2455	E37	SEPT10	
2456	E44	SERP1	
2457	E59	Serpina3f	
2458	E8	SERPINB1	
2459	E40	SERPINB13	
2460	E8	SERPINB5	
2461	E14	SERPINB8	
2462	E54	SERPINB8	
2463	E67	Serpinb8	
2464	E20	SERPINE1	
2465	E60	SERPINE1(PAI1)	
2466	E38	SERPINE2	
2467	E54	SERPINE2	
2468	E57	SERPINE2	
2469	E1	SERPINF1	
2470	E33	SERPINF1	
2471	E40	SERPINF1	
2472	E41	SERTAD4	
2473	E31	SESN3	
2474	E60	SESN3	
2475	E62	SESN3	
2476	E8	SFN	
2477	E60	SFN(14-3-3σ)	
2478	E4	SFRP1	
2479	E41	SFRP1	
2480	E54	SFTPD	
2481	E14	SFXN4	
2482	E14	SGCB	
2483	E1	SGIP1	
2484	E21	SGK223	
2485	E54	SH2D3C	
2486	E40	SH2D5	
2487	E42	SH3BGRL2	

2488	E16	SH3GLB1	
2489	E43	SH3KBP1	
2490	E41	SH3PXD2A	
2491	E66	SH3PXD2B	
2492	E26	Shank1	
2493	E58	SHANK1	
2494	E50	SHC1	
2495	E50	SHC3	
2496	E11	SHCBP1	
2497	E63	SHCBP1	
2498	E1	SHE	
2499	E46	SHH	
2500	E65	SHH	
2501	E2	SHISA2	
2502	E41	SHISA2	
2503	E46	SHISA2	
2504	E56	SHISA2	
2505	E63	SHISA4	
2506	E42	SI	
2507	E63	SIAE	
2508	E45	Sidt2	
2509	E20	SIM1	
2510	E46	SIM2	
2511	E45	Simapos2	
2512	E14	SIRPAP1	
2513	E20	SIX1	
2514	E66	SKI	
2515	E31	SKIL	
2516	E44	SKIL	
2517	E31	SKIV2L	
2518	E35	SKP2	
2519	E37	SLAMF1	
2520	E28	SLAMF7	
2521	E21	SLC04A1	
2522	E66	SLC12A4	
2523	E31	SLC12A6	
2524	E41	SLC14A1	
2525	E14	SLC14A1	
2526	E58	SLC14A1	
2527	E59	Slc16a11	
2528	E8	SLC16A3	
2529	E43	SLC16A3	
2530	E9	SLC16A6	

2531	E26	Slc17a6	
2532	E26	Slc17a7	
2533	E56	SLC18A1	
2534	E4	SLC18A2	
2535	E59	Slc18a2	
2536	E56	SLC18A3	
2537	E14	SLC19A2	
2538	E58	SLC1A1	
2539	E26	Slc1a2	
2540	E51	SLC1A2	
2541	E58	SLC1A2	
2542	E67	Slc1a2	
2543	E51	SLC1A3	
2544	E58	SLC1A3	
2545	E28	SLC1A4	
2546	E39	SLC22A4	
2547	E51	SLC24A3	
2548	E38	SLC25A24	
2549	E27	SLC25A26	
2550	E14	SLC25A42	
2551	E19	SLC26A4	
2552	E2	SLC27A2	
2553	E14	SLC27A3	
2554	E1	SLC28A3	
2555	E43	SLC2A3	
2556	E3	SLC2A5	
2557	E56	SLC30A3	
2558	E67	Slc31a2	
2559	E18	SLC35E3	
2560	E41	SLC35F1	
2561	E58	SLC35F5	
2562	E58	SLC38A4	
2563	E23	SLC38A8	
2564	E7	SLC39A2	
2565	E19	SLC3A1	
2566	E63	SLC3A2	
2567	E29	SLC40A1	
2568	E42	SLC40A1	
2569	E58	SLC40A1	
2570	E42	SLC44A4	
2571	E27	SLC44A5	
2572	E52	SLC45A3	
2573	E58	SLC45A4	

2574	E67	Slc4a4	
2575	E54	SLC4A7	
2576	E42	SLC5A1	
2577	E34	SLC6A1	
2578	E51	SLC6A1	
2579	E26	Slc6a11	
2580	E24	SLC6A12	
2581	E42	SLC6A20	
2582	E65	SLC6A7	
2583	E67	Slc7a1	
2584	E54	SLC7A1	
2585	E5	SLC7A11	
2586	E62	SLC7A11	
2587	E65	SLC7A2	
2588	E67	Slc7a2	
2589	E63	SLC7A5	
2590	E66	SLC7A5	
2591	E58	SLC8A1	
2592	E58	SLC9A2	
2593	E15	SLC9AB	
2594	E54	SLCO2B1	
2595	E21	SLIT1	
2596	E39	SLIT2	
2597	E1	SLIT3	
2598	E41	SLITRK6	
2599	E58	SLITRK6	
2600	E64	SLK	
2601	E43	SLN	
2602	E29	SLPI	
2603	E54	SLURP1	
2604	E41	SMAGP	
2605	E31	SMARCA2	
2606	E35	SMARCA4	
2607	E2	SMARCD3	
2608	E20	SMIM5	
2609	E2	SMO	
2610	E43	SNAI2	
2611	E54	SNAI2	
2612	E65	SNAI2	
2613	E63	SNAP23	
2614	E17	SNAP91	
2615	E49	Snap91	
2616	E66	SNHG3	

2617	E21	SNN	
2618	E43	SNORA12	
2619	E61	SNTA1	
2620	E2	SNX10	
2621	E37	SNX4	
2622	E59	Socs2	
2623	E33	SOCS3	
2624	E60	SOD3	
2625	E66	SOGA1	
2626	E66	SON	
2627	E27	SORCS2	
2628	E2	SORD	
2629	E53	SORD	
2630	E26	Sostdc1	
2631	E35	SOX11	
2632	E65	SOX11	
2633	E4	SOX2	
2634	E12	SOX2	
2635	E41	SOX2	
2636	E46	SOX2	
2637	E65	SOX2	
2638	E46	SOX2/3/8	
2639	E27	SOX2-OT	
2640	E46	SOX3/8	
2641	E33	SOX4	
2642	E24	SOX5	
2643	E65	SOX5	
2644	E24	SOX6	
2645	E59	Sox6	
2646	E46	SOX8	
2647	E24	SOX9	
2648	E51	SOX9	
2649	E56	SOX9	
2650	E2	SP5	
2651	E65	SP5	
2652	E2	SPAG5	
2653	E43	SPANXB1	
2654	E43	SPANXB2	
2655	E26	Sparc	
2656	E40	SPARC	
2657	E14	SPARC	
2658	E66	SPATA18	
2659	E2	SPATA24	

2660	E58	SPDEF	
2661	E54	SPDEF	
2662	E24	SPDYE1	
2663	E54	SPEF1	
2664	E66	SPEN	
2665	E59	Sphk1	
2666	E58	SPI1	
2667	E53	SPIB	
2668	E2	SPICE1	
2669	E33	SPINT2	
2670	E21	SPOCD1	
2671	E43	SPOCD1	
2672	E41	SPOCK1	
2673	E19	SPP1	
2674	E45	Spr2a3	
2675	E41	SPRED3	
2676	E14	SPRED3	
2677	E33	SPRY1	
2678	E49	Spry2	
2679	E51	SPRY4	
2680	E31	SPSB4	
2681	E26	Sptbn2	
2682	E67	Sqstm1	
2683	E66	SRCAP	
2684	E21	SRGAP1	
2685	E27	SRL	
2686	E2	SRL	
2687	E43	SRPX	
2688	E44	SSBP2	
2689	E21	SSTR3	
2690	E65	ST18	
2691	E21	ST3GAL5	
2692	E31	ST3GAL5	
2693	E42	ST6GALNAC1	
2694	E24	ST8SIA1	
2695	E16	STAC	
2696	E66	STAC	
2697	E50	STAM2	
2698	E59	Stap2	
2699	E32	STAR	
2700	E60	STARD4	
2701	E66	STARD4	
2702	E58	STARD8	

2703	E43	STC1	
2704	E22	STC2	
2705	E38	STC2	
2706	E54	STC2	
2707	E8	STEAP1	
2708	E54	STEAP1	
2709	E44	STEAP4	
2710	E54	STEAP4	
2711	E16	STK17A	
2712	E41	STK32B	
2713	E13	STK39	
2714	E63	STMN1	
2715	E17	STMN3	
2716	E17	STMN4	
2717	E27	STON1-GTF2A1L	
2718	E58	STX19	
2719	E59	Stxbp6	
2720	E3	SULT1C2	
2721	E42	SULT1C2	
2722	E32	SULT2A1	
2723	E24	SUZ12	
2724	E26	Sv2b	
2725	E1	SVEP1	
2726	E4	SYN2	
2727	E40	SYNE1	
2728	E41	SYNPO	
2729	E12	SYT1	
2730	E58	SYT1	
2731	E4	SYT2	
2732	E26	Tac1	
2733	E51	TAC1	
2734	E65	TAC4	
2735	E34	TACR2	
2736	E20	TACR3	
2737	E24	TAF13	
2738	E1	TAGLN	
2739	E40	TAGLN	
2740	E43	TAGLN	
2741	E14	TAP1	
2742	E31	TBC1D16	
2743	E62	TBC1D16	
2744	E17	TBC1D30	
2745	E56	TBC1D30	

2746	E65	TBX19	
2747	E23	TBX21	
2748	E24	TBXT	
2749	E41	TCAF2	
2750	E32	TCF21	
2751	E39	TCF4	
2752	E4	TCF7L1	
2753	E26	Tcf7l2	
2754	E27	TCF7L2	
2755	E24	TCFL2	
2756	E4	TDGF1	
2757	E67	Tdrd7	
2758	E2	TEAD2	
2759	E25	TENM1	
2760	E46	TERT	
2761	E42	TESC	
2762	E35	TFAP2B	
2763	E35	TFDP1	
2764	E14	TFE3	
2765	E22	TFF3	
2766	E58	TFF3	
2767	E8	TFPI2	
2768	E21	TFRC	
2769	E19	TG	
2770	E41	TGFA	
2771	E24	TGFB1	
2772	E16	TGFB1	
2773	E21	TGFB1	
2774	E67	Tgif1	
2775	E2	TGIF2	
2776	E29	TGM2	
2777	E33	TGM2	
2778	E43	TGM2	
2779	E59	Tgm2	
2780	E23	TGM4	
2781	E17	TH	
2782	E60	THBS1	
2783	E40	THBS2	
2784	E14	THNSL1	
2785	E1	THY1	
2786	E13	THY1	
2787	E27	TIAM1	
2788	E2	TIFA	

2789	E58	TIMD4	
2790	E2	TIMELESS	
2791	E14	TIMM50	
2792	E21	TIMP1	
2793	E31	TIRAP	
2794	E63	TK1	
2795	E31	TLCD1	
2796	E46	TLE1	
2797	E39	TLE4	
2798	E41	TLE4	
2799	E67	Tlr3	
2800	E41	TLR4	
2801	E42	TM4SF20	
2802	E65	TMBIM6	
2803	E42	TMC5	
2804	E58	TMC5	
2805	E14	TMC8	
2806	E15	TMED1	
2807	E1	TMEM125	
2808	E23	TMEM156	
2809	E43	TMEM158	
2810	E43	TMEM166	
2811	E31	TMEM170A	
2812	E31	TMEM170B	
2813	E29	TMEM176A	
2814	E49	Tmem176a	
2815	E29	TMEM176B	
2816	E49	Tmem176b	
2817	E26	Tmem212	
2818	E54	TMEM22	
2819	E26	Tmem30	
2820	E17	TMEM35	
2821	E65	TMEM38B	
2822	E8	TMEM45B	
2823	E15	TMEM59	
2824	E52	TMEM74	
2825	E26	Tmem88b	
2826	E2	TMEM9	
2827	E29	TMEM91	
2828	E15	TMEM98	
2829	E56	TMIE	
2830	E35	TMIGD2	
2831	E1	TMPRSS13	

2832	E31	TMPRSS5	
2833	E27	TMTC2	
2834	E21	TNC	
2835	E40	TNC	
2836	E57	TNC	
2837	E11	TNF	
2838	E38	TNFAIP3	
2839	E49	Tnfaip3	
2840	E66	TNFRSF10B	
2841	E42	TNFRSF11A	
2842	E8	TNFRSF12A	
2843	E21	TNFRSF12A	
2844	E28	TNFRSF13B	
2845	E28	TNFRSF13C	
2846	E21	TNFRSF14	
2847	E28	TNFRSF17	
2848	E21	TNFRSF19	
2849	E55	Tnfrsf19	
2850	E67	Tnfrsf1b	
2851	E47	TNFRSF21	
2852	E37	TNFRSF8	
2853	E14	TNFRSF9	
2854	E54	TNFRSF9	
2855	E2	TNFSF10	
2856	E44	TNFSF10	
2857	E54	TNFSF4	
2858	E67	Tnfsf9	
2859	E35	TNIK	
2860	E64	TNIK	
2861	E65	TNNI1	
2862	E58	TNNT1	
2863	E49	Tnnt2	
2864	E1	TNS1	
2865	E1	TNS4	
2866	E36	TNS4	
2867	E29	TOP2A	
2868	E63	TOP2A	
2869	E17	TOX	
2870	E37	TOX	
2871	E42	TOX3	
2872	E50	TP53	
2873	E43	TP53INP1	
2874	E60	TP63	

2875	E46	TP73	
2876	E60	TP73	
2877	E39	TPBG	
2878	E41	TPBG	
2879	E12	TPH1	
2880	E29	TPI1	
2881	E41	TPM1	
2882	E1	TPM2	
2883	E37	TPM2	
2884	E43	TPM2	
2885	E19	TPO	
2886	E60	TPO	
2887	E21	TPP1	
2888	E54	TPPP3	
2889	E37	TPST2	
2890	E65	TPT1	
2891	E14	TRAM2	
2892	E47	TRAM2	
2893	E58	TRDC	
2894	E26	Trf	
2895	E11	TRIAP1	
2896	E25	TRIB1	
2897	E49	Trib2	
2898	E24	TRIL	
2899	E7	TRIM29	
2900	E2	TRIM37	
2901	E4	TRIM71	
2902	E51	TRIM9	
2903	E67	Trip10	
2904	E12	TRIT1	
2905	E1	TRO	
2906	E16	TRPC1	
2907	E54	TRPC1	
2908	E15	TRPC6	
2909	E14	TRPM1	
2910	E34	TRPV4	
2911	E7	TRPV6	
2912	E38	TRPV8	
2913	E60	TSC2	
2914	E33	TSC22D3	
2915	E18	TSFM	
2916	E57	TSGA10	
2917	E19	TSHR	

2918	E20	TSHZ1	
2919	E59	Tshz2	
2920	E65	TSHZ2	
2921	E43	TSPAN13	
2922	E18	TSPAN31	
2923	E15	TSPAN8	
2924	E42	TSPAN8	
2925	E63	TSPYL3	
2926	E33	TTC3	
2927	E35	TTC3	
2928	E26	Ttr	
2929	E51	TTYH1	
2930	E11	TUBA4A	
2931	E25	TUBB2B	
2932	E17	TUBB2B	
2933	E58	TUBB2B	
2934	E65	TUBB4A	
2935	E66	TUBB4A	
2936	E2	TXNDC16	
2937	E21	TXNIP	
2938	E33	TXNIP	
2939	E45	Txnip	
2940	E31	TYW1	
2941	E48	UAP1	
2942	E21	UAP1L1	
2943	E50	UBASH3B	
2944	E35	UBB	
2945	E67	Ube216	
2946	E14	UBE2E3	
2947	E14	UBE2H	
2948	E31	UBL3	
2949	E23	UCHL1	
2950	E34	UCN2	
2951	E45	Ugdh	
2952	E45	Ugt2b34	
2953	E23	UGT3A1	
2954	E14	ULBP2	
2955	E4	UNC13C	
2956	E20	UNC5A	
2957	E62	UNC5A	
2958	E17	UNC5C	
2959	E6	UNC5D	
2960	E46	UNCX	

2961	E2	UNG	
2962	E54	UPP1	
2963	E31	USB1	
2964	E42	USH1C	
2965	E62	VAMP7	
2966	E26	Vat1l	
2967	E2	VAV3	
2968	E26	Vcan	
2969	E16	VCAN	
2970	E43	VCAN	
2971	E56	VCAN	
2972	E21	VCL	
2973	E35	VCL	
2974	E2	VDR	
2975	E60	VDR	
2976	E29	VEGFA	
2977	E19	VEGFA	
2978	E54	VEGFA	
2979	E21	VGF	
2980	E21	VGLL4	
2981	E33	VGLL4	
2982	E42	VIL1	
2983	E16	VIM	
2984	E66	VIM	
2985	E65	VIPR1	
2986	E1	VIT	
2987	E31	VKORC1L1	
2988	E31	VMAC	
2989	E29	VMP1	
2990	E30	VPS9D1-AS1	
2991	E32	VSNL1	
2992	E40	VSNL1	
2993	E65	VSTM2A	
2994	E52	VTCN1	
2995	E66	VWA1	
2996	E58	VWA2	
2997	E54	VWA5A	
2998	E66	VWA5B2	
2999	E56	VWDE	
3000	E26	Vxn	
3001	E27	WASF3	
3002	E4	WDFY2	
3003	E14	WDR43	

3004	E16	WDR47	
3005	E23	WDR72	
3006	E58	WDR72	
3007	E2	WDR90	
3008	E25	WFDC1	
3009	E2	WFDC15B	
3010	E29	WFDC2	
3011	E54	WISP2	
3012	E65	WNT16	
3013	E46	WNT3A	
3014	E39	WNT5A	
3015	E46	WNT5A	
3016	E54	WNT6	
3017	E58	WNT6	
3018	E40	WNT7A	
3019	E49	Wnt7a	
3020	E46	WNT7B	
3021	E10	WRN	
3022	E37	WSB2	
3023	E24	WWP2	
3024	E37	XBP1	
3025	E60	XBP1	
3026	E47	XBP1	
3027	E58	XCL2	
3028	E66	XIST	
3029	E14	XKRX	
3030	E24	XYLB	
3031	E35	YAP1	
3032	E54	YARS	
3033	E18	YEATS4	
3034	E33	YPEL3	
3035	E58	YWHAEP7	
3036	E37	ZA20D3	
3037	E35	ZADH2	
3038	E37	ZAP70	
3039	E54	ZBED2	
3040	E65	ZBED2	
3041	E67	Zbp1	
3042	E37	ZBT20	
3043	E2	ZBTB12	
3044	E26	Zbtb18	
3045	E31	ZBTB41	
3046	E35	ZBTB7A	

3047	E21	ZCCHC12	
3048	E33	ZCCHC24	
3049	E62	ZCCHC3	
3050	E39	ZEB1	
3051	E33	ZFAND5	
3052	E66	ZFHX3	
3053	E2	ZFP566	
3054	E65	ZFPM2	
3055	E26	Zic1	
3056	E65	ZIC2	
3057	E46	ZIC5	
3058	E65	ZIC5	
3059	E2	ZKSCAN17	
3060	E43	ZMAT3	
3061	E66	ZMAT3	
3062	E23	ZMAT4	
3063	E65	ZMAT4	
3064	E66	ZMIZ1	
3065	E54	ZMYND10	
3066	E27	ZMYND8	
3067	E60	ZNF185	
3068	E65	ZNF385B	
3069	E31	ZNF396	
3070	E66	ZNF428	
3071	E65	ZNF536	
3072	E14	ZNF704	
3073	E35	ZNF704	
3074	E65	ZNF750	
3075	E14	ZNF75D	
3076	E61	ZNF791	
3077	E65	ZNF804A	
3078	E4	ZSCAN10	
3079	E21	ZYX	
3080	E43	ZYX	
3081	E26	1110017D15Rik	
3082	E45	1700030C14Rik	
3083	E45	1700031L13Rik	
3084	E26	1700094D03Rik	
3085	E26	2900040C04Rik	